

https://dspace.org/

Wind loading on catenary domes

Van Gool, Richard Marc

2020
https://hdl.handle.net/10539/31200

Downloaded from a DSpace repository. https://dspace.org/



UNIVERSITY OF THE WITWATERSRAND

SCHOOL OF CIVIL AND ENVIRONMENTAL ENGINEERING

MASTERS RESEARCH REPORT

Title:	Wind Loading on Catenary Domes
Supervisor:	Prof. M. Gohnert
Co. Supervisor:	Mr R. A. Bradley
Student Name:	Richard Marc van Gool
Student no:	348658
Date:	March 2020

DECLARATION

I declare that this research report is my own unaided work. It is being submitted for the Degree of Master of Science to the University of the Witwatersrand, Johannesburg. It has not been submitted before for any degree or examination to any other University.

_____

Richard Marc van Gool

__31st__ day of ____March___ year 2020

ABSTRACT

The research aimed at understanding the pressure patterns induced by wind loading on thin shelled catenary dome structures. This unique shape of a “catenary” is able to further optimise material usage by only transmitting compressive stresses within the shape. A circular dome was tested along with the catenary domes to ensure the external wind pressure distributions were in agreement with previously conducted research on circular domes. Once validated, this research will be valuable in design, as there is no guidance given on wind pressures for catenary domes. Codes used by engineers provide external pressure coefficients for vaulted circular roofs with rectangular bases and for circular domes with circular bases. If external pressure coefficients are made available for catenary domes, this may offer guidance in design.

ACKNOWLEDGEMENTS

I would like to acknowledge and thank the following people who have assisted me throughout my Masters:

- My supervisor, Prof. M. Gohnert, for his continued assistance and patience.
- My co-supervisor, Mr. R. Bradley, for his continued support, experience and help throughout.
- Dr. A.M. Goliger, for his valuable input and guidance.
- Mr. T. van Wyk, for his technical support and testing of the dome models in the wind tunnel.
- The Council for Scientific and Industrial Research (CSIR) for the use of the Boundary-Layer Wind-Tunnel.

TABLE OF CONTENTS

Declaration ii

Abstract iii

Acknowledgements iv

Table of Contents v

List of Figures viii

List of Tables xii

List of Symbols xiii

1 Introduction 1

1.1 Background 1

1.2 Objectives 3

1.3 Scope 3

2 Literature Review 8

2.1 Prior Research on Catenary Domes 8

2.2 Prior Research of Relevance 8

2.2.1 Wind Loading on Catenary Vault Structures 8

2.2.2 Wind Loading on Catenary Earth Shells 9

2.2.3 Wind Loads on a Circular Dome in Smooth and Turbulent Boundary Layer Flow 9

2.2.4 Wind loads on curved roofs 11

2.2.5 Wind pressure on circular cylinder structures 13

2.2.6 Wind pressure on hemispherical dome geometry 16

2.3 Gaps in Research 17

3 Experimental Methodology 18

3.1 Boundary Layer Wind Tunnel 18

3.1.1 Wind tunnel facility 18

3.1.2 Instrumentation 19

3.2 Boundary Layer Simulation 21
3.3 Surface Pressure, Measurements and Calculation 22
3.3.1 Reference dynamic pressure 22
3.3.2 Reference static pressure 22
3.3.3 Data processing 22
3.4 Wind tunnel models 23
3.5 Simulation of Surface Roughness 24
3.6 Wind Speed Profile 27
3.7 Pressure Tap Placement 29
3.8 Initial Test Results 31
3.8.1 Small Size Domes 31
3.8.2 Large Size Domes 33
3.9 Repeatability of Measurements 37
3.10 Summary of Chapter 38
4 Analysis and Results 39
4.1 Boundary Layer 39
4.2 Reynolds Number 40
4.3 The Influence of Geometry 42
4.4 Influence of Walls 44
4.5 Summary of Chapter 48
5 Discussion 49
5.1 Boundary Layer and Reynolds Number 49
5.1.1 Overview 49
5.1.2 Influence of Geometrical Size 49
5.1.3 Influence of Wind Speed 50
5.1.4 Pressure Distribution Discussion 51
5.2 The Influence of Geometry 53
5.3 Influence of Walls 55
6 Development of The Design Graph 60

6.1 Development of graph 60

6.2 Comparison of Dome and Catenary Design Graphs 66

6.3 Catenary Design Graph 73

7 Future Work 76

8 Conclusion 77

9 Works Cited 78

LIST OF FIGURES

Figure 1: Pantheon, Rome (Walks of Italy) 1
Figure 2: Cross-section (Wikipedia, 2018) 1
Figure 3: St. Paul's Cathedral, London (Wikipedia) 1
Figure 4: Cross-Section of St. Paul's (Media Storehouse) 1
Figure 5: The Gateway Arch (Quora, 2011) 2
Figure 6: Catenary Curves (Auroville Earth Institute) 2
Figure 7: Thrust Line within an Arch Cross-Section (Auroville Earth Institute) 3
Figure 8: 2D Catenary Dome Shape - Various H/R Ratios 4
Figure 9: 2D Catenary Dome Shape - Domes at lower H/R Ratios 5
Figure 10: Recommended values of external pressure coefficients for domes with circular base (SANS 10160-3:2010) 6
Figure 11: Definition of wind direction and distribution of measuring points, (R A Bradley, 2016) 8
Figure 12: Correlation coefficient of pressure distributions at various Reynolds number in smooth flow, Re, ref = 3 x 10^5 (C.M. Cheng, 2009) 10
Figure 13: Correlation coefficient of pressure distributions at various Reynolds number in turbulent boundary layer flow, Re, ref = 2 x 10^5 (C.M. Cheng, 2009) 10
Figure 14: Comparison of Cpe values for curved roofs with h/d = 0.5 (or h/r = 1.0), and f/d = 0.1 (Blackmore & Tsokri, 2006) 11
Figure 15: Comparison of Cpe values for curved roofs with h/d = 0 (no wall), and f/d = 0.3 (Blackmore & Tsokri, 2006) 11
Figure 16: Recommended values of external pressure coefficients $c_{pe,10}$ for vaulted roofs with rectangular base (BS EN 1991-1-4:2005) 12
Figure 17: Proposed revision to EN1991-1-4 Fig. 7.11 for curved roofs (Blackmore & Tsokri, 2006) 13
Figure 18: Distribution of local mean pressure coefficient around a circular cylinder at different Reynolds numbers (Liu, 1990) 14
Figure 19: Pressure distributions around a two-dimensional flow over a circular cylinder at subcritical and supercritical Reynolds numbers (Holmes, 2001) 15
Figure 20: Effect of aspect ratio (height/diameter) on pressure distributions around circular cylinders (Holmes, 2001) 15

Figure 21: Effect of rise ratio on spherical-section dome by relative position along (Cook, 1990) 16
Figure 22: Schematic Diagram of the Boundary Layer Wind Tunnel 18
Figure 23: Wind Tunnel Facility (Photo 1) 18
Figure 24: Wind Tunnel Facility (Photo 2) 19
Figure 25: Pressure taps 19
Figure 26: Schematic Diagram of the Rad3200 System (Mistry & Bhayroo, 2014) 20
Figure 27: Pitot Static Tube (placed 750mm above the turn table) 20
Figure 28: Dome model placed on turn table for testing 21
Figure 29: Corrugated Cardboard within 16m Fetch for Boundary Layer Simulation .. 21
Figure 30: Small 3D Printed Domes 23
Figure 31: ESDU P12 to P40 Grit Graph 25
Figure 32: ESDU P100 to P220 Grit Graph 25
Figure 33: ESDU P600 Grit & Fibreglass Graph 26
Figure 34 & Figure 35: Applying Sandpaper to Models 26
Figure 36: Glue Sand Particles to 3D Models 27
Figure 37: Wind Speed Profiles 28
Figure 38: Placement of Pressure Taps on the Models 29
Figure 39: Tap Placement Sketch (Example for CAT 1.4) 30
Figure 40: Small Dome Model Comparison to the graph collated by (Taylor, 1991) 32
Figure 41: Peak Pressure Error for Small Domes - SC5.0 Rough BL 33
Figure 42: Large 250mm Diameter Hand-crafted Domes 33
Figure 43: Large Dome Model Comparison to the graph collated by (Taylor, 1991) ... 34
Figure 44: Turbulence Intensity Profile (R A Bradley, 2016) 34
Figure 45: Peak Pressure Error for Large Domes - SC5.0 Rough BL (old) 36
Figure 46: Repeatability of Results - Dome 1.0 37
Figure 47: Repeatability of Results - CAT 1.0 38
Figure 48: Comparison of Sub-critical and Super-critical flow regimes to the graph collated by (Taylor, 1991) 39
Figure 49: Large & Small Circular Domes (Rough BL) - Reynolds Number 40
Figure 50: Large & Small Catenary Domes (Rough BL) - Reynolds Number 41
Figure 51: Dome Models Tested (Geometry) 42
Figure 52: Effect of Geometry on Large Domes, Rough BL, SC5.0 42
Figure 53: 3D Pressure Contour, Dome (L) 1.0 43
Figure 54: 3D Pressure Contour, CAT (L) 0.6 43

Figure 55: 3D Pressure Contour, CAT (L) 1.0 43
Figure 56: 3D Pressure Contour, CAT (L) 1.4 43
Figure 57: 3D Pressure Contour, CAT (L) 2.0 44
Figure 58: Large Domes on Walls, Rough BL, SC5.0 (40mm Wall)..... 45
Figure 59: Large Domes on Walls, Rough BL, SC5.0 (100mm Wall)..... 45
Figure 60: Large Domes on Walls, Rough BL, SC5.0 (160mm Wall)..... 46
Figure 61: 3D PC, DOME (L) 1.0, (40 Wall)..... 46
Figure 62: 3D PC, CAT (L) 0.6, (40 Wall)..... 46
Figure 63: 3D PC, CAT (L) 1.0, (40 Wall)..... 47
Figure 64: 3D PC, CAT (L) 1.4, (40 Wall)..... 47
Figure 65: 3D PC, DOME (L) 1.0, (100 Wall)..... 47
Figure 66: 3D PC, CAT (L) 0.6, (100 Wall)..... 47
Figure 67: 3D PC, CAT (L) 1.0, (100 Wall)..... 47
Figure 68: 3D PC, CAT (L) 1.4, (100 Wall)..... 47
Figure 69: 3D PC, DOME (L) 1.0, (160 Wall)..... 48
Figure 70: 3D PC, CAT (L) 0.6, (160 Wall)..... 48
Figure 71: 3D PC, CAT (L) 1.0, (160 Wall)..... 48
Figure 72: 3D PC, CAT (L) 1.4, (160 Wall)..... 48
Figure 73: Rough BL, Large, SC4.0/4.4/5.0 (Combined) 50
Figure 74: Example of Taps Spaced at Varies Degrees (0 to 180)..... 53
Figure 75: Peak Pressure Error for Large Domes - SC5.0 Rough BL..... 54
Figure 76: 40/100/160mm Walls (Photo) 55
Figure 77: Incident Angle of Dome Models (e.g. CAT 0.6) 56
Figure 78: Negative Pressure Distribution Zone for Low H/R Ratios 59
Figure 79: Design Graph Development (Step 1 of 4)..... 61
Figure 80: Design Graph Development (Step 2 of 4)..... 62
Figure 81: Design Graph Development (Step 3 of 4)..... 62
Figure 82: Design Graph Development (Step 4 of 4)..... 63
Figure 83: DOME 1.0 Test Data vs. Dome Design Graph..... 66
Figure 84: Dome and Catenary Dome Design Graph (Comparison)..... 68
Figure 85: Illustration of CAT 2.0 Dome on a Wall (f/d = 1.0) 69
Figure 86: Catenary Dome Design Graph 73
Figure 87: Illustration for Application of Wind Loads (f/d > 0.3) 74

Figure 88: Positive and Negative Pressure Coefficients for Member Design (loading area >10m^2)..... 75

LIST OF TABLES

Table 1: Three ranges of Reynolds numbers with shedding characteristics (Liu, 1990) 13
Table 2: Small Dome Dimensions 24
Table 3: Small Dome Velocity SC5.0 28
Table 4: Model Tap Spacing and No. of Taps 29
Table 5: Tap Spacing Error (Design vs. Actual) 31
Table 6: Large Dome Velocity SC4.0, SC4.4, and SC5.0 35
Table 7: Large Dome Velocity SC4.0, SC4.4, and SC5.0 (with Walls) 35
Table 8: Peak Negative Pressures for Varying Reynolds Numbers 52
Table 9: h/d ratios used for testing 61
Table 10: Zone C - Maximum Pressure Coefficients for 150 to 210 Degrees 67
Table 11: Pressure Coefficient Readings from 0 to 45 Degrees at Varying h/d Ratios . 70
Table 12: Defining dimension "a" 75

LIST OF SYMBOLS

H/R	Height of dome/ Radius of dome
C_p or C_{pe}	Mean Pressure coefficient
C_{pe10}	Mean pressure coefficient (Area $\geq 10m^2$)
P_i	i^{th} Pressure (at tap positions)
P_{Ref}	Freestream Dynamic Pressure (at the pitot static tube)
N	Number of samples
R	Ratio of the square free stream reference velocities
V_{RH}	Velocity Measured at the Peak Dome Roof Height
V_{PH}	Velocity Measured at the Pitot Static Tube
R_e	Reynolds number
ρ	Density of fluid
v	Velocity of the fluid (m/s)
D	Diameter of the model (m)
μ	Kinematic viscosity
h/d	Wall height the dome is placed on/ diameter of the dome
f/d	height of the dome/ diameter of the dome
CAT (0.6/1.0/1.4/2.0)	Catenary Domes with varying H/R ratios
DOME (1.0)	Circular (i.e. hemispherical) Dome with a H/R ratio = 1.0
CSIR	Council for Scientific and Industrial Research
SC	Speed Conditions used in the CSIR Wind Tunnel
ESDU	Engineering Sciences Data Unit

1 INTRODUCTION

1.1 BACKGROUND

Thin shell structures have been around for many years, with construction dating back to 125 AD, an example being the Pantheon in Rome (Figure 1 and Figure 2). A thin shell structure is one in which the shape allows the forces applied to transmit by compressive and tensile stresses, which act in the plane of the surface.

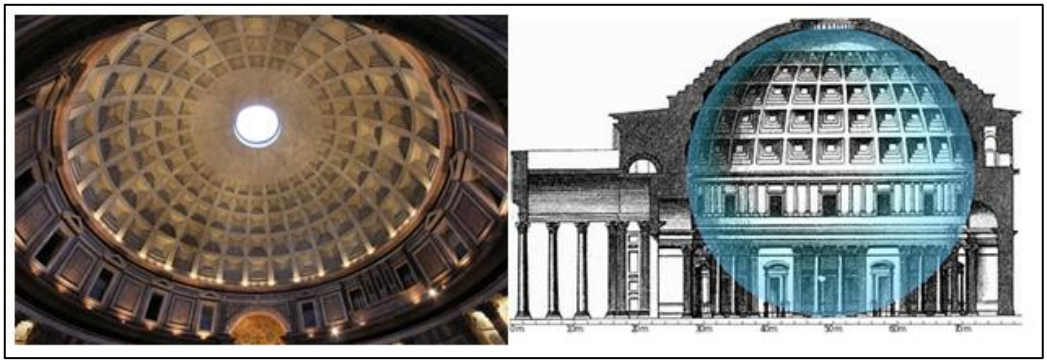


Figure 1: Pantheon, Rome (Walks of Italy)

Figure 2: Cross-section (Wikipedia, 2018)

Construction of domes in the sixteenth and seventeenth centuries used empirical techniques and oral traditions. During the seventeenth and eighteenth centuries, statics was used to determine the most stable form for domes. This was called “the catenary curve”. The Pantheon’s outer roof profile is a catenary (Figure 2) and the compressive forces flow within the shape. St. Paul’s Cathedral in London (Figure 3), which has an inner dome being in the shape of a catenary curve (Figure 4).



Figure 3: St. Paul's Cathedral, London (Wikipedia)

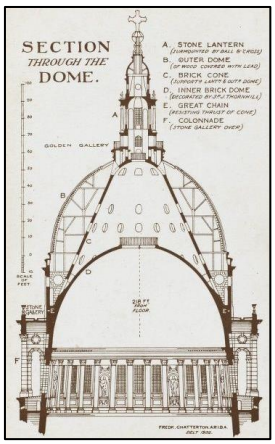


Figure 4: Cross-Section of St. Paul's (Media Storehouse)

The identification that an inverted chain was comparable to a thin arch was deduced by Robert Hooke. This unique shape called a “catenary” is able to further optimise material usage by only transmitting compressive stresses within the shape. A catenary is defined as the form a chain makes when it hangs freely between two supports (Figure 6). For an inverted catenary (Figure 5), the compressive forces are the least at the highest point (i.e. apex) and increase towards the base of the structure.



Figure 5: The Gateway Arch (Quora, 2011)

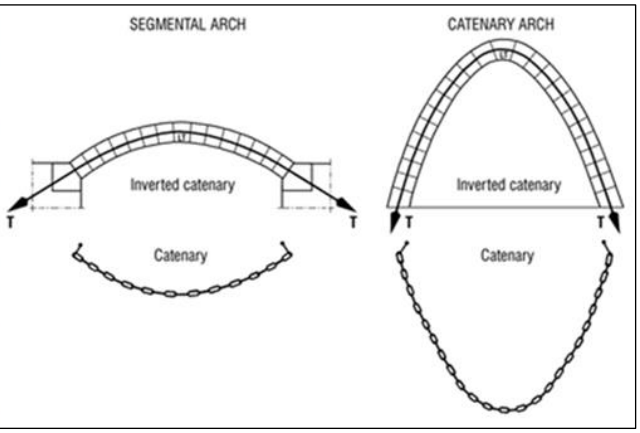


Figure 6: Catenary Curves (Auroville Earth Institute)

Catenary domes have a funicular geometry and are used because their shape responds to loads applied to the structure. Due to these types of domes being tension free structures, masonry can be used. On the other hand, a circular dome is not a tension free structure.

The general principle regarding arch design for thin shelled structures is to ensure the line of thrust (LT) is within the middle third of the arch’s cross-section (Figure 7). If this principle is followed, the arch will be stable. However, if the line of thrust moves to the inner third, the arch will tend to burst outwards. And, if the line of thrust moves to the outer third, the arch will tend to collapse inwards. These same principles apply to catenary domes.

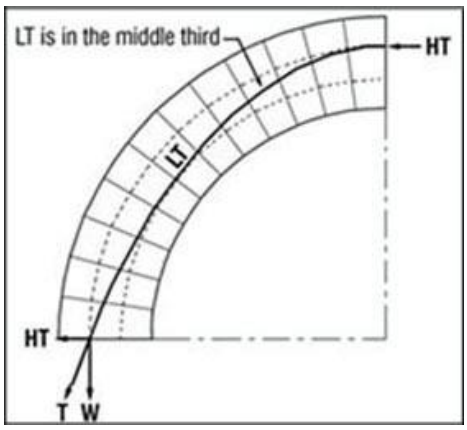


Figure 7: Thrust Line within an Arch Cross-Section (Auroville Earth Institute)

1.2 OBJECTIVES

The main aim of the research is to examine the wind pressure distributions over catenary domed structures, which may then give guidance in the design. No wind data currently exists for catenary domes, so such a study could be of benefit to designers. Currently, the engineer would use circular dome wind data, as published in various design codes, or seek specialist advice. This research would give the end user (the engineer) more guidance and establish the differences between a hemispherical dome and a catenary dome.

1.3 SCOPE

To research the effects of wind on catenary domes, experimentation is required. Scaled models tested have been printed on a 3D printer at CSIR (Council for Scientific and Industrial Research). The CSIR wind tunnel was used to perform the tests. Scale models vary in height to radius (H/R) ratios. The domes which were tested are plotted in Figure 8.

$$H/R\ ratio\ = \frac{Height\ of\ Dome}{Radius\ of\ Dome}$$

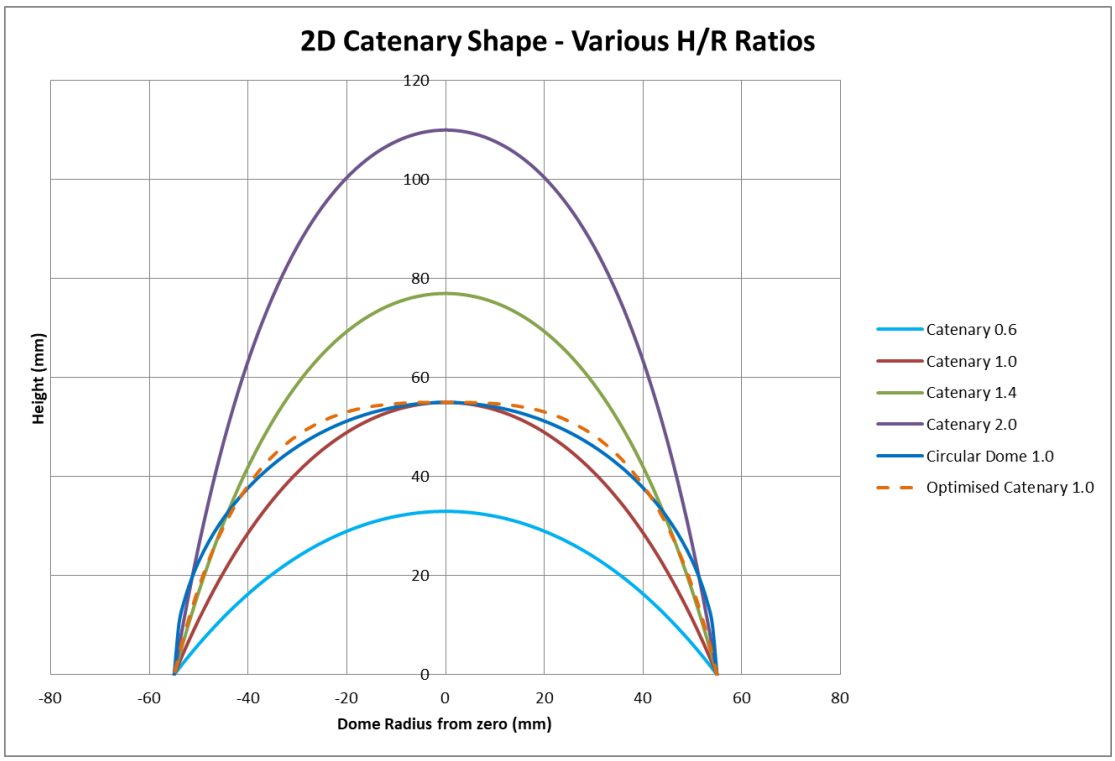


Figure 8: 2D Catenary Dome Shape - Various H/R Ratios

The shapes of catenary domes are the same as a 2D catenary, but rotated 360 degrees around the central axis. A catenary can be described by the following equation:

$$y = a.cosh\left(\frac{x}{a}\right) \qquad \text{Eqn. (1)}$$

Where;

x, y rectangular coordinates of an arbitrary point along the catenary

a parameter in the catenary equation

The ideal/optimised catenary domed shapes are given in *"Building with Earth: Design and Technology of a Sustainable Architecture"* (Minke, 2009). A table was used to plot the optimised catenary dome shape seen in Figure 8. The optimised catenary dome is based on a statics engineering method used to derive an ideal curve. The shape accounts for self-weight only. The shape ensures that no tensile ring forces are developed. The theoretical catenary curve described by Eqn. (1) is drastically different from the optimised catenary shape.

It was decided that in the current research the typical catenary shape be tested, with the inclusion of one optimised catenary dome of ratio H/R = 1.0. These catenary dome test specimens are to be 110mm in diameter at the base. By changing the apex height, the catenary domes change in shape according to the following height to radius (H/R) ratios; 0.6, 1.0, 1.4, and 2.0. Therefore, there are five catenary dome models which were constructed and tested.

Figure 9 represents a comparison between circular domes and catenary domes at varying H/R ratios. It can be seen that at a H/R ratio of 0.3, the circular dome and the catenary dome shapes are almost identical and will therefore respond similarly to load. A H/R ratio for testing at the lower range was chosen as 0.6, based on this graph. This was chosen because the differences between the circular and catenary domes become evident.

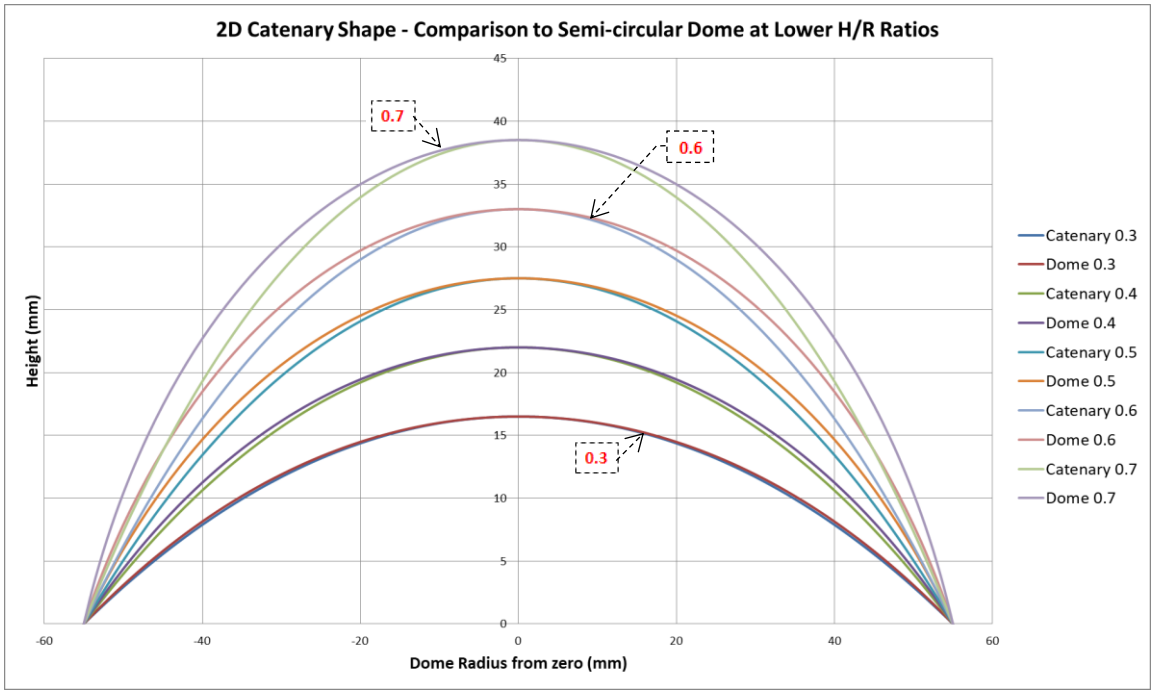


Figure 9: 2D Catenary Dome Shape - Domes at lower H/R Ratios

Blackmore and Tsokri (2006) during testing of the semi-circular vault, placed the vault on a limited height wall which would provide a more realistic pressure distribution over the shape being tested, since most domes are used as roof structures. The same principle was applied to the tests carried out on the catenary domes. Cylindrical walls were

placed below the catenary dome models to avoid any windward vortices affecting the pressure distribution over the shape being tested. A HDPE pipe of 110mm diameter was used as the wall for the model to sit on. Wall heights of 20, 55, and 100mm will be used.

A circular dome model was also tested. This allowed for comparisons with other research results of circular domes. If the results are in agreement, this indicates that the test data of the catenary domes have a high probability of being reliable. Once the final design graph is developed, it will be compared to the pressure coefficients for domes with a circular base in the SANS 10160-3:2010 code of practice, represented by Figure 10.

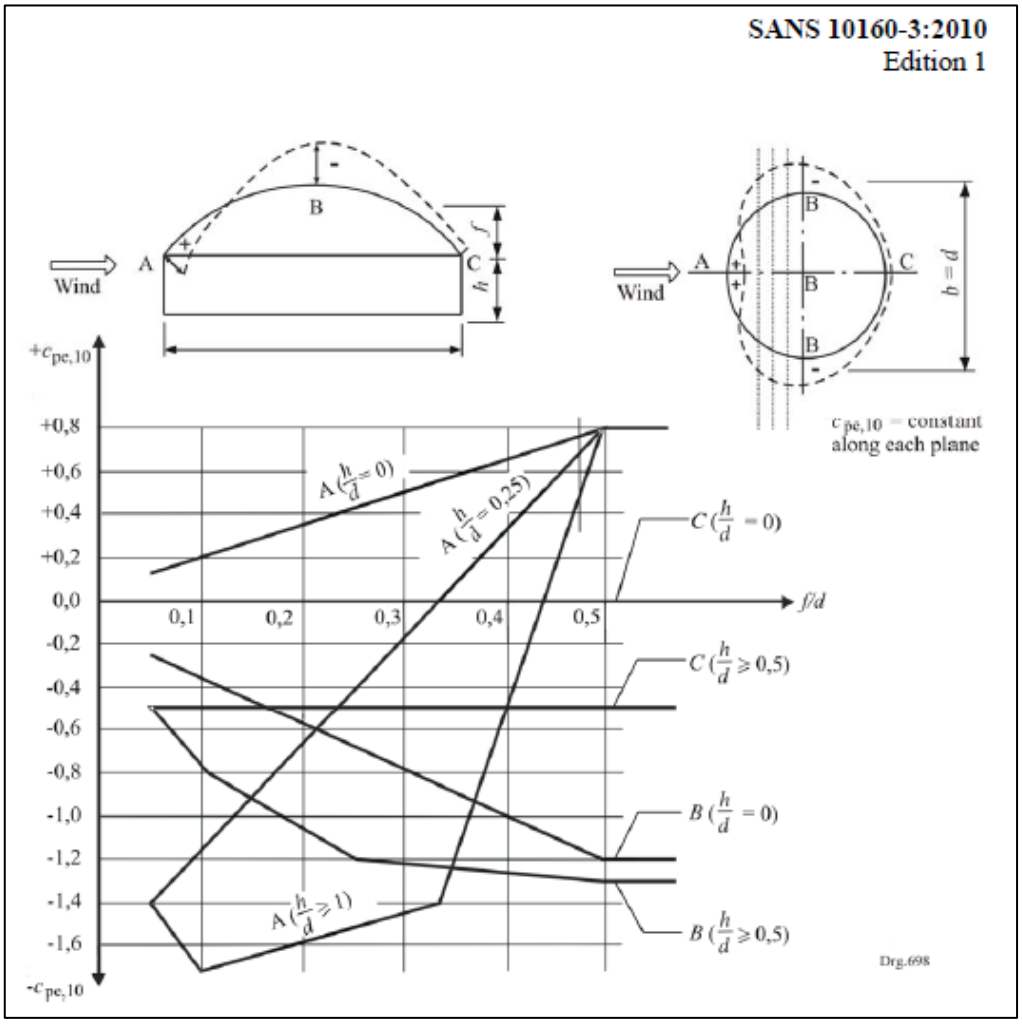


Figure 10: Recommended values of external pressure coefficients for domes with circular base (SANS 10160-3:2010)

These small dome sizes of 110mm diameter were modelled at scale of 1:545 which is within the acceptable range for scaled boundary layer modelling at the CSIR's wind tunnel (between 1:400 and 1:600). In Section 3.7 it is shown that these small dome sizes did not meet the required flow characteristics (i.e. Reynolds Number) and a scope change was required. The scope changed to testing larger domes sizes of 250mm diameter (i.e. model scale of 1:240), which then fell outside the aforementioned scaling range, i.e. the domes were not assessed in a scaled boundary layer. This in turn limits this study.

2 LITERATURE REVIEW

2.1 PRIOR RESEARCH ON CATENARY DOMES

Literature read indicates that no study into wind loading on catenary domes has been published. Only research on circular/hemispherical domes, vaulted structures, and circular cylinders could be found. Since catenary domes are being used more extensively in recent years, the need for wind testing has become apparent.

2.2 PRIOR RESEARCH OF RELEVANCE

2.2.1 Wind Loading on Catenary Vault Structures

Wind loading on catenary vaults was compared to SANS 10160-3 circular vaults or duo-pitched roof pressure coefficients. The important conclusions made by Bradley (2016), who conducted a series of wind tunnel experiments, are summarised below.

- The critical wind orientation for catenary vaults with a H/R ratios ≤ 1.2 correspond to an incident angle of $\alpha = 30^{o}$.
- The critical wind orientation for catenary vaults with a H/R ratio of 1.6 corresponds to an incident angle of $\alpha = 0^{o}$.

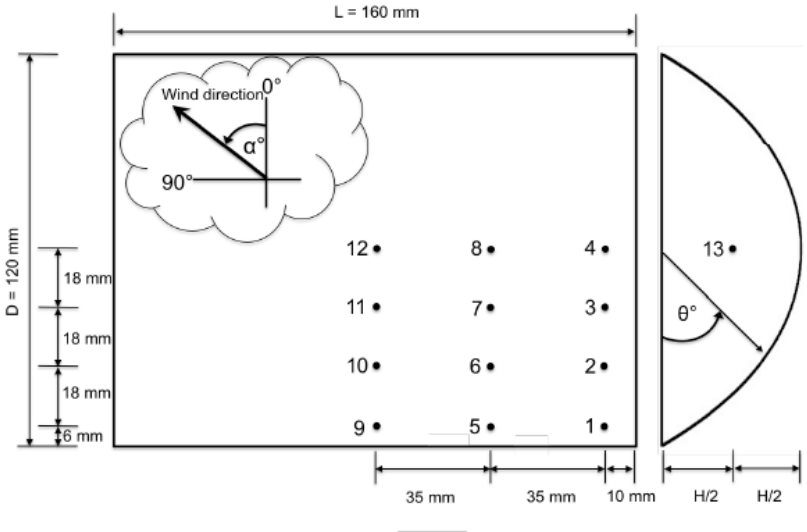


Figure 11: Definition of wind direction and distribution of measuring points, (R A Bradley, 2016)

- For catenary vaults with low H/R ratios, the pressure coefficients show the greatest similarity to the circular vault pressure coefficients as per SANS 10160-3:2011 code. For H/R $\geq$ 1.2 ratio, the pressure coefficients show the greatest similarity to the duo-pitch roof pressure coefficients from the SANS code.
- When using H/R ratios $\geq$ 1.2, which is approximated by the duo-pitch roof data in the code, the roof pitch (ψ) can be approximated using $\psi = \tan^{-1}(H/R)$.
- Wind blowing parallel to the gable end ($\alpha = 90^{o}$), is not a critical orientation for all catenary geometries.

2.2.2 Wind Loading on Catenary Earth Shells

Bradley (2016) further concluded for wind loads on catenary vault earth shells;

- Wind loads dominate as the main force, as the span/height increases.
- For steep and complex unreinforced earth shell, expert advice should be acquired before adopting pressure coefficients.
- Adopting pressure coefficients from a circular vault to design a H/R = 1.6 catenary vault, resulted in an almost 20% under design.

2.2.3 Wind Loads on a Circular Dome in Smooth and Turbulent Boundary Layer Flow

Wind tunnel tests were performed on circular domes in smooth and turbulent boundary layer flows by C.M. Cheng (2009), to determine the effects of Reynolds number. Various Reynolds numbers were tested ranging from 5.3×10^4 to 2.0×10^6. The results are summarized below:

- In smooth flow (Figure 12);
    - The transition of separation flow occurs between Re =$1.8 - 3.0 \times 10^5$. In this Reynolds number region, separation/reattachment occurs.
    - Pressure distributions become relatively stable after Re > 3.0×10^5.
- In turbulent flow (Figure 13);
    - The transition of separation flow occurs where Re < 1.1×10^5. In this Reynolds number region, separation/reattachment occurs.

- Pressure distributions become Reynolds number independent at Re = 1.0 - 2.0 x 10^5.

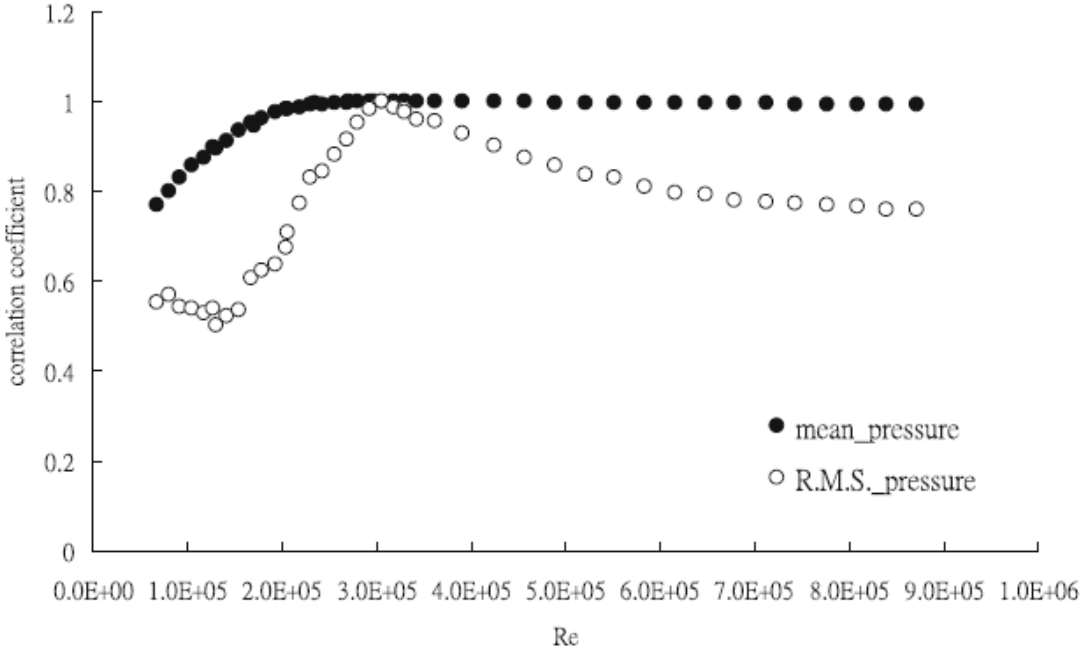


Figure 12: Correlation coefficient of pressure distributions at various Reynolds number in smooth flow, Re, ref = 3 x 10^5 (C.M. Cheng, 2009)

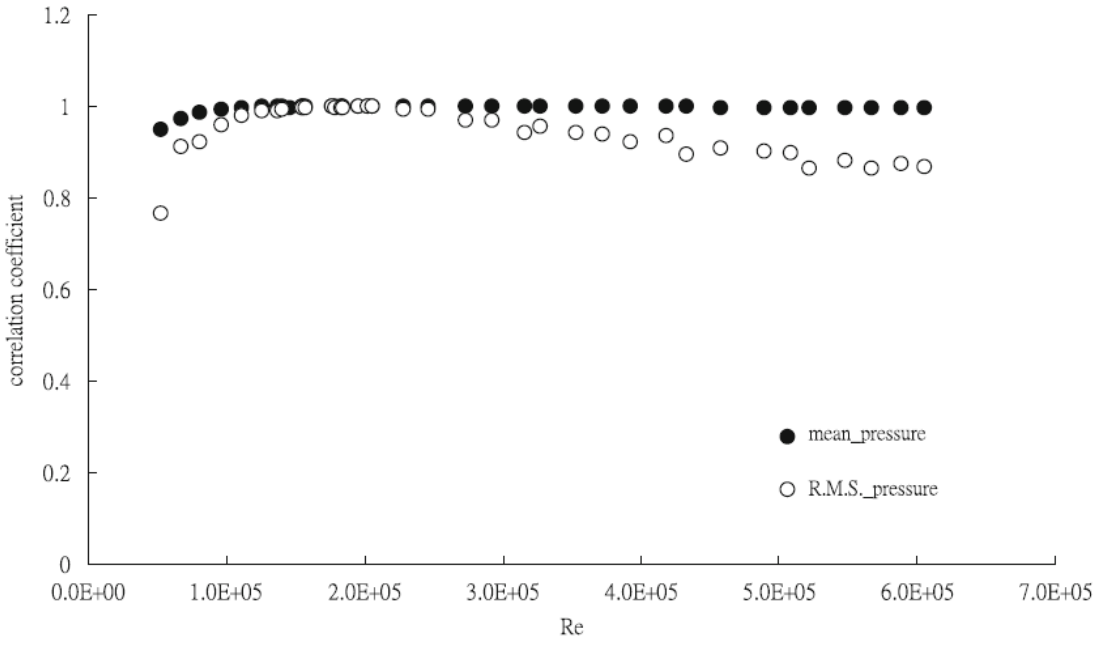


Figure 13: Correlation coefficient of pressure distributions at various Reynolds number in turbulent boundary layer flow, Re, ref = 2 x 10^5 (C.M. Cheng, 2009)

2.2.4 Wind loads on curved roofs

The Eurocode (EN1991-1-4) for wind actions includes pressure coefficients for cylindrical roofs for wind blowing normal to the eaves. Blackmore and Tsokri (2006) stated several concerns when testing cylindrical vault roofs.

Wind pressure coefficients were compared between several published journals and codes (Figure 14 and Figure 15). It is clear that there is a wide variability between data sets.

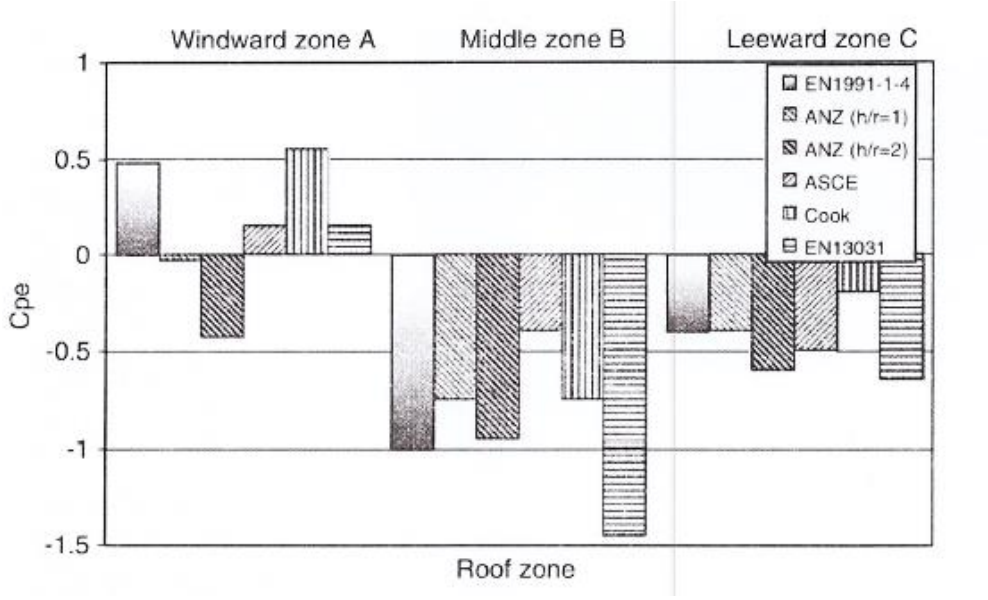


Figure 14: Comparison of Cpe values for curved roofs with h/d = 0.5 (or h/r = 1.0), and f/d = 0.1 (Blackmore & Tsokri, 2006)

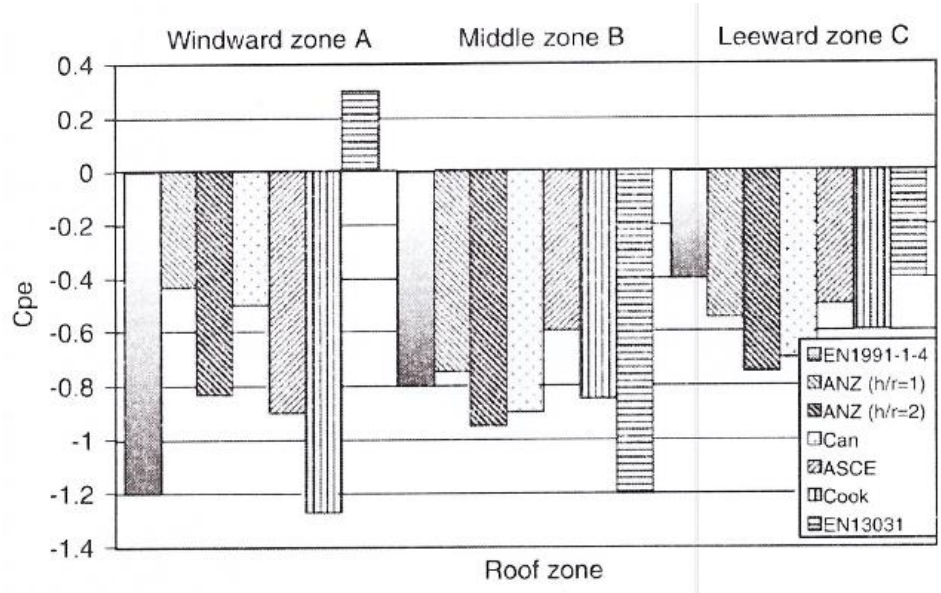


Figure 15: Comparison of Cpe values for curved roofs with h/d = 0 (no wall), and f/d = 0.3 (Blackmore & Tsokri, 2006)

Furthermore, Blackmore and Tsokri (2006) concluded by stating:

- For wind angle 0 ± 45^{o} (wind normal to the ridge); the wind pressure graph published in the EN1991-1-4 code for circular vault roofs requires some modifications to ensure the design engineer will have a safe an economical design.
- For wind angle 90 ± 45^{o} (wind parallel to the ridge); the wind pressure graph published in the EN1991-1-4 code for duo-pitched roofs may be used to reasonably approximate wind pressures on curved roofs. To determine the respective pitch to be used for the curved roof being considered, the pitch angle should be taken as $\alpha = \tan^{-1}\left(\frac{f}{0.5d}\right)$.

The proposed revision to Figure 16 from the EN1991-1-4 code, for circular vault roofs recommended by Blackmore and Tsokri (2006) is shown in Figure 17.

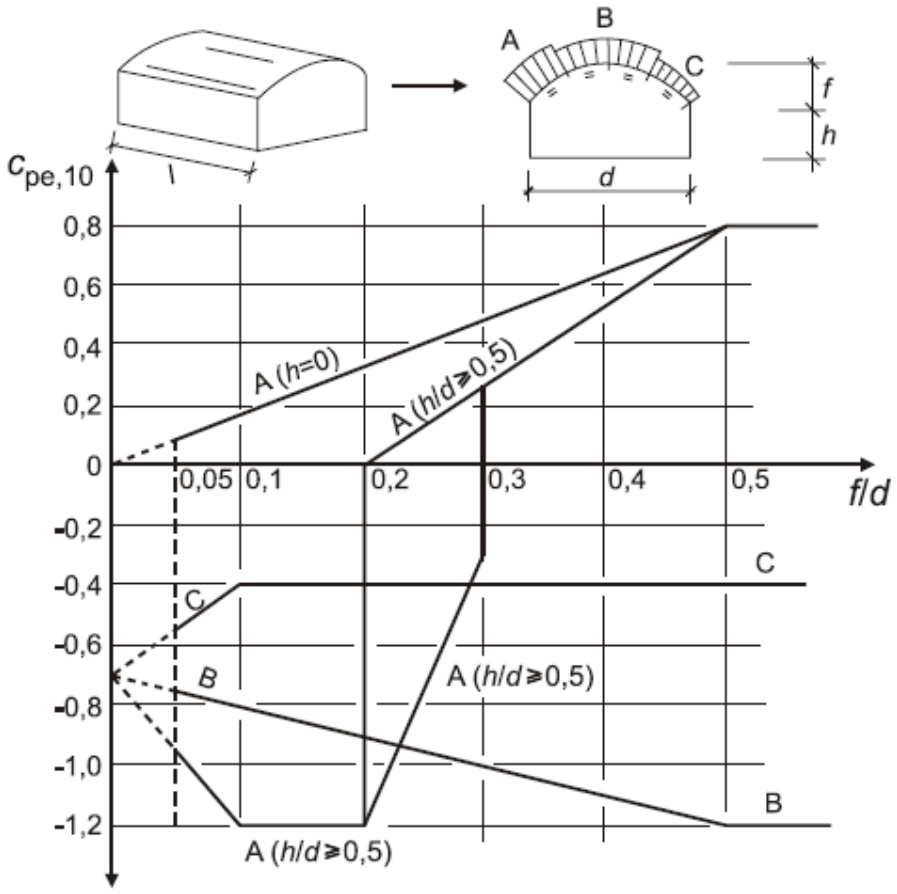


Figure 16: Recommended values of external pressure coefficients $c_{pe,10}$ for vaulted roofs with rectangular base (BS EN 1991-1-4:2005)

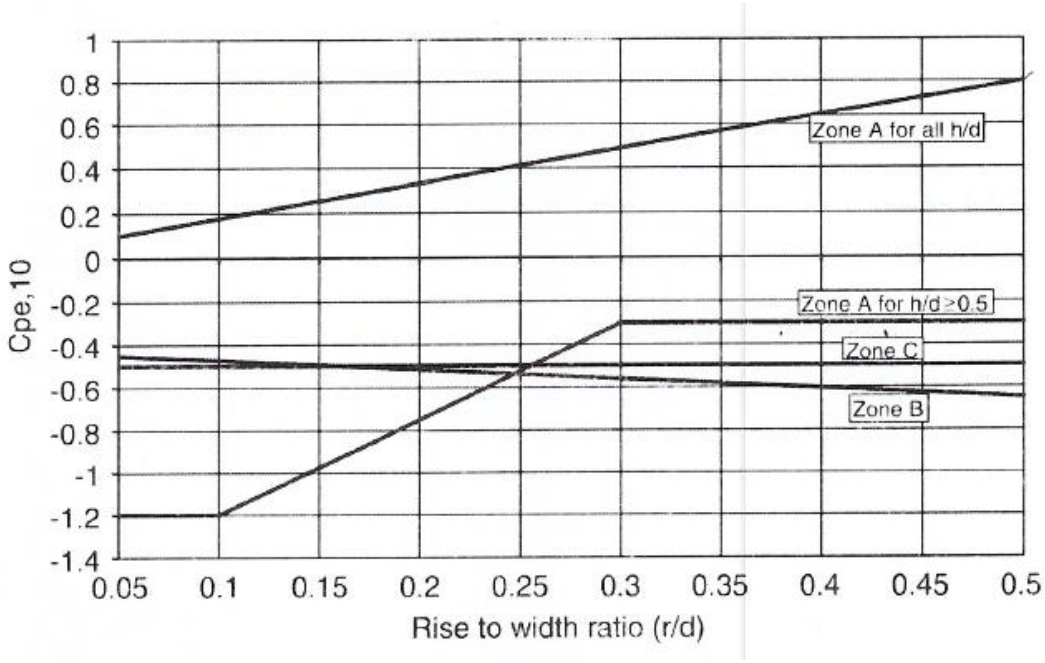


Figure 17: Proposed revision to EN1991-1-4 Fig. 7.11 for curved roofs (Blackmore & Tsokri, 2006)

2.2.5 Wind pressure on circular cylinder structures

Liu (1990) describes the distribution of pressures in terms of Reynolds number ranges for Subcritical, Supercritical, and Hypercritical flows. Refer to Table 1 and Figure 18.

Table 1: Three ranges of Reynolds numbers with shedding characteristics (Liu, 1990)

Range	Re	Shedding Characteristics
Subcritical	30 to 2×10^5	Regular (constant frequency)
Supercritical	2×10^5 to 4×10^6	Random (variable frequency)
Hypercritical	$> 4 \times 10^6$	Regular (constant frequency)

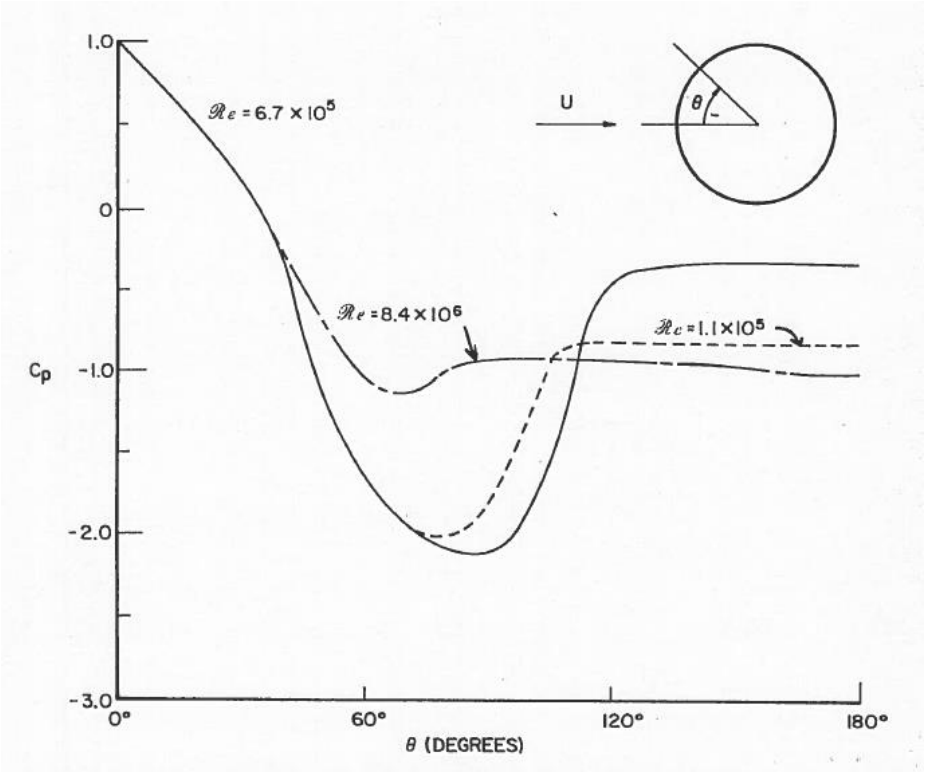


Figure 18: Distribution of local mean pressure coefficient around a circular cylinder at different Reynolds numbers (Liu, 1990)

The results by Liu (1990) are based on a smooth cylinder exposed to a uniform flow without free-stream turbulence. Should the cylinder be rough or exposed to turbulence induced in the free-stream, the critical Reynolds number will be $< 2 \times 10^5$. The transition between each range of critical flow would also not be as distinct. It is concluded that the variation of pressure coefficients around a cylinder depend on:

- Reynolds number
- Surface roughness
- Turbulence characteristics of the free stream

Holmes (2001) provided pressure distribution values at the supercritical and subcritical Reynolds numbers for a 2D flow over a circular cylinder, shown in Figure 19.

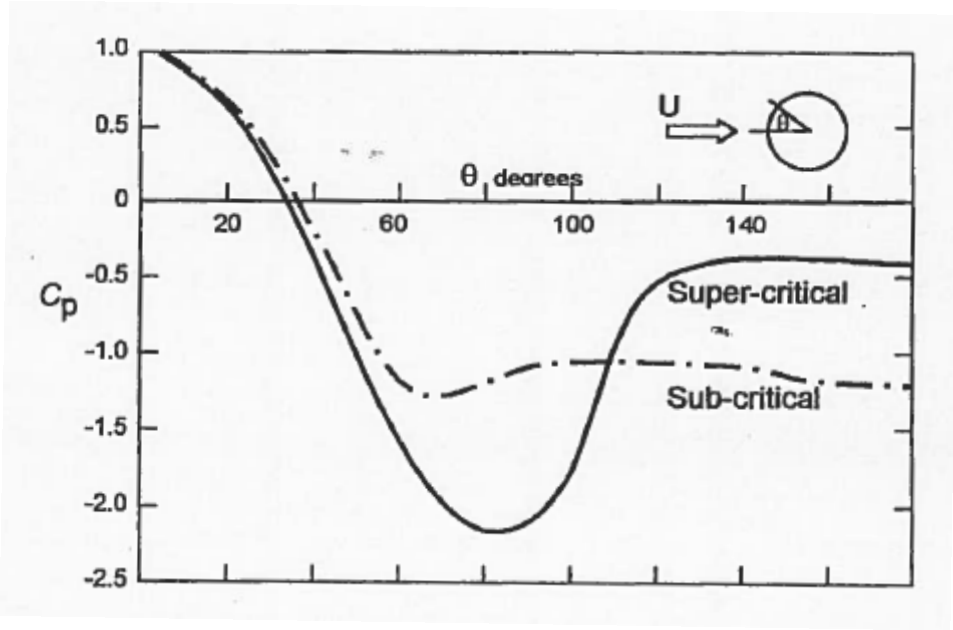


Figure 19: Pressure distributions around a two-dimensional flow over a circular cylinder at subcritical and supercritical Reynolds numbers (Holmes, 2001)

Circular cylinder pressure coefficients are also shown by Holmes (2001) for varying height to diameter aspect ratios, given in Figure 20.

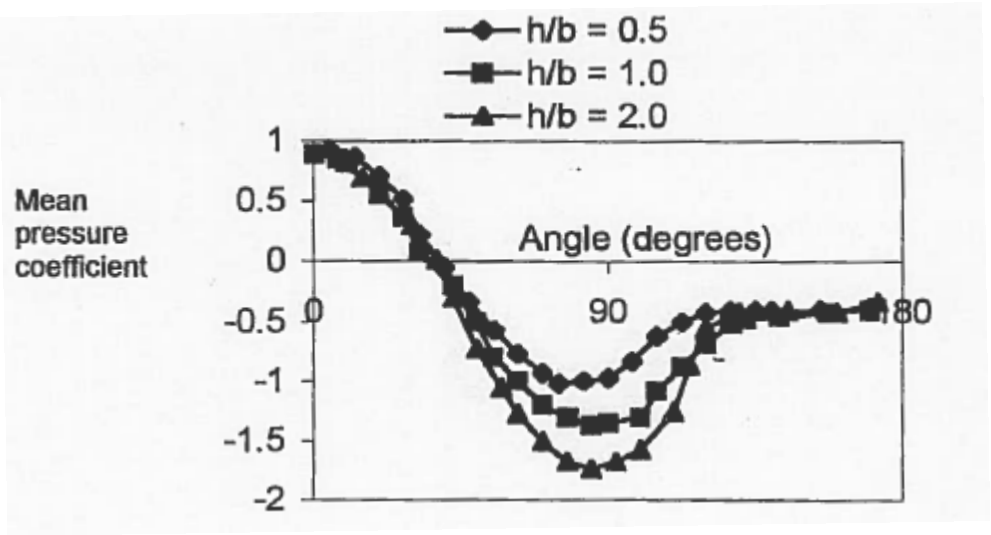


Figure 20: Effect of aspect ratio (height/diameter) on pressure distributions around circular cylinders (Holmes, 2001)

2.2.6 Wind pressure on hemispherical dome geometry

Wind tunnel tests were performed on hemispherical domes, and the results were summarised by Cook (1990), as follows:

- For a hemispherical dome in smooth uniform flow located on the ground (i.e. no wall), pressure coefficients were similar to a half sphere. However, the pressure at the base was affected by the thin boundary layer that forms on the ground surface.
- Pressures contours follow lines of latitude over the dome.
- Due to horse-shoe vortices near the base of the dome, pressures are reduced.
- The largest suction occurs at s/S = 0.5 ().

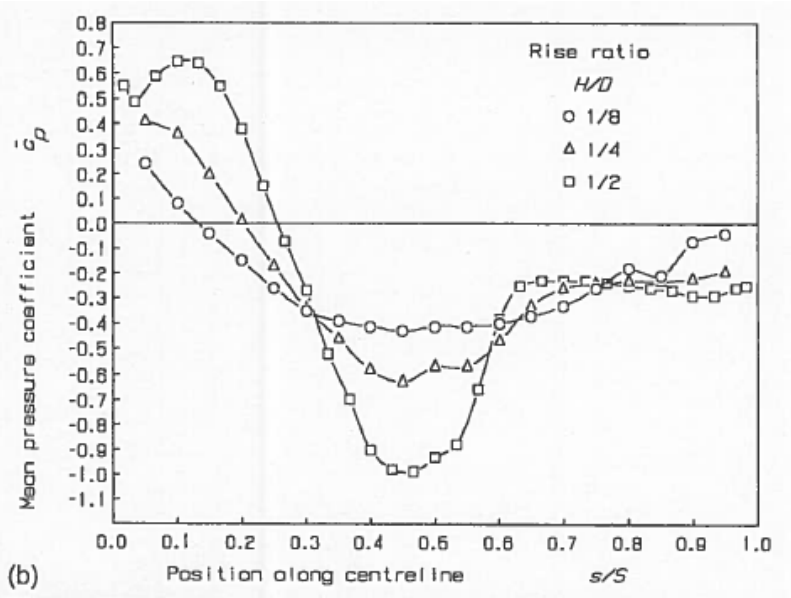


Figure 21: Effect of rise ratio on spherical-section dome by relative position along (Cook, 1990)

2.3 GAPS IN RESEARCH

No literature could be found on the following:

- Wind pressure coefficients acting on catenary domes with and without walls.
- Using catenary ribs of varying dimensions on the thin shelled catenary domes for high wind speeds. This would give an idea of what pressure coefficients could be expected by using ribs to strengthen the catenary dome against high winds. In essence, the ribs would resist the extreme wind forces. This information would be valuable to designers in tornado and hurricane zones throughout the world.
- Small openings within the catenary dome and the affect this has on external and internal pressure coefficients.

3 EXPERIMENTAL METHODOLOGY

The purpose of this Chapter is to discuss how the wind tunnel testing was setup, how the models were developed and prepared for testing, and the cause of the scope change requiring the small domes to be increase in size through analysis of the initial data.

3.1 BOUNDARY LAYER WIND TUNNEL

3.1.1 Wind tunnel facility

The wind tunnel facility located at the Council for Scientific and Industrial Research (CSIR) in Pretoria, South Africa, was used to conduct these tests. The internal dimensions of the wind tunnel was approximately 1000x2000x18000mm (H x W x L). Features of the wind tunnel, as seen from the schematic diagram in Figure 22 include:

- A development length of approximately 18m;
- A turn table to rotate a model 360 degrees (see Figure 23); and
- Instrumentation for pressure measurements and other readings.

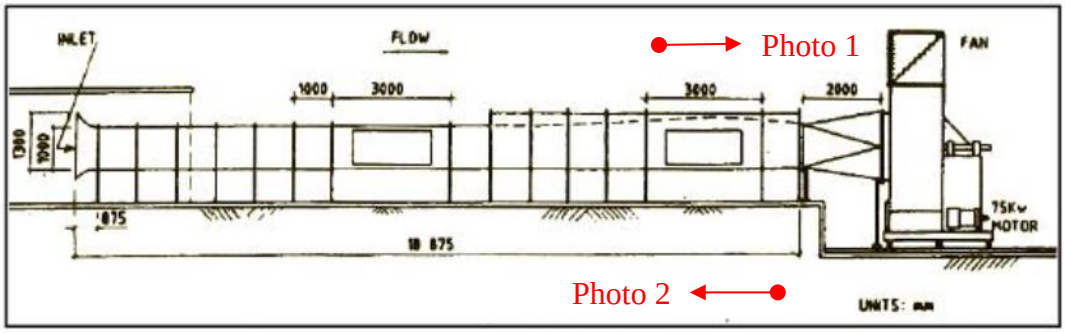


Figure 22: Schematic Diagram of the Boundary Layer Wind Tunnel



Figure 23: Wind Tunnel Facility (Photo 1)

Figure 23 and Figure 24, show the wind tunnel at the CSIR looking firstly towards the fan and then in the 2nd photo towards the inlet. Reference is made in Figure 22 with arrows showing the direction the photos were taken.



Figure 24: Wind Tunnel Facility (Photo 2)

3.1.2 Instrumentation

The initial data is read via pressure taps placed onto the models being tested. The tubes are hidden inside the domes (see Figure 25).



Figure 25: Pressure taps

The Synchronous Multi-Pressure Scanning System (SM-PSS) was used to obtain the pressure measurements from the tests. This system is based on the the RAD3200 system, developed by Scanivalve (see Figure 26). A sampling frequency of 625 Hz was used in this study.

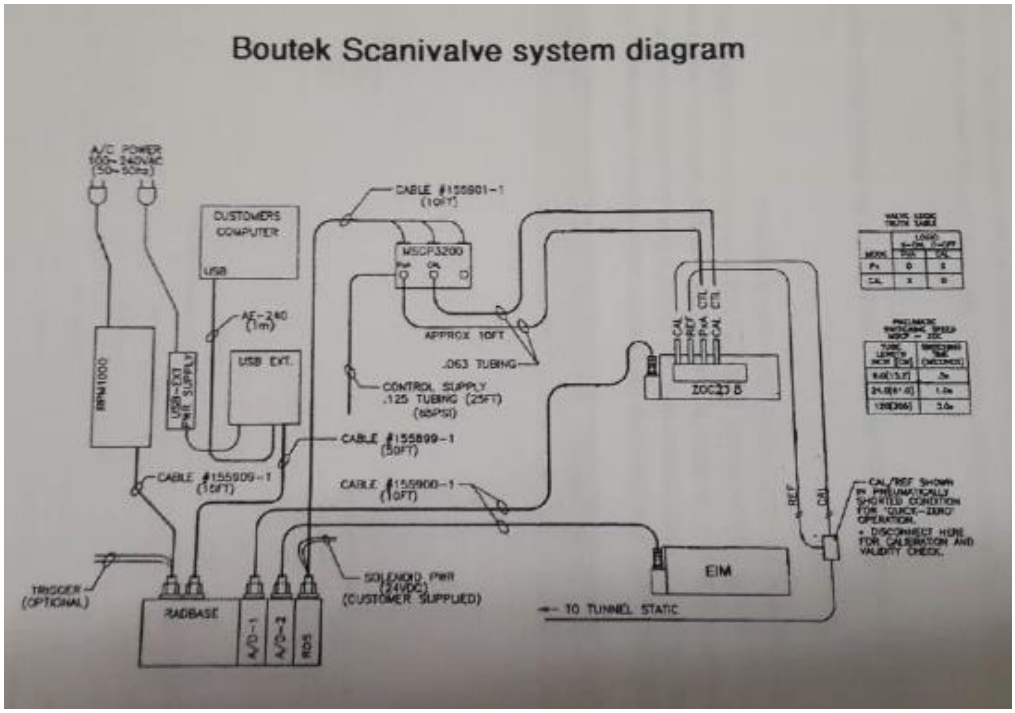


Figure 26: Schematic Diagram of the Rad3200 System (Mistry & Bhayroo, 2014)

The Pitot Static Tube was placed 750mm above the wind tunnel turn table (see Figure 27). The blockage introduced by the model was approximately 4.2% and 2.2% for the largest cross-section catenary dome with and without a wall respectively. This is below the value of 5% blockage noted in literature (e.g. Stathopoulos & Baniotopoulos, 2007). Therefore, the effect of blockage was considered to be negligible. See Figure 28, which shows a dome model placed on the turn table for testing.



Figure 27: Pitot Static Tube (placed 750mm above the turn table)



Figure 28: Dome model placed on turn table for testing

3.2 BOUNDARY LAYER SIMULATION

The wind tunnel was modified to simulate an “open terrain” boundary layer profile, as specified according to literature (Davenport A G, 2000). At the start of the wind tunnel there is a honeycomb structure to create the initial small scale turbulence. This is then followed by four 100x250mm (WxH) spires and a tripping wall 50mm high to create a wind speed deficit near the floor of the wind tunnel. The remaining portion of the wind tunnel floor leading up to the test model is called the “fetch”, and is covered with 2.5mm high corrugated cardboard to allow for an open country terrain wind profile to be generated. The 16m fetch including the corrugated cardboard can be seen in Figure 29.



Figure 29: Corrugated Cardboard within 16m Fetch for Boundary Layer Simulation

3.3 SURFACE PRESSURE, MEASUREMENTS AND CALCULATION

3.3.1 Reference dynamic pressure

External pressure coefficients were normalised by the free-stream dynamic pressure at apex height of the relevant dome model. However, the pitot static tube could not be placed at the peak height of the dome roof, since this would influence the pressure readings. Instead, the pitot static tube was placed 750mm above the wind tunnel floor. Separate wind speed measurements were then taken using a hot-wire anemometer at dome apex height. Consequently, pressures were factored by the free stream pressure at the dome peak height to the free stream pressure measured by the pitot static tube at 750mm, referred to as normalising the free stream dynamic pressure.

3.3.2 Reference static pressure

The static reference pressure was measured from a tap placed on the wind tunnel ceiling. This tap was placed directly above the centre of the turn table, and hence above the models being tested.

3.3.3 Data processing

Mean pressure coefficients were calculated using the following equations:

$$R = \left(\frac{V_{PH}}{V_{RH}}\right)^2 \qquad \text{Eqn. (2)}$$

$$C_p = \frac{R}{N}\sum_{i=1}^{N}\frac{P_i}{P_{Ref}} \qquad \text{Eqn. (3)}$$

Where;

P_i	ith Pressure (at tap positions)
P_{Ref}	Freestream Dynamic Pressure (at the pitot static tube)
N	Number of samples

R	Ratio of the square free stream reference velocities (which will normalise the measured pressures)
V_{RH}	Velocity Measured at the Peak Dome Roof Height
V_{PH}	Velocity Measured at the Pitot Static Tube
C_p	Mean Pressure coefficient

3.4 WIND TUNNEL MODELS

For the most accurate shape, it was decided to make the test specimen with a 3D printer. To print the domes, the following input was required:

- Draw the shape in AutoCAD 2D.
- Export the file to SketchUp and manipulate into a 3D shape with a wall thickness of 3mm (for robustness).
- The drawings are saved in a STL file format using a 'Plug-In' for sketchup, called "sketchup-stl-2.1.6.rbz". (free to download)

These domes were then printed at the CSIR (see Figure 30).

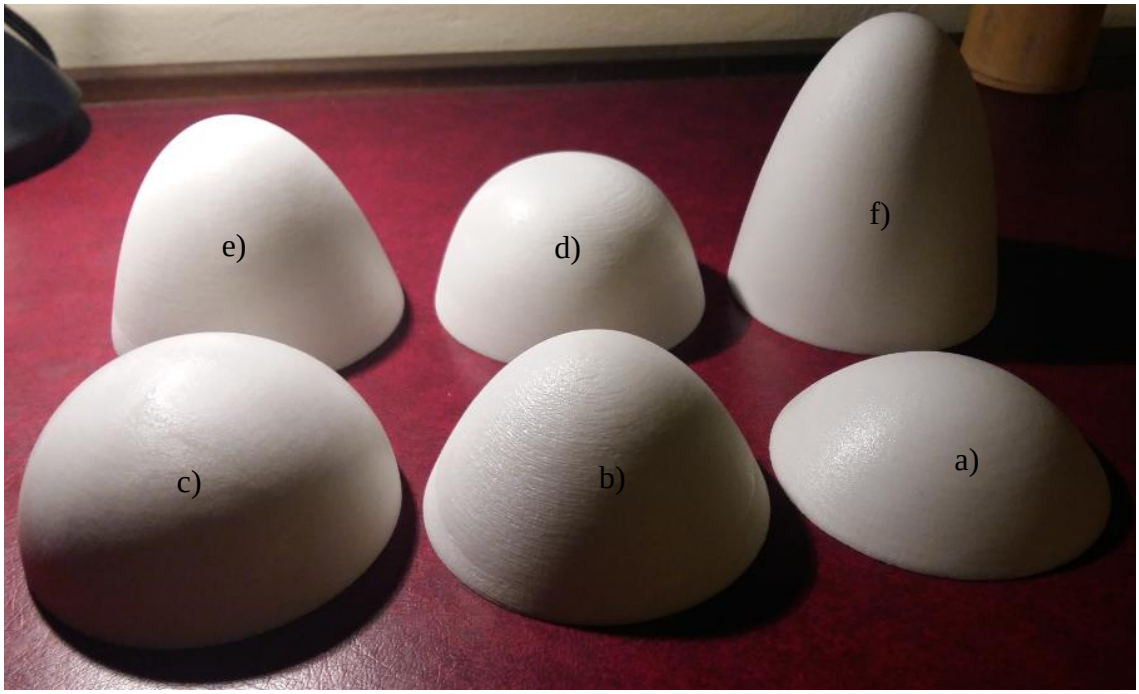


Figure 30: Small 3D Printed Domes

Each dome is described below, according to the labels seen on Figure 30:

a) Catenary H/R = 0.6
b) Catenary H/R = 1.0
c) Dome H/R = 1.0
d) Optimised Catenary H/R = 1.0
e) Catenary H/R = 1.4
f) Catenary H/R = 2.0

The choice of these ratios was as follows. A ratio of 0.6 was chosen as this is when the differences in the catenary dome and circular dome become more pronounced (refer to Section 1.3). A ratio of 1.0 was a clear choice so as to be able to correlate directly to a hemispherical dome, which has vast research data to be able to make reference to. An upper ratio limit of 2.0 was chosen as this was a point determined by the Author who felt that the catenary dome may become unstable, and also unpractical to build. A ratio of 1.4 was then chosen to not only provide data between H/R =1.0 and 2.0, but also to be a linear relationship between the first three domes height to radius ratios (i.e. 0.6, 1.0 and 1.4).

The dimensions of each dome printed can be seen in Table 2 below.

Table 2: Small Dome Dimensions

H/R Ratio	Height/ Radius
0.6	33 / 55
1.0	55 / 55
1.4	77 / 55
2.0	110 / 55

3.5 SIMULATION OF SURFACE ROUGHNESS

A particularly important factor in testing of scale models was to ensure one achieves similitude in the Reynolds number. An ESDU (Engineering Sciences Data Unit) procedure was carried out using an excel spreadsheet programmed by Bradley R.A. (2011), to evaluate the drag coefficients for various roughness's. Three types of

roughness magnitudes, of much greater variation than that assessed by Mistry and Bhayroo (2014) was assessed to see their influence on Reynolds number for catenary domes. Sandpaper was used to determine the roughness characteristics, refer to Figure 31, Figure 32, and Figure 33.

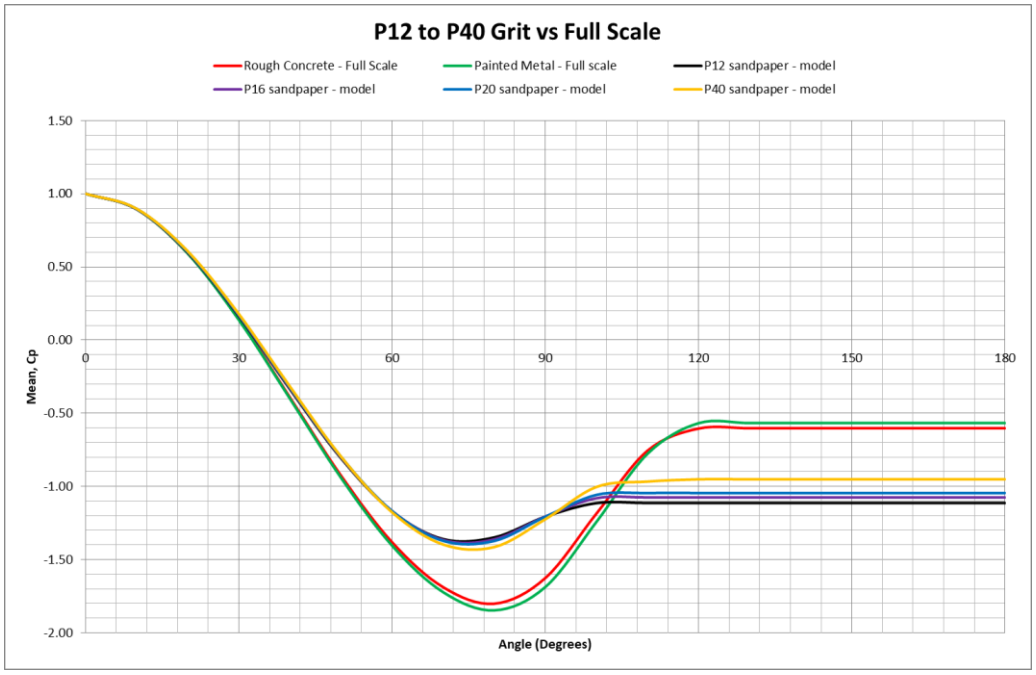


Figure 31: ESDU P12 to P40 Grit Graph

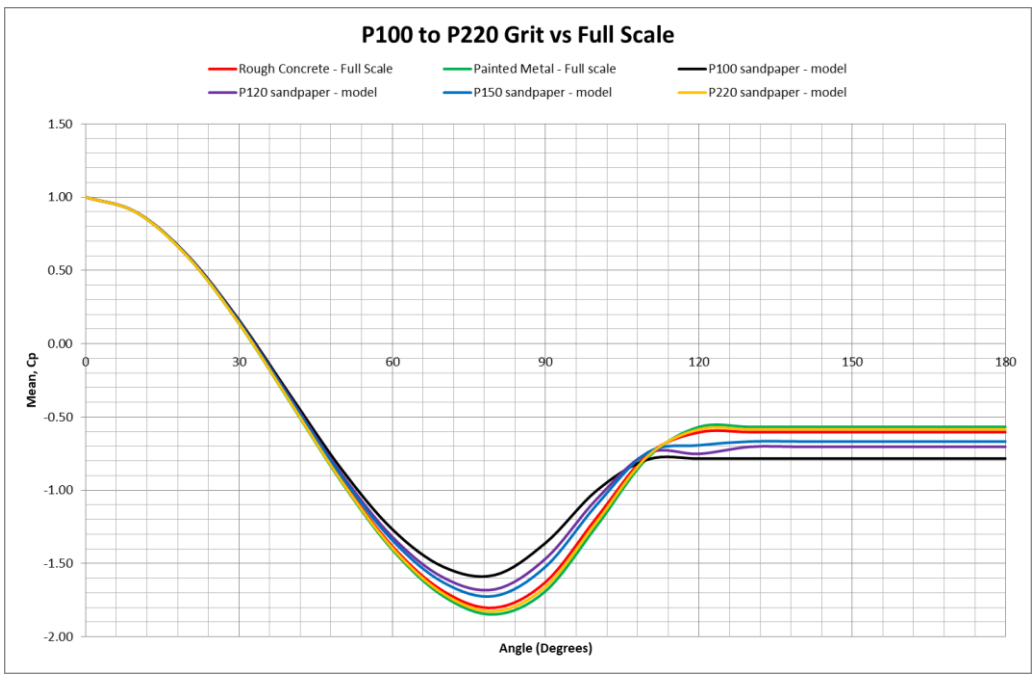


Figure 32: ESDU P100 to P220 Grit Graph

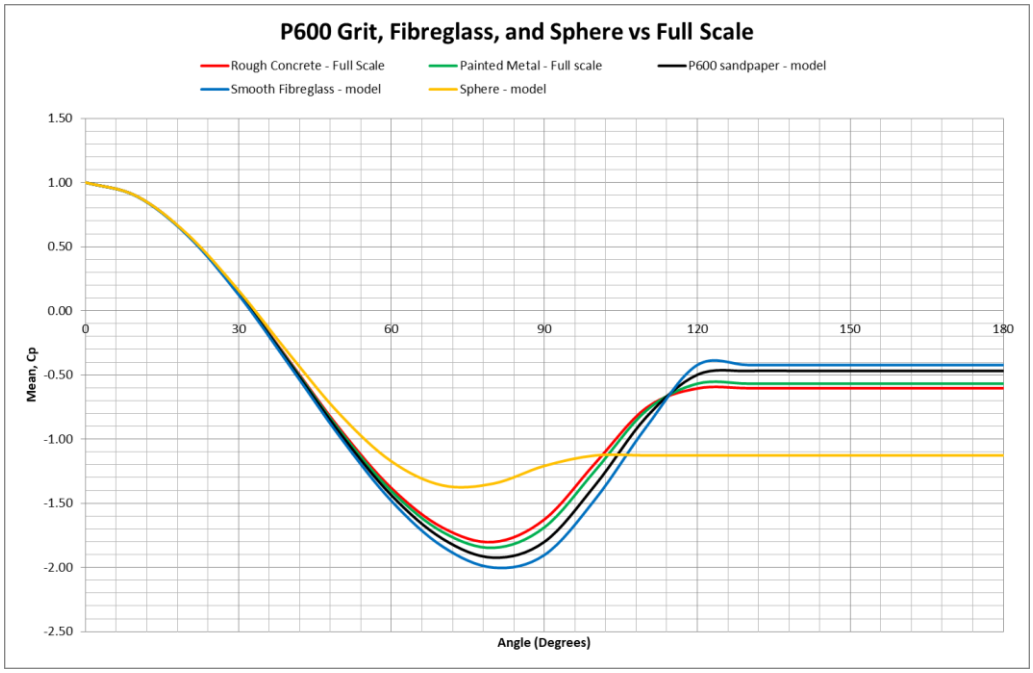


Figure 33: ESDU P600 Grit & Fibreglass Graph

It was determined from Figure 32, that the "P220 grit sandpaper" curve most closely approximated the "rough concrete full scale" curve. Thus, P220 grit sandpaper was to be used to meet the Reynolds number similitude.

Some difficulty was found applying sandpaper to the outer surface of the dome. Grit P150 sandpaper was used, due to having it available over the Grit P220 sandpaper, to test the application method. The ridges created between sandpaper segments were large enough to alter the results (Figure 34 & Figure 35: Applying Sandpaper to Models). Another approach needed to be taken.



Figure 34 & Figure 35: Applying Sandpaper to Models

Gluing sand particles to the outer surface was also attempted (Figure 36), but without success. The surface became too rough.



Figure 36: Glue Sand Particles to 3D Models

The roughness between the printed surface of the 3D domes and the P220 grit sandpaper appeared to be similar (by touch). Therefore, it was decided to keep the 3D printed domes at their current roughness, without any additions. Once analysed, the models roughness would be adjusted, if required.

3.6 WIND SPEED PROFILE

The CSIR Wind Tunnel has various dial settings which each represent different wind speeds. This paper will address the three examined wind speeds for ease of reference as speed conditions (SC) 4.0, 4.4, and 5.0. With an increase in the speed condition, there was an increase in the wind speed the model was being subjected to. Wind profiles were plotted for each, which can be seen in Figure 37. An exponential curve was used to smooth the data for SC 5.0, as there seems to have been an inconsistency during data capturing for this particular speed condition.

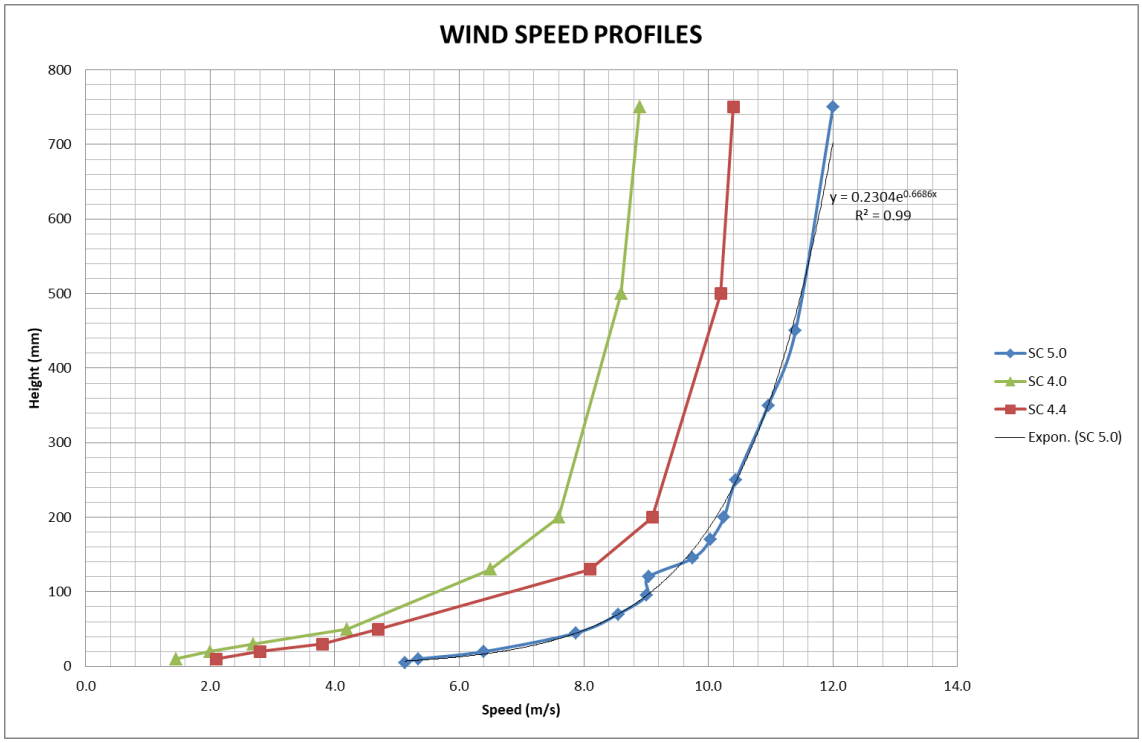


Figure 37: Wind Speed Profiles

For the test specimens with varying H/R ratios, each velocity used for the calculation of the domes mean pressure coefficient, can be read from Table 3. These velocities are read at the apex of the domes and assume a speed condition of 5.0.

Table 3: Small Dome Velocity SC5.0

Small Domes	
h (mm)	SC 5.0 (m/s)
33	7.43
55	8.19
77	8.69
110	9.23

3.7 PRESSURE TAP PLACEMENT

Due to the geometric symmetry of a dome, pressure taps were placed in-line on a single axis. This allows for the measurement of wind pressure data at any orientation required. The locations of the taps are given in Figure 38.

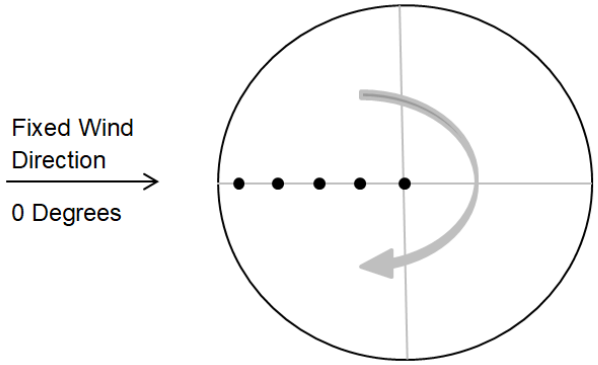


Figure 38: Placement of Pressure Taps on the Models

To identify the number of taps required per dome, Dome 1.0 was divided up into multiple arc lengths by the number of taps (i.e. 5 taps, which was decided to be suitable for measurements). This arc spacing was then matched by either increasing or decreasing the number of taps required per dome, based on the overall arc length to the apex. Table 4 refers to the spacing and number of taps required by each dome.

Table 4: Model Tap Spacing and No. of Taps

Model Type	Arc Length (mm)	1st tap spacing (mm)	# of taps	# of gaps	Tap Arc Spacing (mm)	% diff. to Dome
Dome 1.0	392.70	13	5	4	45.8	-1%
Catenary 0.6	302.35	13	4	3	46.1	-2%
Catenary 1.0	373.95	13	5	4	43.5	4%
Catenary 1.4	457.46	13	6	5	43.1	5%
Catenary 2.0	592.74	13	7	6	47.2	-4%
Opt. Catenary 1.0	394.97	13	5	4	46.1	-2%
Average Tap Arc Spacing (mm)					45.3	

The acceptable range based on the average tap arc spacing was ±5%, which these results fall within. This was seen as being an acceptable range, as it allowed spacing of taps to be defined to ensure all domes were recording wind pressures at a regular arc

length interval. Thus, these taps were placed into the respective models (see Figure 39 for an illustration).

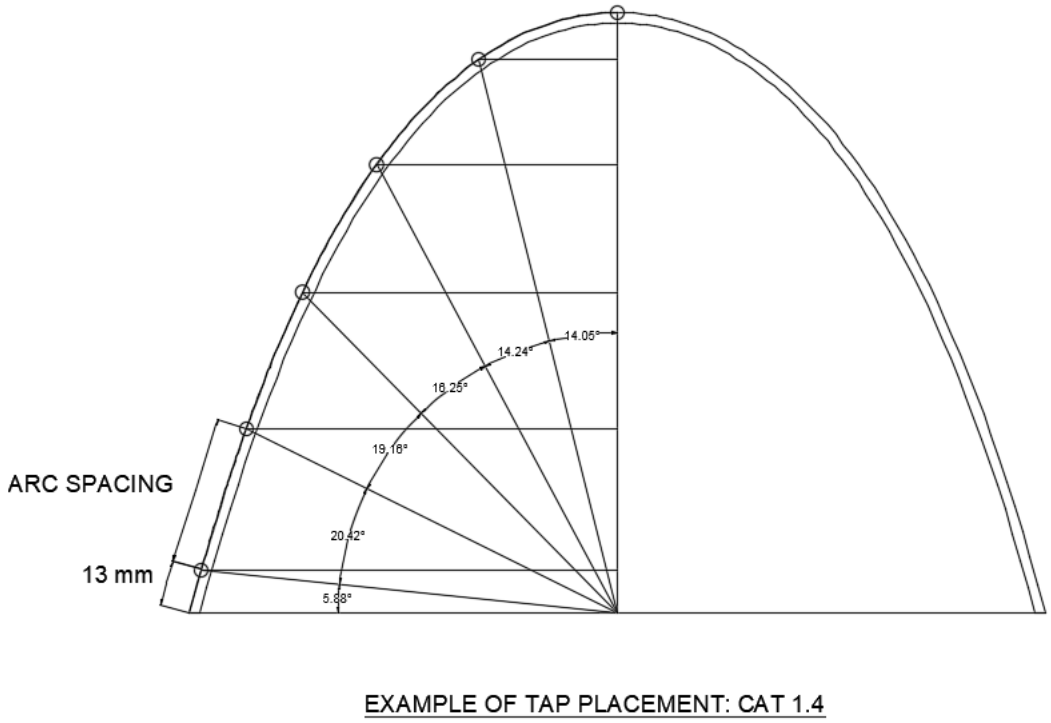


Figure 39: Tap Placement Sketch (Example for CAT 1.4)

A comparison is then made between the designed (i.e. planned) arc lengths and the actual arc lengths measured off the models tested can be seen in Table 5.

The acceptable range was ±5%, which these results fall within. The chosen acceptable range is a practical consideration and determined from scale and constructability limits. For Cat 1.4, the error was seen to be 8%, but this equates to 1mm difference to the planned arc length. Hence, tap spacing was deemed acceptable.

Table 5: Tap Spacing Error (Design vs. Actual)

Model Type	Comparison	No. of Taps						
		1	2	3	4	5	6	7
Dome 1.0	Design	13	58.8	104.6	150.4	196.2		
	Actual	13	60	106.5	155	201		
	% Error	0%	2%	2%	3%	2%		
Catenary 0.6	Design	13	59.1	105.2	151.3			
	Actual	12.5	58	105	150.0			
	% Error	-4%	-2%	0%	-1%			
Catenary 1.0	Design	13	56.5	100	143.5	187		
	Actual	12.5	58.5	103	148.0	192.5		
	% Error	-4%	4%	3%	3%	3%		
Catenary 1.4	Design	13	56.1	99.2	142.3	185.4	228.5	
	Actual	12	56	100	144.0	189.5	234	
	% Error	-8%	0%	1%	1%	2%	2%	
Catenary 2.0	Design	13	60.2	107.4	154.6	201.8	249	296.2
	Actual	13.3	61	110	158	207	255	303.0
	% Error	2%	1%	2%	2%	3%	2%	2%

3.8 INITIAL TEST RESULTS

3.8.1 Small Size Domes

The first sets of testing were done on the 3D Printed domes, printed with a fine nozzle for accuracy of the shapes. These domes were printed at the CSIR. Each dome had a base diameter of 110mm, with varying height to radius ratios (H/R).

Once the data was captured, the first analysis completed was the comparison of the graph collated by (Taylor, 1991) from several wind-tunnel studies and that of the circular domes test results (see Figure 40). A comparison to the graph collated by (Taylor, 1991) indicates if the dome sizes being tested are large enough to create the correct flow characteristics.

A comparison was made between Figure 19 and Figure 40, this showed that the mean pressure coefficient distribution of the small size dome tested corresponds to sub-critical flow. To achieve super-critical flow, either the flow velocity or the dome diameter needed to be increased. The CSIR wind tunnel had a limited wind speed achievable of 22m/s. Thus, it was decided to manufacture larger size domes to achieve super-critical flow, which is what we would see for full-scale structures.

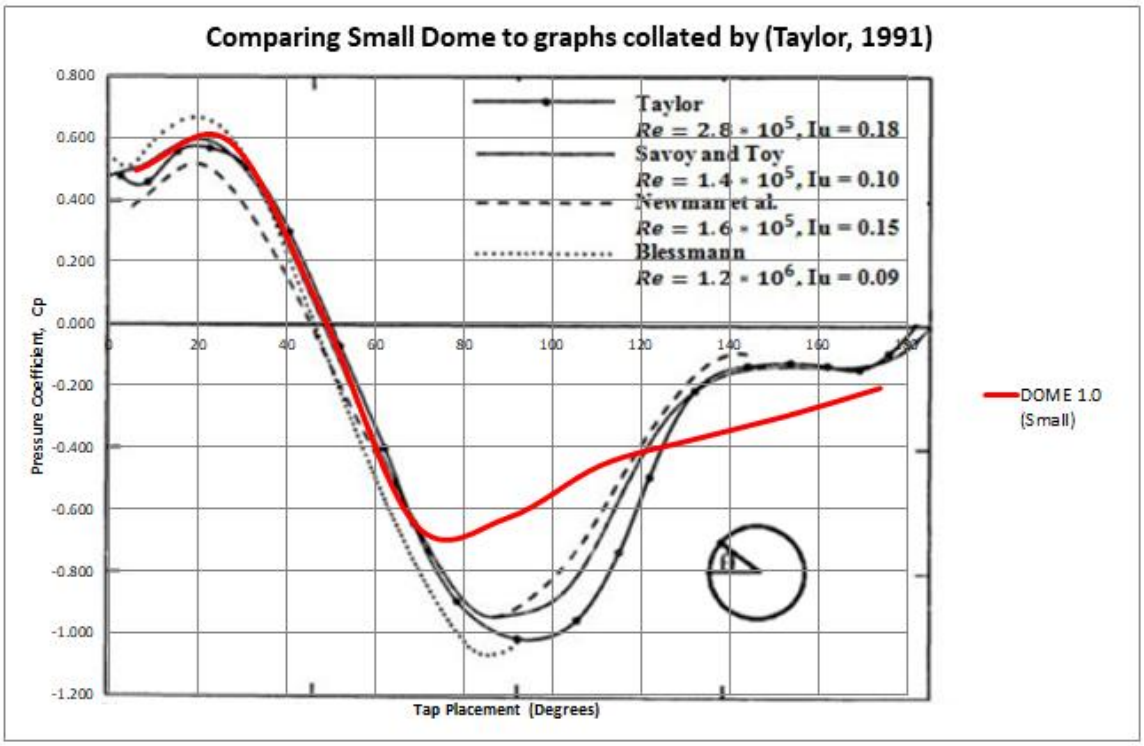


Figure 40: Small Dome Model Comparison to the graph collated by (Taylor, 1991)

While having available data on hand obtained from the small domes, it was decided to assess the accuracy of the geometry and the effect on the pressure readings. Wind directions of 0 & 180 degrees were considered for this comparison, presented in Figure 41.

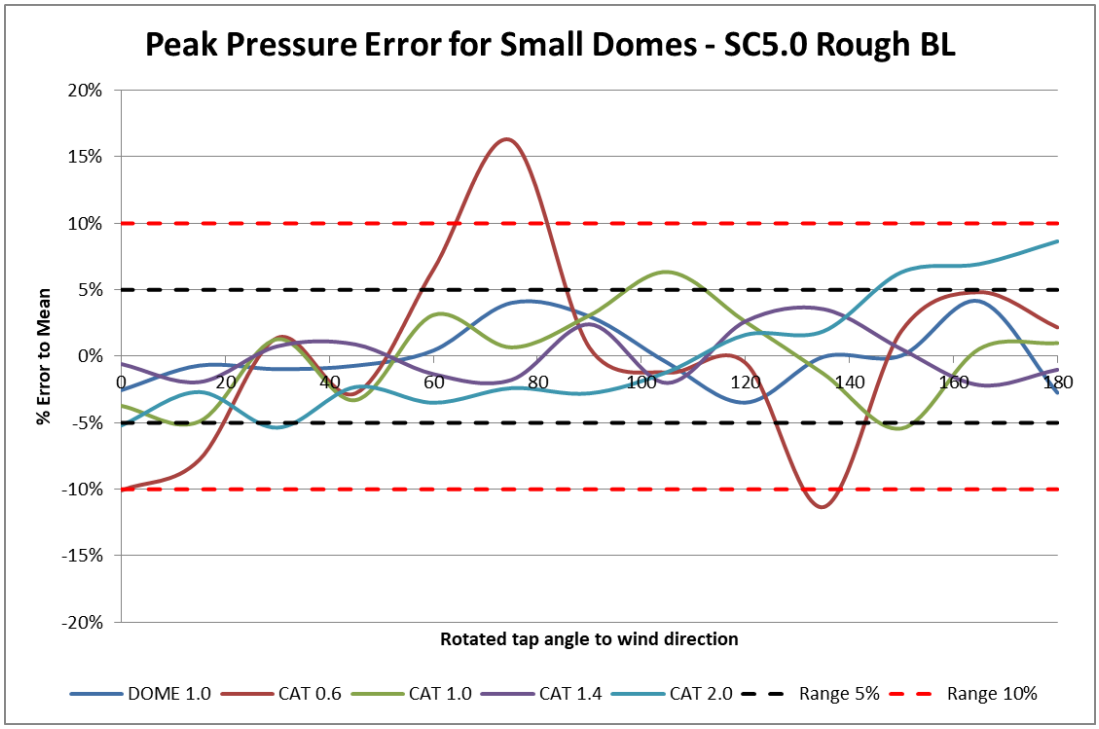


Figure 41: Peak Pressure Error for Small Domes - SC5.0 Rough BL

This graph (Figure 41) was developed using the constant tap position at the domes peak for wind directions 0 to 180 in increments of 15 degrees. The percentage variation to the average pressure coefficient at this tap position was then calculated. Reviewing Figure 41, it was noted that the majority of domes tested fall within an error range of +/- 5%. However, it was also noted that CAT0.6 and CAT2.0 fall outside this error range.

3.8.2 Large Size Domes

New hand-crafted set of domes were manufactured, with a diameter of 250mm (see Figure 42). When comparing these test results to the graph collated by (Taylor, 1991), the larger size dome specimens appear to achieve super-critical flow and correlate well with existing experimental results (Figure 43).



Figure 42: Large 250mm Diameter Hand-crafted Domes

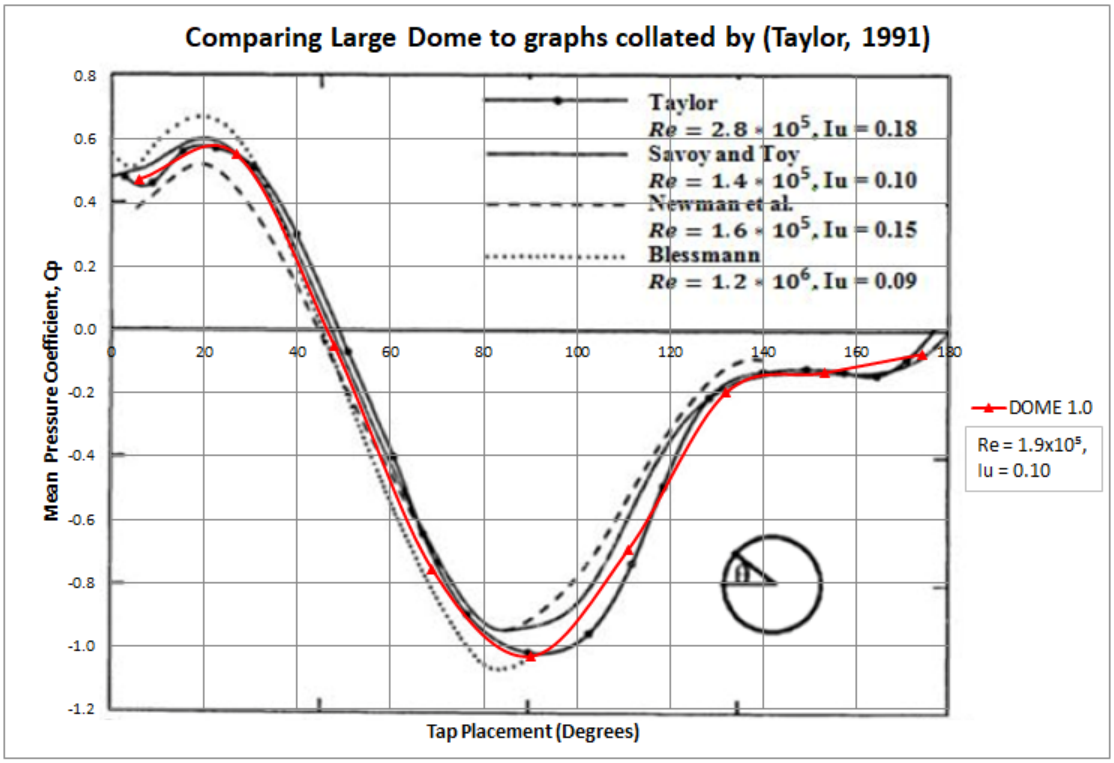


Figure 43: Large Dome Model Comparison to the graph collated by (Taylor, 1991)

The turbulence intensity profile for the circular dome tested is shown in Figure 44. Because larger size domes were required to achieve supercritical flow, the boundary layer scaling was affected and no longer fully representative for a realistic full-scale structure. The characteristics of the CSIR wind-tunnel limited the modelling scale to between 1 to 400 and 1 to 600. Nevertheless, the domes were still examined in a turbulent boundary layer.

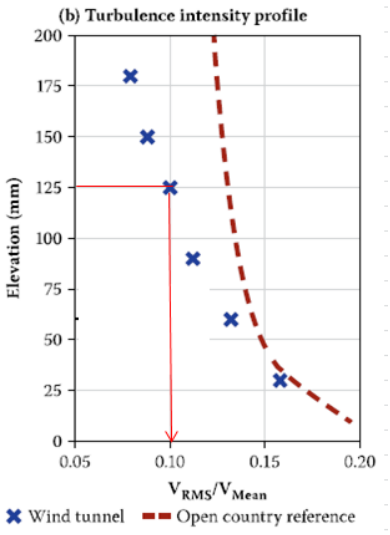


Figure 44: Turbulence Intensity Profile (R A Bradley, 2016)

The respective wind speed velocities at the apex of the models used to analyse data of the larger domes, are based on Table 6 and Table 7.

Table 6: Large Dome Velocity SC4.0, SC4.4, and SC5.0

Large Domes			
h (mm)	SC 4.0 (m/s)	SC 4.4 (m/s)	SC 5.0 (m/s)
75	4.92	5.76	8.65
125	6.36	7.89	9.42
175	7.21	8.74	9.92
250	7.77	9.28	10.44

Table 7: Large Dome Velocity SC4.0, SC4.4, and SC5.0 (with Walls)

Large Domes					
40mm Wall		100mm Wall		160mm Wall	
h (mm)	SC 5.0 (m/s)	h (mm)	SC 5.0 (m/s)	h (mm)	SC 5.0 (m/s)
115	9.29	175	9.92	235	10.36
165	9.83	225	10.30	285	10.65
215	10.23	275	10.60	335	10.89

Testing proceeded on the five larger domes seen in Figure 42. These results were analysed and it was noticed that these domes were displaying a fairly large variance in results. Figure 45 shows these errors with CAT 1.0, CAT 1.4 and CAT 2.0 clearly falling out of the 5% and 10% error ranges.

After an in-depth investigation, it was found that these domes were not symmetrical, but had slight variances in geometry. The domes were then re-shaped for further testing.

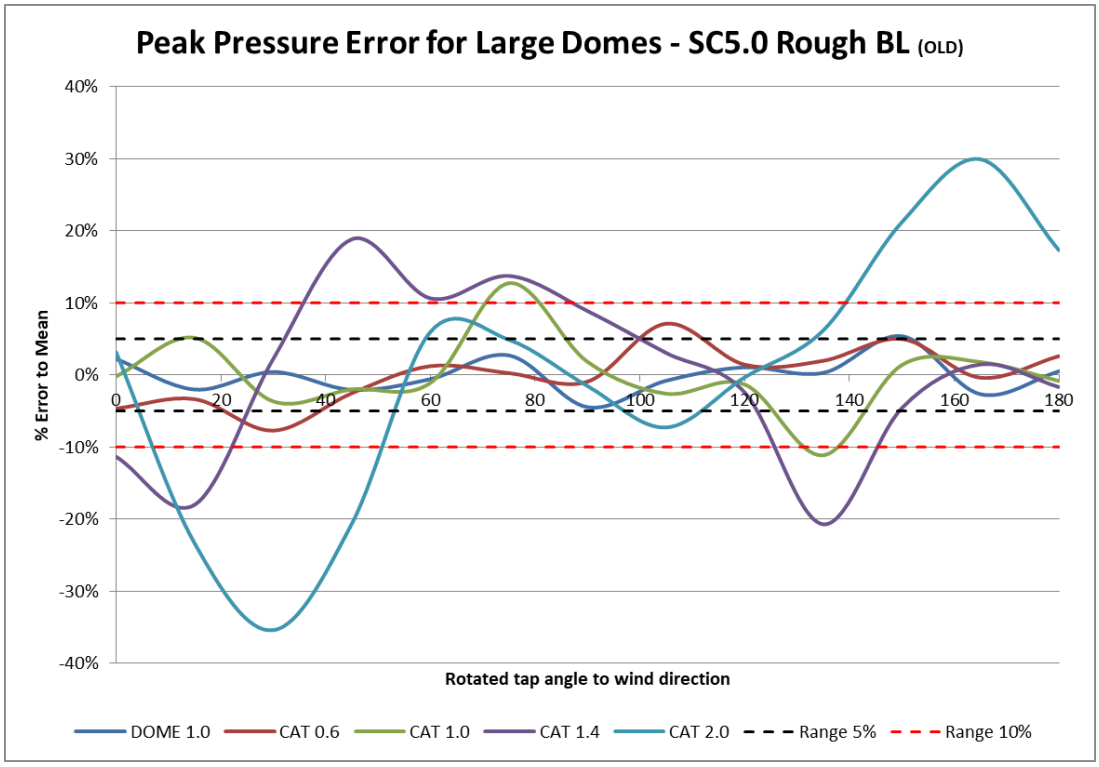


Figure 45: Peak Pressure Error for Large Domes - SC5.0 Rough BL (old)

Final results of tests are found in Section 4 of this report.

3.9 REPEATABILITY OF MEASUREMENTS

To have repeatable measurements is vital for research. Figure 46 and Figure 47 represent tests on different days, on two different models, and the R squared value is indicated to show the repeatability of the tests.

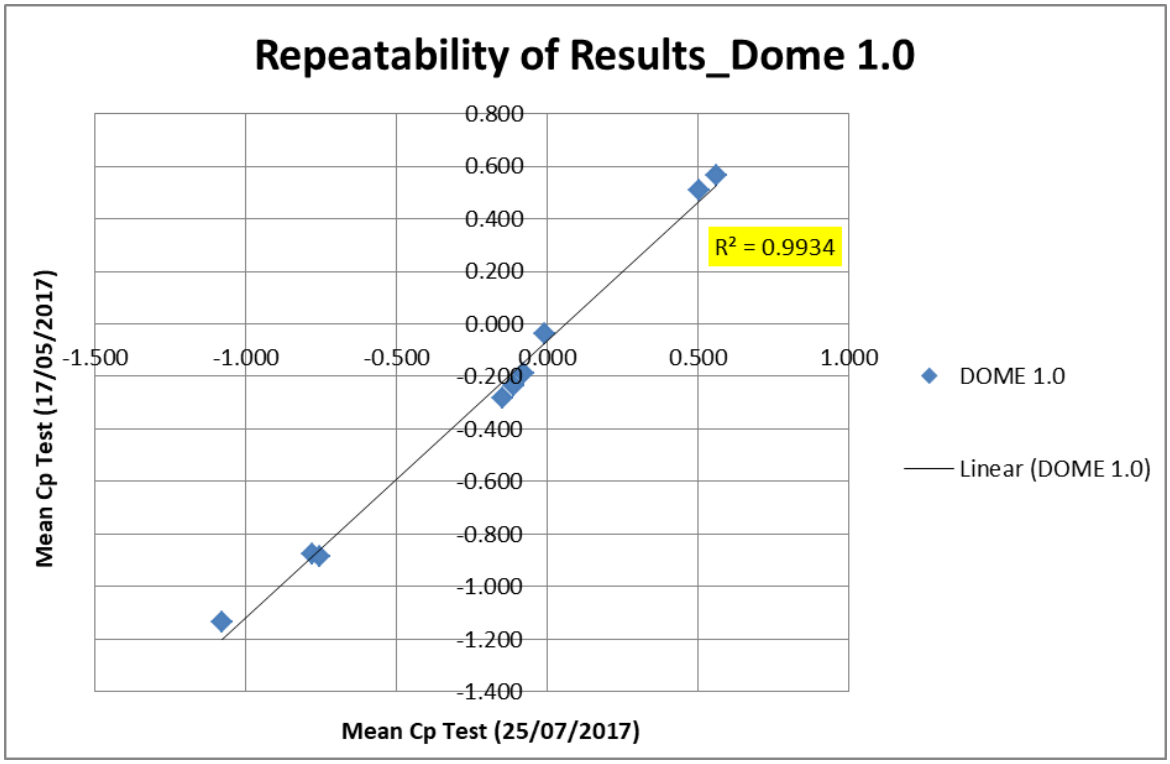


Figure 46: Repeatability of Results - Dome 1.0

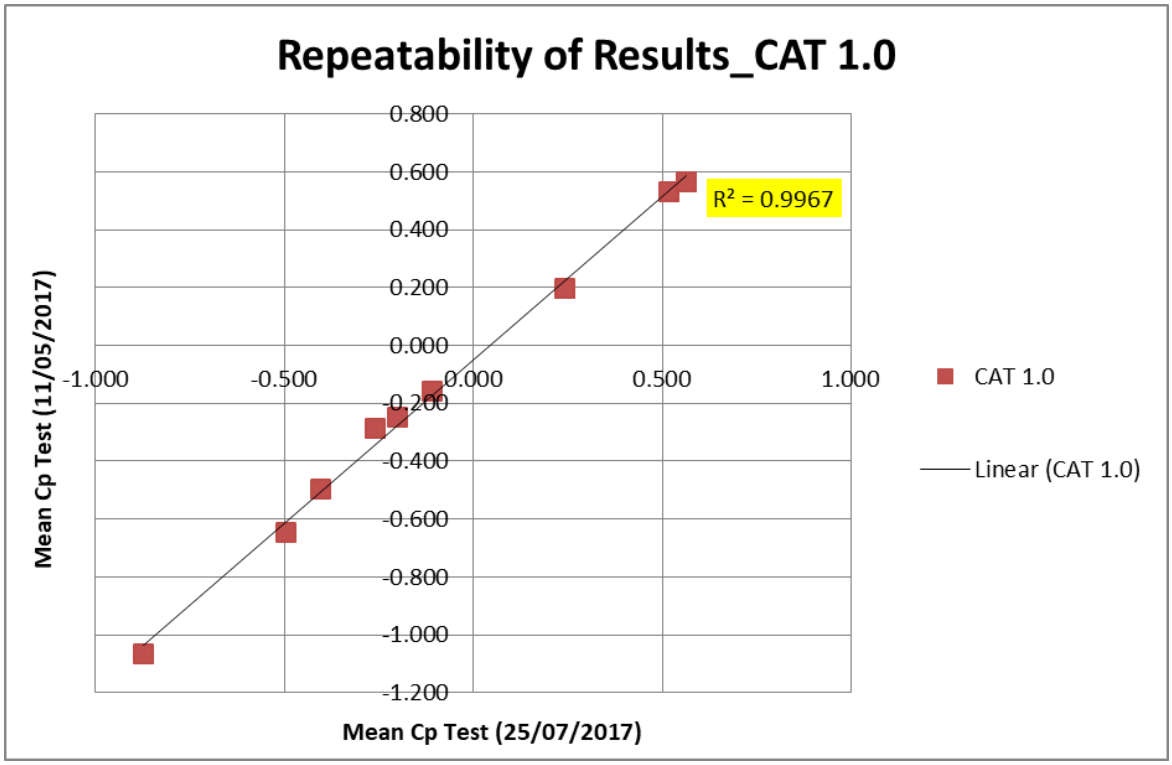


Figure 47: Repeatability of Results - CAT 1.0

These graphs show that the data was repeatable due to the R squared value being approximately equal to 1.0. Therefore, this comparison can be represented by a linear line, and confirms the repeatability of the measurements. The discrepancies could be attributed to variations in weather and temperature at the time of testing.

3.10 SUMMARY OF CHAPTER

The process of how the wind tunnel was setup as well as the apparatus used was discussed. The initial size of the catenary dome models chosen being 110mm in diameter was identified to be too small to achieve the flow characteristics required for testing when compared to previous hemispherical dome research, see Figure 40. Hence, the dome models were increased in size to 250mm in diameter, which then did correlate well to the flow characteristics compared to previous hemispherical dome research, see Figure 43.

4 ANALYSIS AND RESULTS

The main aim of the study was to investigate the effects of:

- Boundary layer;
- Reynolds number;
- Geometry of the domes; and
- The effect of raising these domes on cylindrical walls.

4.1 BOUNDARY LAYER

The larger 250mm diameter circular dome tested in a turbulent boundary layer was similar to the graphs collated by (Taylor, 1991) at speed condition 5.0 (see Figure 48). From the literature (Figure 19) this flow regime was observed to be super-critical, whereas the flow regime for the smaller size dome was seen to be sub-critical.

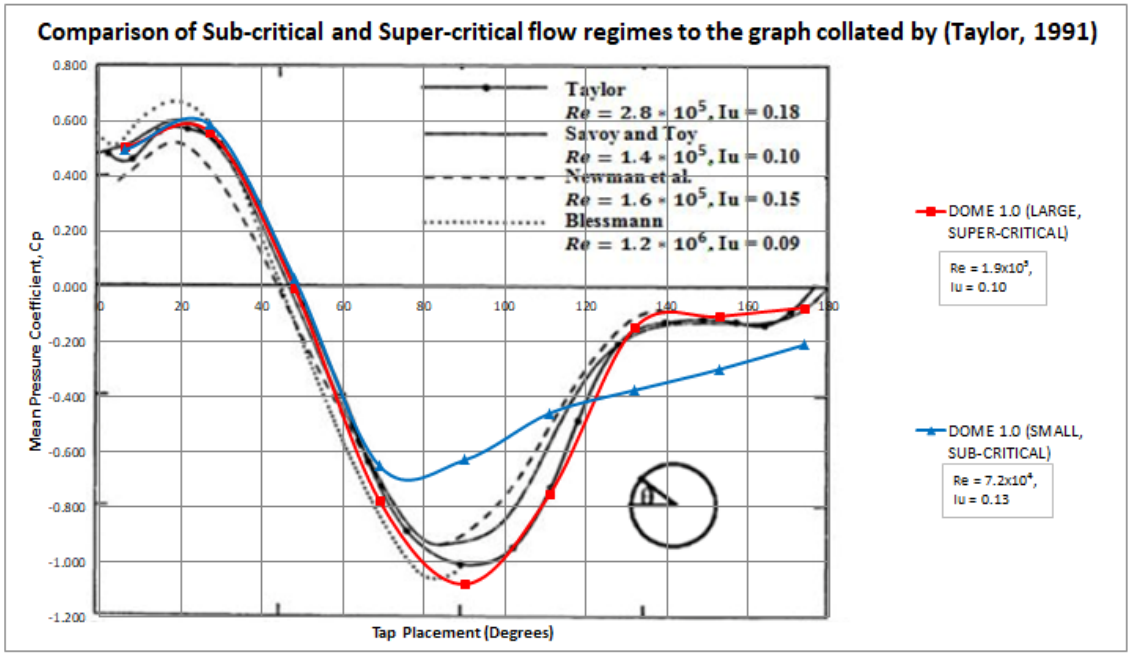


Figure 48: Comparison of Sub-critical and Super-critical flow regimes to the graph collated by (Taylor, 1991)

The error's in data due to smoothening the domes have also been reduced to acceptable ranges, similar to those for the small domes printed with a 3D printer. This is discussed in Section 5.2.

4.2 REYNOLDS NUMBER

During analysis of Reynolds Number, three main variances in the wind speed setting were adjusted. These are;

- SC5.0 Rough Boundary Layer,
  - Re = 1.9 x 10^5 for Large Domes and Re = 7.2 x 10^4 for Small Domes
- SC4.4 Rough Boundary Layer, Re = 1.6 x 10^5 (Large Domes)
- SC4.0 Rough Boundary Layer, Re = 1.3 x 10^5 (Large Domes)

The graphs in Figure 49 and Figure 50 show the corresponding Circular Dome (H/R = 1.0) pressure coefficients and the Catenary Dome (H/R = 1.0) pressure coefficients at varying Reynolds numbers.

$$Reynolds\ number, R_e = \frac{\rho v D}{\mu}$$

Where;

R_e	Reynolds number
ρ	Density of fluid (i.e. Air = 1.205 kg/m^3 @ 20℃)
v	Velocity of the fluid w.r.t. the model (m/s)
D	Diameter of the model (m)
μ	Kinematic viscosity = 1.511×10^{-5} m^2/s @ 20℃

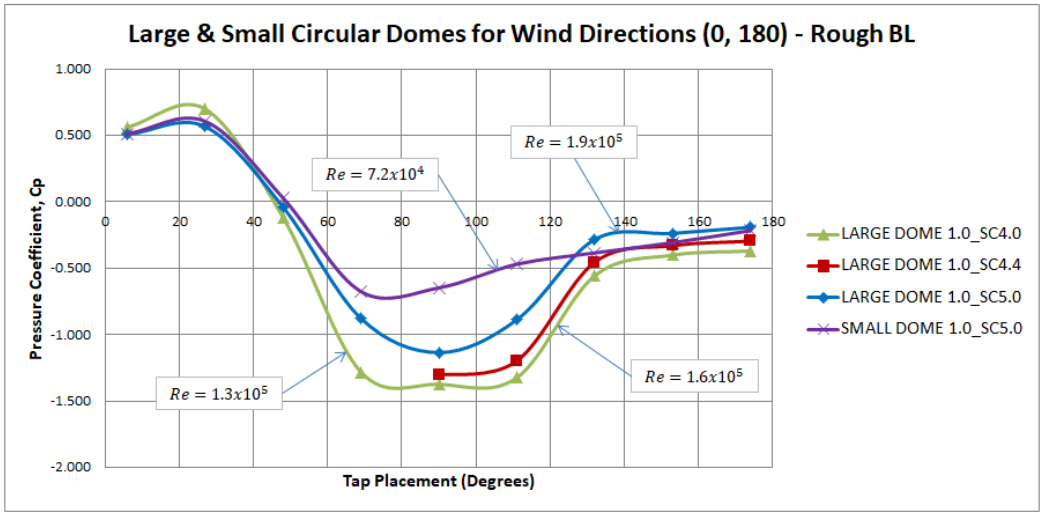


Figure 49: Large & Small Circular Domes (Rough BL) - Reynolds Number

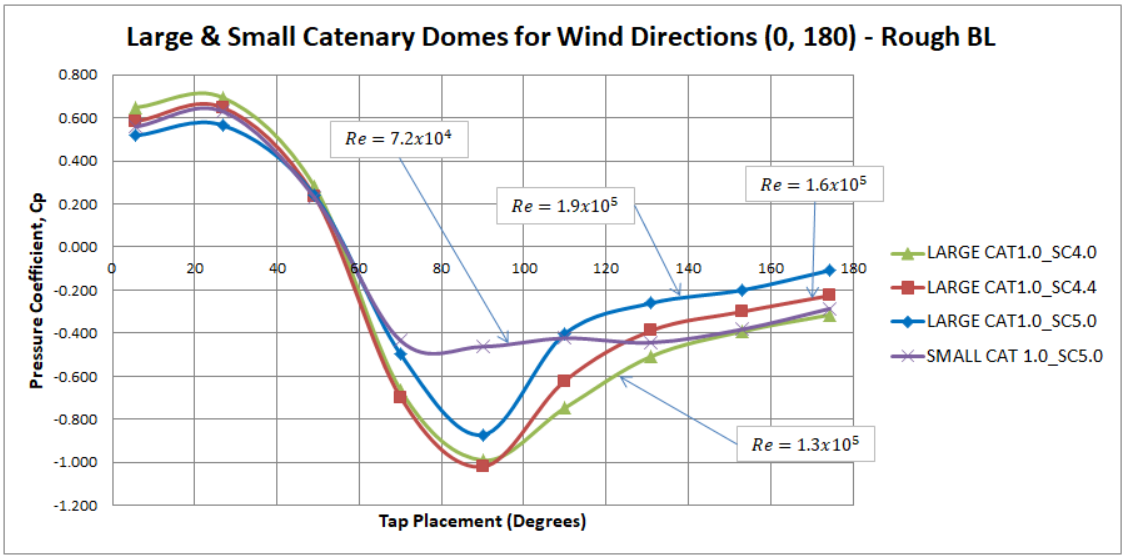


Figure 50: Large & Small Catenary Domes (Rough BL) - Reynolds Number

There was missing data in Figure 49 for the Circular Dome 1.0 at a wind direction of 0 degrees and at a speed condition (SC) of 4.4. Even though the data was misplaced for the 0 degree angle, it was decided to plot the 180 degree angle, as this shows that the Circular Dome 1.0 pressure curve follows the same trend as seen with the plots for SC4.0 and SC5.0. This will be explained further in Section 5.

It was observed that the data presented in Figure 49 and Figure 50 was unexpected and in contrast to the results from other wind-tunnel studies on curved roof structures. It was expected that the peak positive and negative pressure coefficients would increase with increased wind speed (i.e. increased Reynolds Number). However, from the output data the opposite was observed. The Author looked into this, but a reason for this could not be identified in this study.

4.3 THE INFLUENCE OF GEOMETRY

During analysis, each catenary dome was tested to see the effect of different H/R ratios. The catenary domes tested are depicted in Figure 51. Dome 1.0 was included to compare to CAT 1.0, and more importantly to ensure the results were in-line with previous hemispherical/circular dome research conducted.

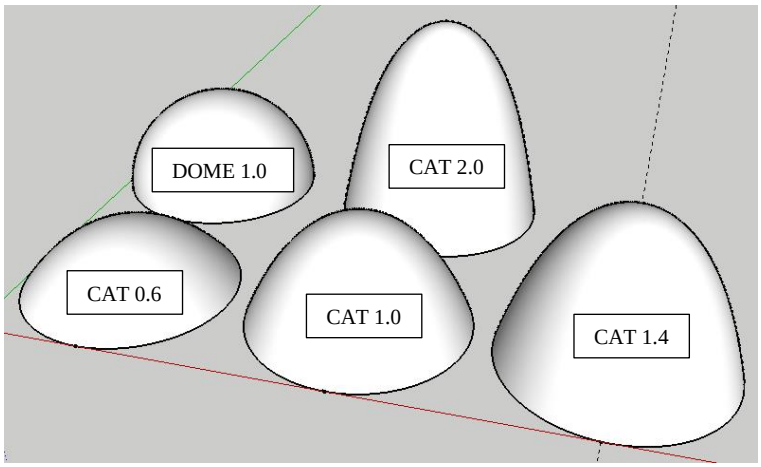


Figure 51: Dome Models Tested (Geometry)

All of the results were combined into a single graph (Figure 52). This graph only shows the pressure coefficients on the domes at 0 and 180 degrees.

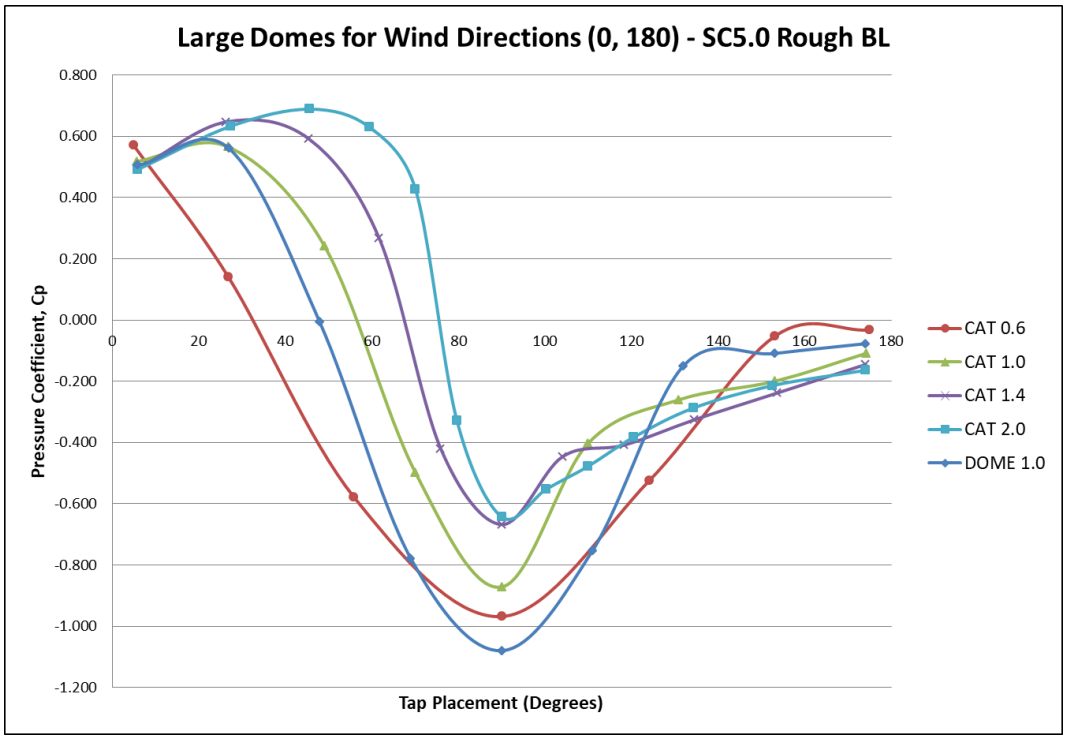


Figure 52: Effect of Geometry on Large Domes, Rough BL, SC5.0

In order to visualise the pressure distribution on the 3D models, it was decided to plot pressure coefficient contours, which can be seen in Figure 53 to Figure 57 below. These pressure plots were generated in MATLAB from the test data for the full 360 degree rotation, in 15 degree increments.

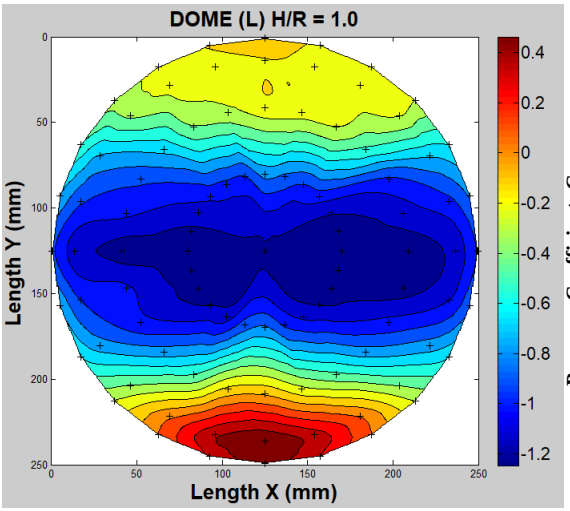


Figure 53: 3D Pressure Contour, Dome (L) 1.0

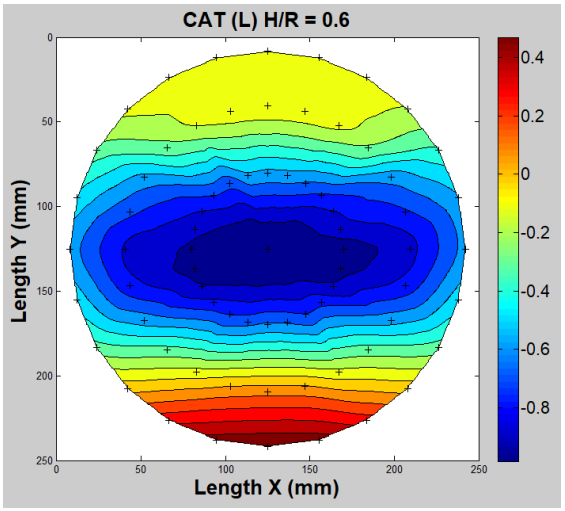


Figure 54: 3D Pressure Contour, CAT (L) 0.6

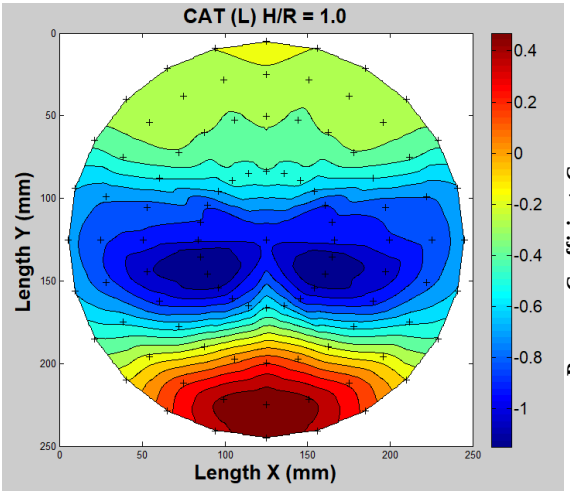


Figure 55: 3D Pressure Contour, CAT (L) 1.0

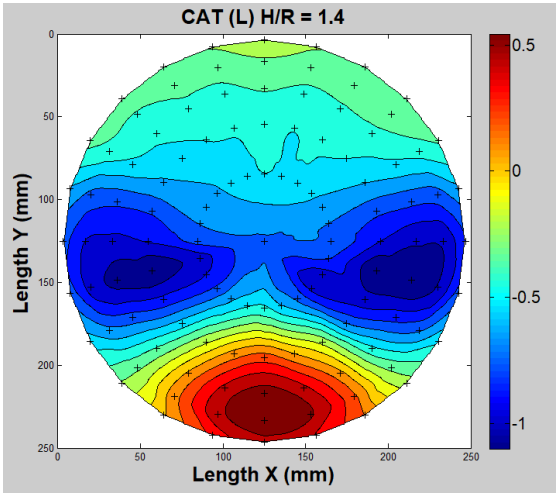


Figure 56: 3D Pressure Contour, CAT (L) 1.4

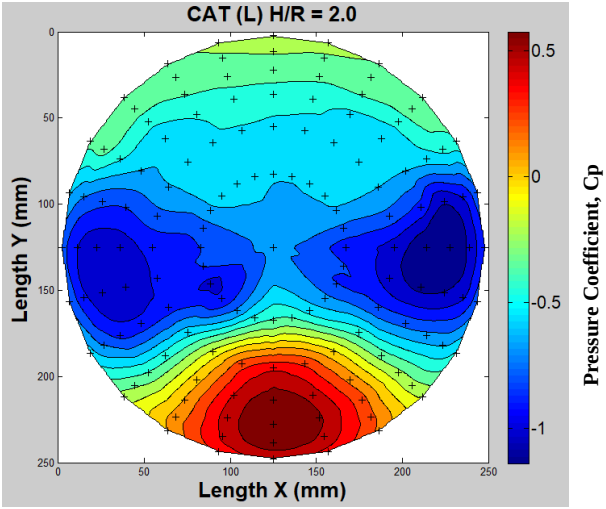


Figure 57: 3D Pressure Contour, CAT (L) 2.0

It was observed that with an increased H/R ratio, the peak negative pressure started to diverge from the catenary domes peak. The peak positive pressure zone started as an elliptical shape (Figure 55) and was tending towards a circular shape as the H/R ratio increased (Figure 57).

4.4 INFLUENCE OF WALLS

Subsequently, the domes were placed on cylindrical walls to elevate them, and hence obtain pressures at different elevations. The wall heights chosen were 40, 100, and 160mm (with a diameter of 250mm, as per the dome models). The joint between the wall and the models base was sealed using masking tape, to create a seamless joint. The CAT 2.0 model was not tested, as this model ratio was seen as being impractical, due to its extreme H/R ratio. The results of the tests are given in Figure 58 to Figure 60.

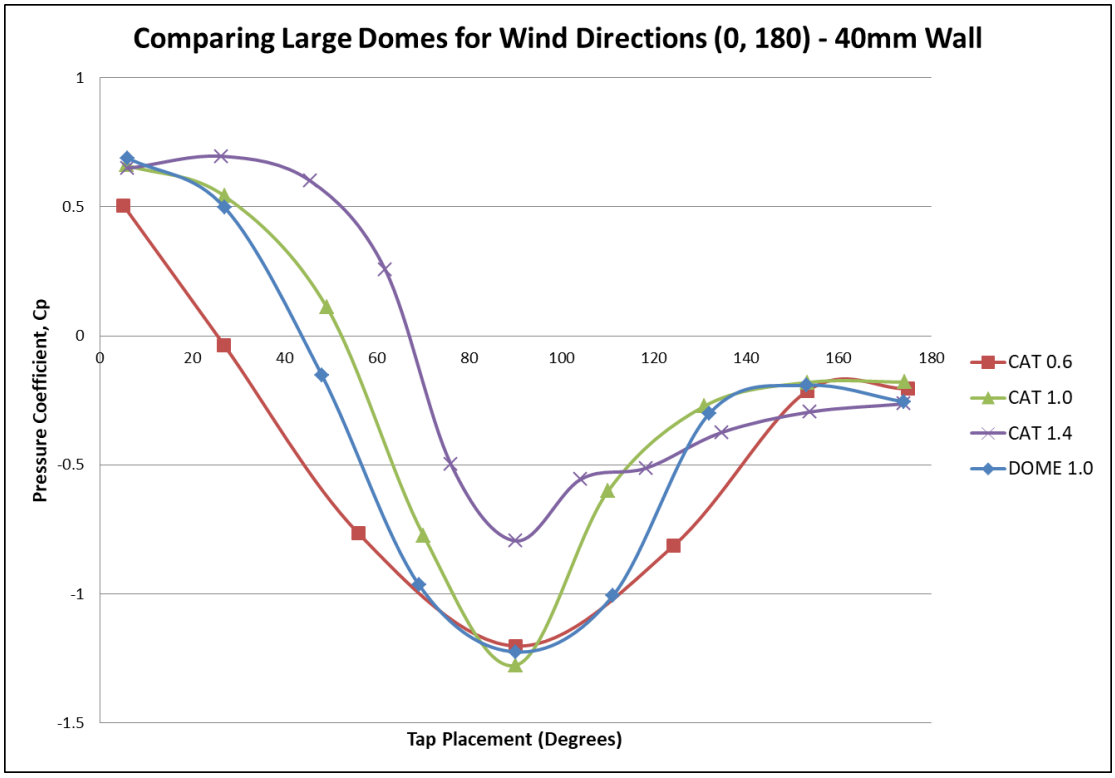


Figure 58: Large Domes on Walls, Rough BL, SC5.0 (40mm Wall)

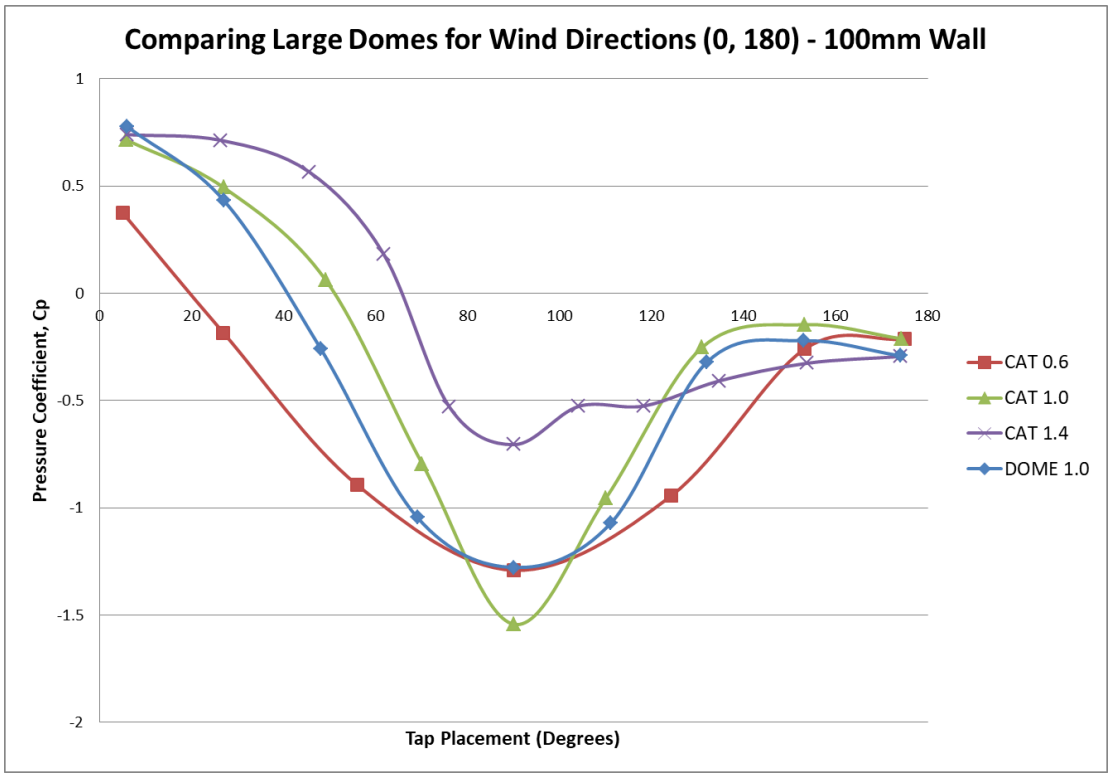


Figure 59: Large Domes on Walls, Rough BL, SC5.0 (100mm Wall)

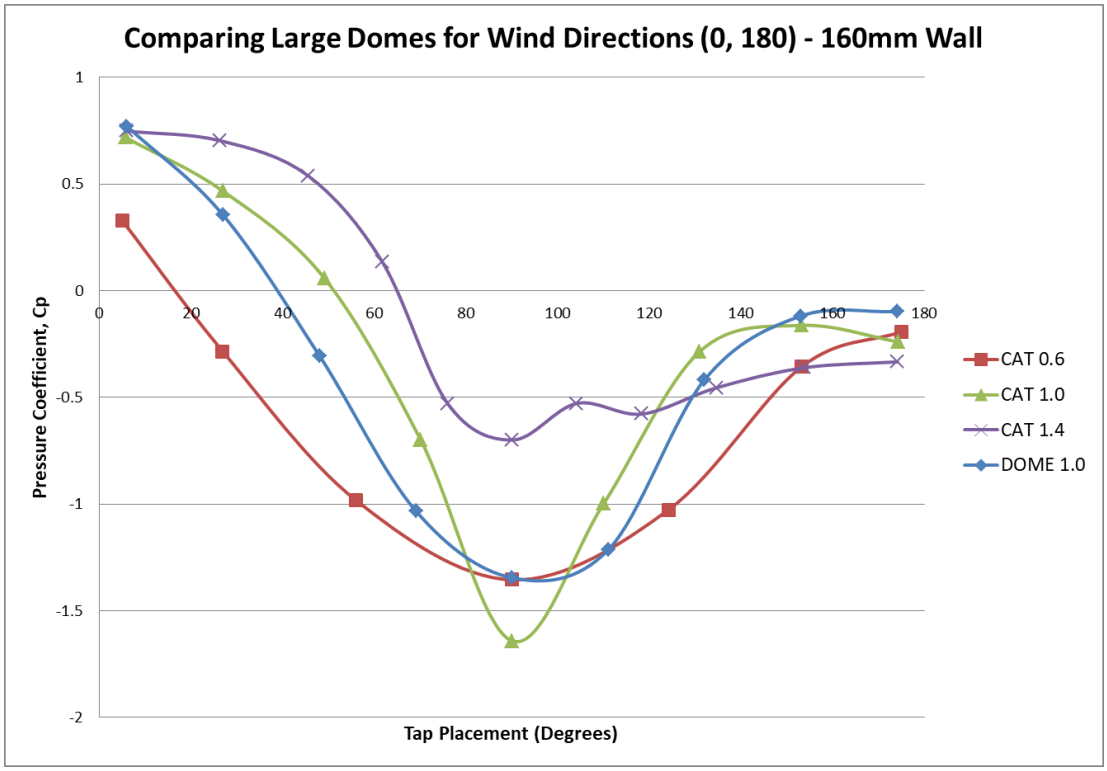


Figure 60: Large Domes on Walls, Rough BL, SC5.0 (160mm Wall)

3D external pressure coefficient (Cpe) plots were also generated (see Figure 61 to Figure 72). However, data for these elevated dome models were only measured in increments of 15 degrees until 180 degrees. Hence, the symmetry of the pressure plots.

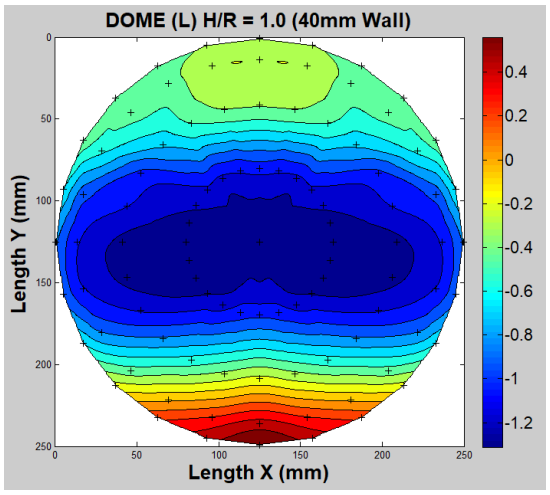


Figure 61: 3D PC, DOME (L) 1.0, (40 Wall)

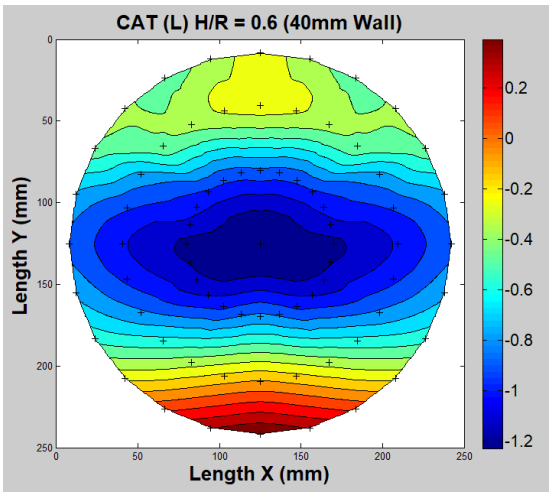


Figure 62: 3D PC, CAT (L) 0.6, (40 Wall)

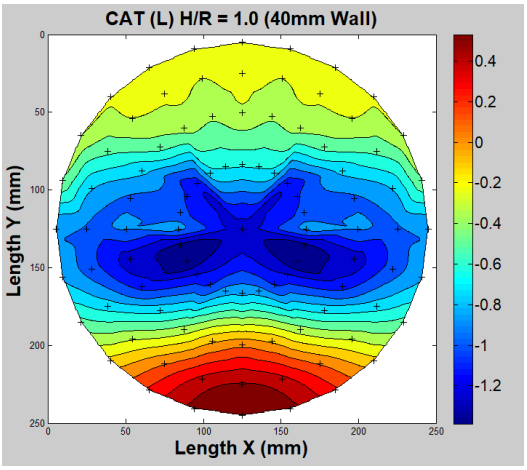


Figure 63: 3D PC, CAT (L) 1.0, (40 Wall)

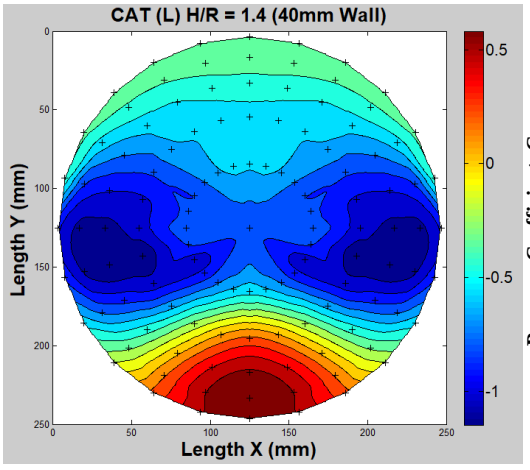


Figure 64: 3D PC, CAT (L) 1.4, (40 Wall)

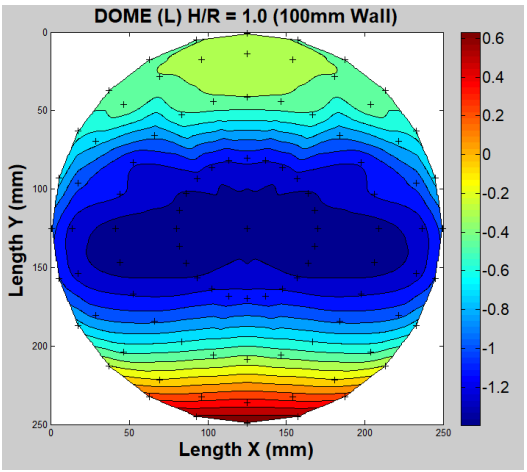


Figure 65: 3D PC, DOME (L) 1.0, (100 Wall)

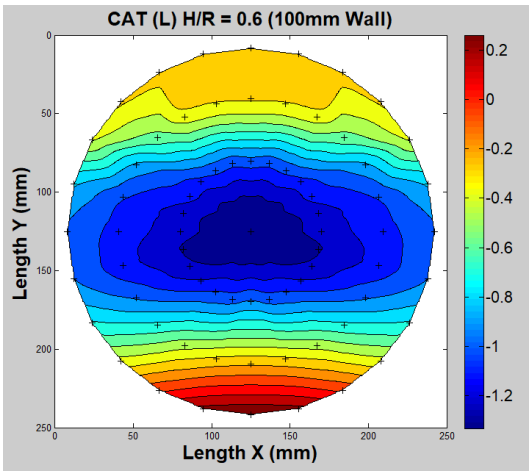


Figure 66: 3D PC, CAT (L) 0.6, (100 Wall)

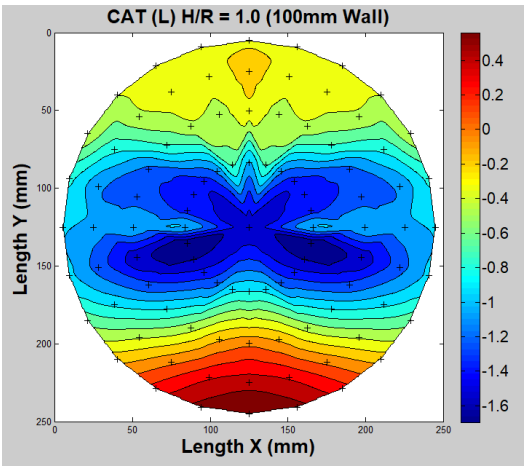


Figure 67: 3D PC, CAT (L) 1.0, (100 Wall)

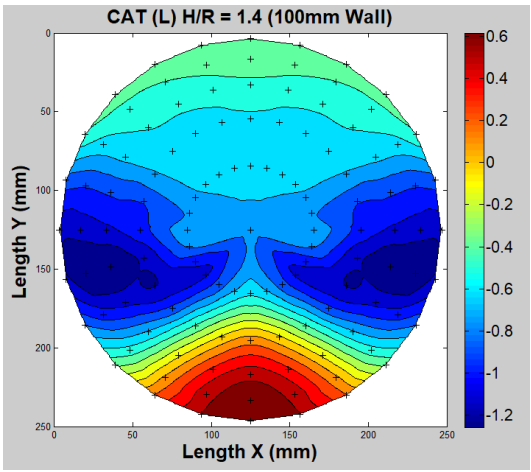


Figure 68: 3D PC, CAT (L) 1.4, (100 Wall)

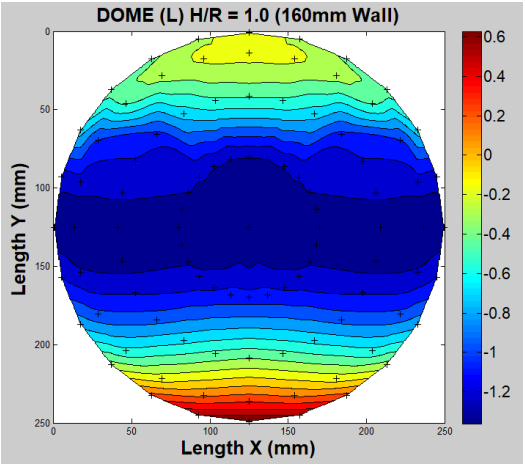


Figure 69: 3D PC, DOME (L) 1.0, (160 Wall)

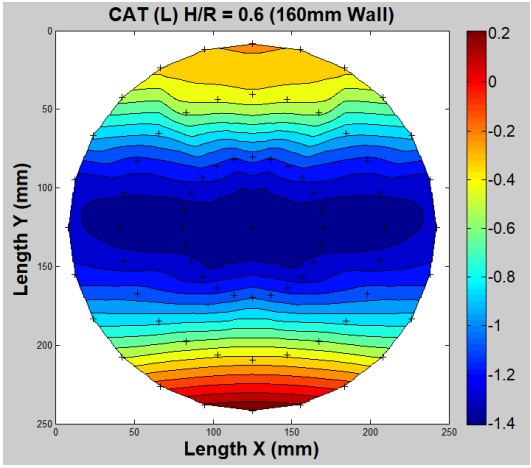


Figure 70: 3D PC, CAT (L) 0.6, (160 Wall)

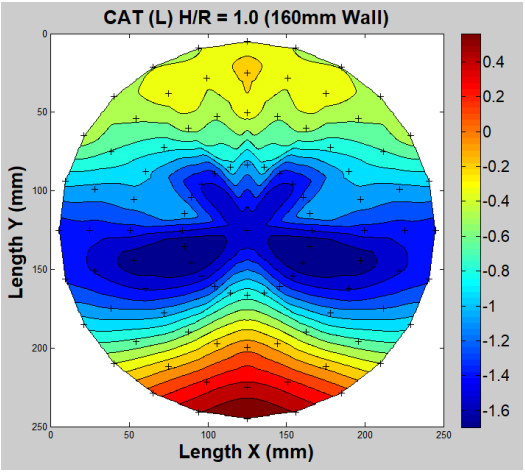


Figure 71: 3D PC, CAT (L) 1.0, (160 Wall)

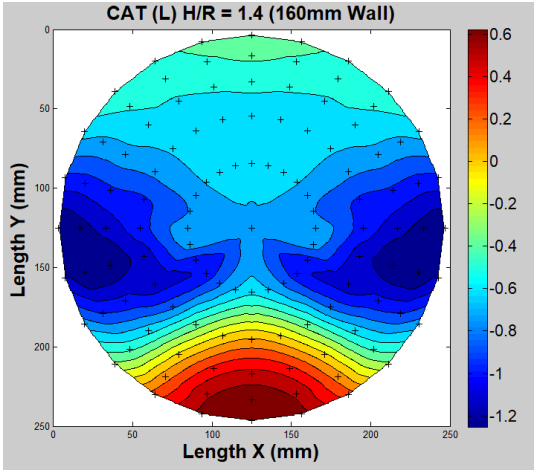


Figure 72: 3D PC, CAT (L) 1.4, (160 Wall)

4.5 SUMMARY OF CHAPTER

The agreement of the flow regime to previous hemispherical domes results provided the basis to proceed with the large size domes for further tests. The results illustrated for Reynolds Number were unexpected. For both cases where the domes were placed on a flat surface or raised on walls, the peak negative pressure started to diverge from the catenary domes peak, as the H/R ratio increased.

5 DISCUSSION

The purpose of this Chapter is to discuss the results of the tests performed and presented in Section 4, focusing on:

- Boundary layer and Reynolds number;
- The influence of geometry; and
- The effect of raising these domes on cylindrical walls of varying heights.

5.1 BOUNDARY LAYER AND REYNOLDS NUMBER

5.1.1 Overview

It is important to ensure that the set of results can be repeatable and justified as being true and correct. It was shown in Section 3.9 the results are repeatable. However, it must be noted that the boundary layer scaling is not representative of full-scale structures, as the physical characteristics of the wind-tunnel limited the modelling scale to between 1 to 400 and 1 to 600. The small domes model scale was 1:545, which falls within this acceptable range. On the other hand as explained in Section 3.7, larger size domes were required in order to achieve supercritical flow regime. These large domes had a model scale of 1:240, which does not fall within the acceptable range. This constitutes the limitation of the study.

5.1.2 Influence of Geometrical Size

It is necessary to assess how varying the domes dimensions (i.e. the Reynolds Number) will affect the pressure distribution over the domes.

Figure 48 shows comparisons of the Circular Dome of H/R = 1.0, both large and small scale tested during this research, to the results from previously conducted research (Taylor, 1991). The flow generated by the small domes of 110mm in diameter was sub-critical and the results differed from previous research by (Taylor, 1991), etc.

On the other hand, when testing the large domes of 250mm diameter, this created a super-critical flow regime which closely matched the research data on Circular Domes. This agreement with the data confirms the Reynolds Number is representative for real life size domes, and further testing of catenary domes could proceed.

5.1.3 Influence of Wind Speed

In this section the influence of varying the wind speed (i.e. the Reynolds Number) was done in order to determine the effect this has on the pressure distribution over the domes. This was to determine the sensitivity of the different domes wind pressure distribution to a varying Reynolds number. The large size domes were only tested for this section.

This set of testing was restricted to the circular dome (DOME 1.0) and a catenary dome (CAT 1.0). Figure 73 combines the graphs from Figure 49 and Figure 50 into a single graph for ease of reference.

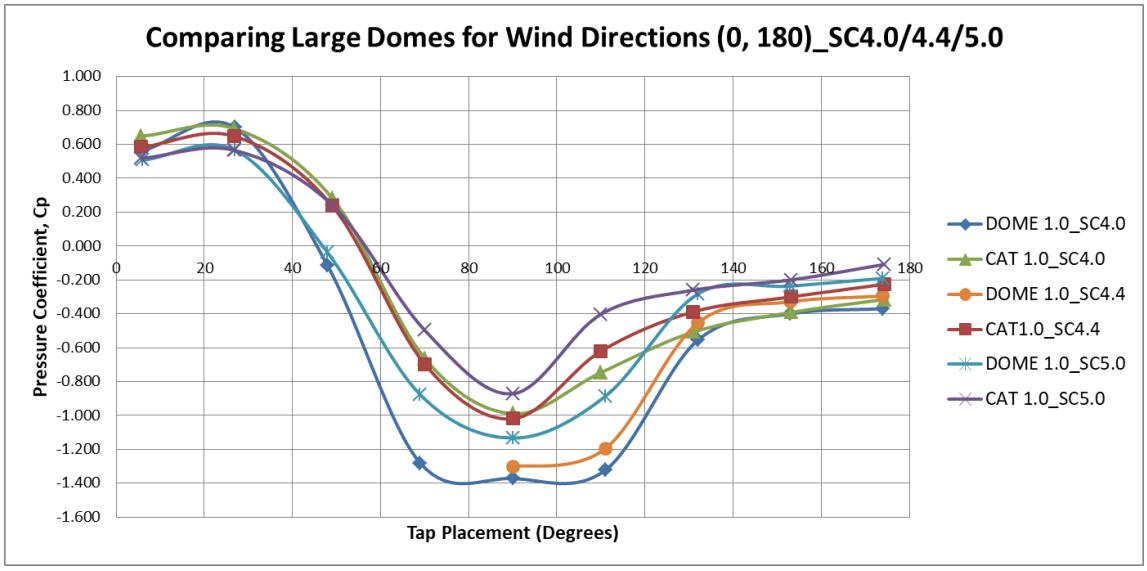


Figure 73: Rough BL, Large, SC4.0/4.4/5.0 (Combined)

In Figure 49, the circular domes (H/R = 1.0) have an almost equal positive pressure coefficient generated at zero degrees, which peaks at around 22 degrees. The domes positive pressure gradient is sharper than that of the catenary domes, and crosses into the negative pressure zone at around 47 degrees. The maximum negative pressure

coefficient for the circular domes occurs at 90 degrees, as expected. The pressures then remain negative and decrease until the pressure graphs tend to plateau at a constant pressure coefficient, at approximately 140 to 180 degrees. This is due to flow separation.

In Figure 50, the catenary domes (H/R = 1.0) tend to have a linear variance in the positive pressure generated at zero degrees, which peaks at around 22 degrees. The catenary domes positive pressure gradient is not as steep as the circular domes and crosses into the negative pressure zone at around 55 degrees. The maximum negative pressure coefficient for the catenary domes occurs at 90 degrees, as expected. The pressures then remain negative and continue to decrease until 180 degrees.

The main observations were:

- The peak positive pressure coefficient occurred at 22 degrees, after which the catenary and dome graphs diverged.
- The peak negative pressure coefficient occurred at 90 degrees, and the circular dome graphs had a greater negative pressure coefficient than the catenary dome graphs. This is discussed further in Section 5.2, which explains that for catenary domes, the peak negative pressure coefficient is only truly represented with a 3D pressure contour graph.
- The circular dome graphs plateaued at 140 degrees, whereas the catenary dome graphs continued to decrease up to 180 degrees.

The Reynolds number is seen to have a significant influence on the pressure distribution and magnitude of pressures coefficients.

5.1.4 Pressure Distribution Discussion

From Figure 73, it is clear to see that varying the Reynold's number has a dramatic effect on the pressure distribution. Interestingly, when reviewing the results in-depth, it

seems that with an increase in the Reynolds number there was a decrease in magnitude of pressure coefficient values (see Table 8).

Table 8: Peak Negative Pressures for Varying Reynolds Numbers

Speed Condition (SC)	Dome 1.0	CAT 1.0
4.0	-1.37	-0.99
4.4	-1.30	-1.02
5.0	-1.13	-0.87

These results are in conflict with circular dome literature and further testing would be required to determine the cause. This was not carried out in this study.

5.2 THE INFLUENCE OF GEOMETRY

All dome results were plotted from 0 to 180 degree angles, see Figure 52 for an example. Taps were placed away from the edge of the models base, thus the actual reading for the CAT 1.0 graph would start at 6 degrees and end at 174 degrees, as an example (see Figure 74). This varies slightly per dome, and was approximated to 0 and 180 degrees. Figure 52 shows that the initial positive pressure coefficients increased with increase in catenary dome height. With an increase in height, it was also determined that the peak positive pressure coefficient shifted higher up the dome face (i.e. away from the base of the dome). This makes the gradient of the line from positive peak pressure coefficient to negative peak pressure coefficient increasingly steep.

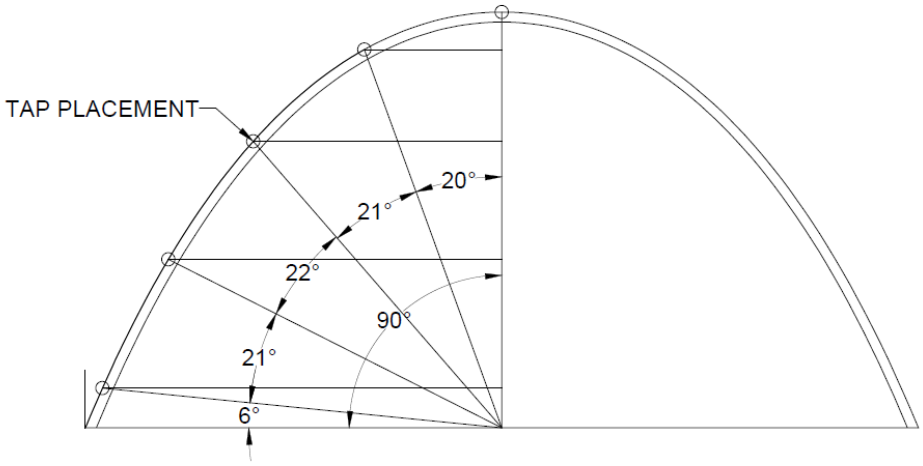


Figure 74: Example of Taps Spaced at Varies Degrees (0 to 180)

It was observed from Figure 52, that the pressure decreased at the catenary dome peak (i.e. 90 degree tap) with an increase in the catenary aspect ratio (H/R). This initially seemed strange, as it would naturally seem that with increased aspect ratio there would also be an increase in the negative peak pressure coefficient at the catenary dome roof.

This was only made clear once the 3D pressure contours were generated. Looking at each dome aspect ratio, the following was determined:

- From Figure 54, the CAT 0.6 model still had the maximum negative peak pressure coefficient at the highest point of the dome (i.e. dome apex).
- From Figure 55, the CAT 1.0 models negative peak pressure coefficients were seen to be starting to diverge from the peak. The maximum negative pressure

coefficient was now located near the 4th tap position at approximately 70 degrees (total taps = 5). From Figure 53, the results of DOME 1.0 seem to fall between the CAT 0.6 and CAT 1.0 models. The flow was starting to diverge.

- From Figure 56, the CAT 1.4 models negative peak pressure coefficients were moderately divergent. The maximum negative pressure coefficient was now located near the 3rd and 4th tap position at approximately 50 degrees (total taps = 6).
- From Figure 57, the CAT 2.0 models negative peak pressure coefficients were highly divergent, to the point of being very low near the base of the test model. The maximum negative pressure coefficient was located near the 3rd and 4th tap position, also at approximately 50 degrees (total taps = 7).

For higher aspect ratios, the flow tends to go around the dome rather than over the apex. This same logic would be adopted by other fluids and is easy to understand if compared to water flowing around a submerged dome. Overall, it can be seen that a H/R ratio ≥ 1.0 will lead to the peak negative pressure moving away from the domes peak (refer to Figure 56). A H/R ratio < 1.0, the maximum negative pressure zone tended to remain at the highest point (i.e. peak) of the dome (refer to Figure 54).

Peak pressure coefficient errors were plotted from the new data having corrected any inconsistences in the models geometry. These errors are presented in Figure 75.

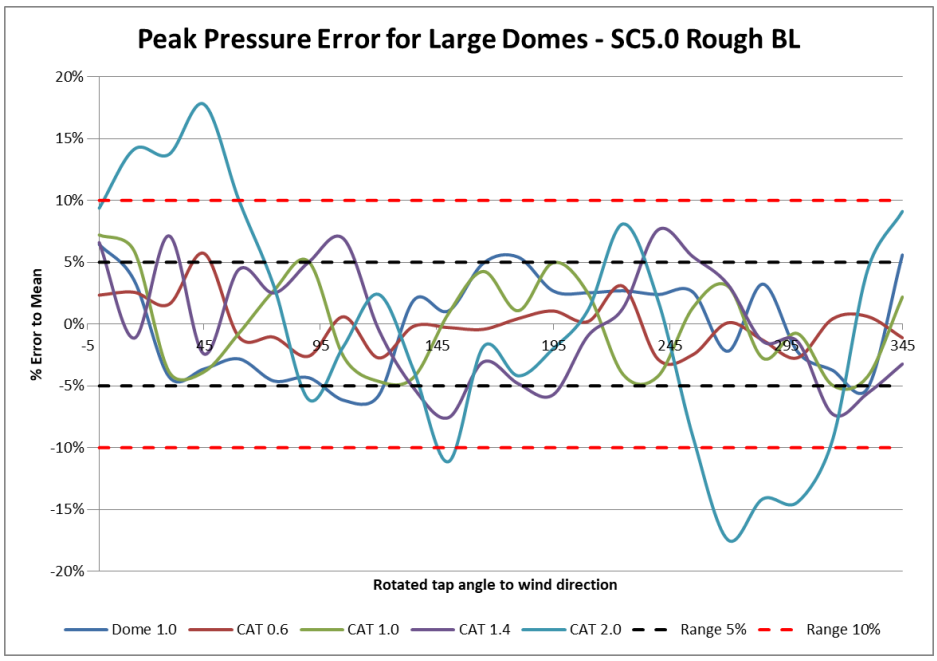


Figure 75: Peak Pressure Error for Large Domes - SC5.0 Rough BL

These errors seem to correlate with the geometry errors of the ‘almost perfect’ 3D printed “small” dome models (see Figure 41). In Figure 45, the CAT 1.0, CAT 1.4 and CAT 2.0 models fall outside the 10% error range. With the newly shaped models, only the CAT 2.0 model falls outside the 10% error range, with the maximum error halved for this dome. This was a significant improvement. The larger errors for the CAT 2.0 model may be caused by a few geometric inconsistencies when rotating at 15 degree increments (e.g. local ridge or roughness in the model). Thus, geometric inconsistency has an effect on any pressure tap for which flow is influenced.

Note: The unsymmetrical nature of the 3D pressure coefficient plots is due to a full range of data (i.e. 360 degrees) with 15 degree increments.

5.3 Influence of Walls

For a fully comprehensive study into wind loads on catenary domes to be conducted, it was necessary to include results where the models were placed on cylindrical walls. This allows for more real-life applications, and a more complete design graph. The walls being 40mm, 100mm, and 160mm in height can be seen in Figure 76. These wall heights were chosen by the Author as they seemed to be practical and would give a good data spread (i.e. lower and upper limits).



Figure 76: 40/100/160mm Walls (Photo)

Upon developing the catenary dome design graph in Section 6, it was observed that the current design graph for circular domes as published in SANS 10160-3:2010 had h/d ratios of 0, 0.25, 0.5, and 1.0. In hindsight, it would have been good to have matched these as the tested h/d ratios in this research report was 0, 0.16, 0.4, and 0.64.

From Figure 58, it was noticeable that the CAT 0.6 model does not achieve the same peak positive pressure coefficient that the other models (CAT 1.0, CAT 1.4 and DOME 1.0) achieve. This was also noticeable in Figure 59 and Figure 60. This was due to a difference in flow regime and also might be due to a slight separation of the flow based on the sharper angle created between the wall and the CAT 0.6 model. See the illustration in Figure 77 for an example showing the incident angle of the CAT 0.6 model. The incident angle was measured from the bottom of the dome models to the 1st tap position.

- CAT 0.6 – 38 degrees (i.e. sharpest incident angle)
- DOME 1.0 – 3 degrees (approximately zero)
- CAT 1.0 – 23 degrees
- CAT 1.4 – 15 degrees

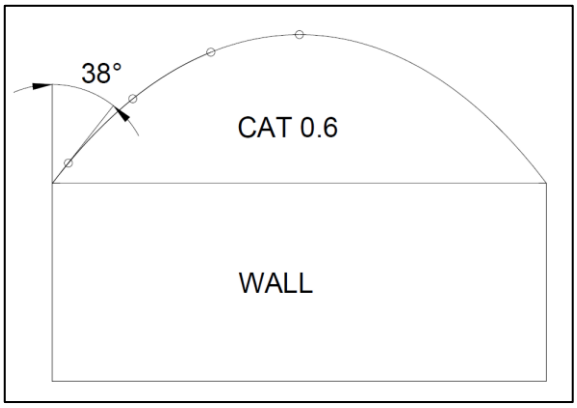


Figure 77: Incident Angle of Dome Models (e.g. CAT 0.6)

Comparisons made at the 90 degree/peak tap:

- In Figure 58, the peak pressure coefficient from CAT 1.4 was lower than that of CAT 1.0, which is expected due to flow around the model instead of over the model. However, what slightly differs from the previous discussion, was that the CAT 1.0 peak is higher than that of the CAT 0.6 model. This may be due to the

flow around the model instead of over the model not occurring as rapidly due to the models being raised on walls. This was not seen as an error due to CAT 1.0 increasingly having a greater peak negative pressure coefficient compared to CAT 0.6 for Figure 59 and Figure 60 (i.e. three data sets), with increased wall height. As identified previously, the accurate pressure distribution cannot be obtained from a single 2D graph.

Looking at each domes aspect ratio for a wall height of 40mm (h/d = 0.16), the following was identified:

- From Figure 62, the CAT 0.6 model still had the maximum negative peak pressure coefficient at the highest point of the dome. From Figure 61, the DOME 1.0 model was similar to CAT 0.6, with the highest flow over the dome remaining at the domes peak (i.e. a more uniform flow).
- From Figure 63, the CAT 1.0 models maximum negative peak pressure coefficients were seen to be starting to diverge from the domes peak. The maximum negative pressure was now located near the 4th tap position at approximately 70 degrees (total taps = 5).
- From Figure 64, the CAT 1.4 models maximum negative peak pressures were more divergent from the domes peak in comparison to CAT 1.0. The maximum negative pressure coefficient was now located near the 3rd tap position, at approximately 45 degrees (total taps = 6).

Looking at each domes aspect ratio for a wall height of 100mm (h/d = 0.4), the following was identified:

- From Figure 66, the CAT 0.6 model still had the maximum negative peak pressure coefficient at the highest point of the dome. From Figure 65, the DOME 1.0 model was similar to CAT 0.6, with the maximum negative pressure coefficient over the dome remaining at the domes peak (i.e. a more uniform flow).
- From Figure 67, the CAT 1.0 models maximum negative peak pressure coefficients were seen to be starting to diverge from the domes peak. The maximum negative pressure coefficient was now located near the 4th tap position at approximately 70 degrees (total taps = 5).

- From Figure 68, the CAT 1.4 models maximum negative peak pressure coefficients were more divergent from the domes peak in comparison to CAT 1.0. The maximum negative pressure coefficient was now located near the 2nd and 3rd tap position at approximately 36 degrees (total taps = 6).

Looking at each domes aspect ratio for a wall height of 160mm (h/d = 0.64), the following was identified:

- From Figure 70, the CAT 0.6 model still had the maximum negative peak pressure coefficient at the highest point of the dome. From Figure 69, the DOME 1.0 model was similar to CAT 0.6. Both models had a fairly even distribution of negative pressure coefficients along the middle section of the models perpendicular to the wind flow.
- From Figure 71, the CAT 1.0 models maximum negative peak pressure coefficients were seen to be starting to diverge from the domes peak. The maximum negative pressure coefficient was now located near the 3rd and 4th tap position at approximately 65 degrees (total taps = 5).
- From Figure 72, the CAT 1.4 models maximum negative peak pressure coefficients were more divergent from the domes peak in comparison to CAT 1.0. The maximum negative pressure coefficient was now located near the 2nd and 3rd tap position at approximately 32 degrees (total taps = 6).

This comparison allows for the determination that for high H/R aspect ratios, the higher the dome from ground level, the lower the negative (suction) pressures develop on the catenary dome faces. For low H/R aspect ratios and the higher the dome from ground level, the more distributed the peak pressure becomes over the catenary domes width. This distribution zone is illustrated below in Figure 78.

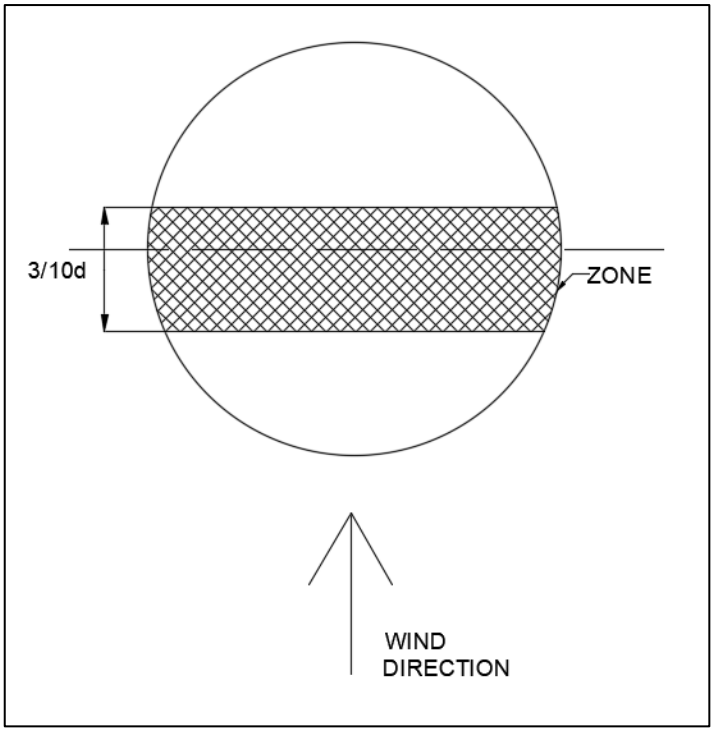


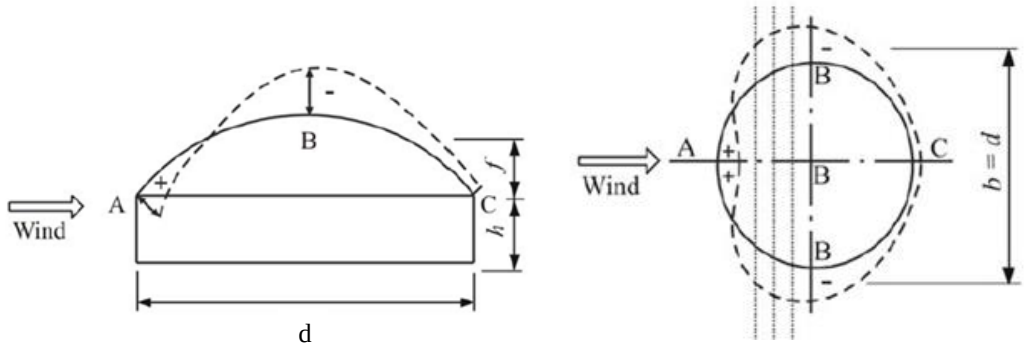
Figure 78: Negative Pressure Distribution Zone for Low H/R Ratios

6 DEVELOPMENT OF THE DESIGN GRAPH

The purpose of this Chapter is to discuss the process the Author used to develop the final design graph for catenary domes with varying base heights and catenary dome diameters, as well as make comparisons between the published SANS 10160-3-2010 hemispherical dome and catenary dome graph developed in this research.

6.1 DEVELOPMENT OF GRAPH

This section gives a breakdown of the process taken to develop the final proposed catenary design graph, for assistance to designers. The two images below are extracted from Figure 15 of SANS Wind Loading code, and define pressure zones for design purposes (i.e. A, B, and C).



Figures from (SANS 10160-3:2010)

The graphs developed in this study assume a loading area > $10m^2$, and the overall pressure coefficients are representative of $c_{pe,10}$. These values are used to design the overall structure and are not intended for the design of small elements and fixings with an area per element of $1m^2$ or less.

Step 1, the maximum external pressure coefficients at each zone measured at the pressure tap positions placed on the models, are plotted for the various wall height/diameter (h/d) ratios (see Figure 79). The h/d ratios used are 0, 0.16, 0.4, and 0.64 (see Table 9).

Table 9: h/d ratios used for testing

h/d Ratio	Wall height/ model diameter (mm)/(mm)
0	No Wall
0.16	40 / 250
0.4	100 / 250
0.64	160 / 250

CAT 2.0 model was not tested with walls, therefore no data was included for dome height/ model diameter (f/d) = 1.0 ratio. The data also only started from f/d = 0.3 ratio, as the smallest catenary dome tested was CAT 0.6.

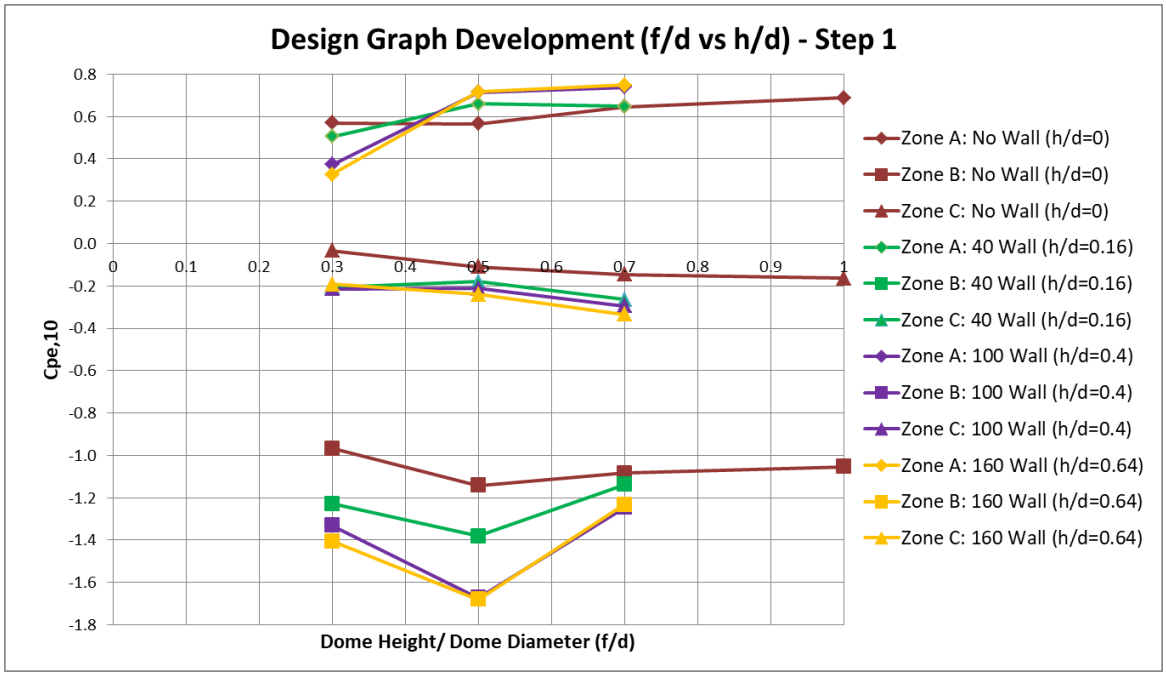


Figure 79: Design Graph Development (Step 1 of 4)

In step 2, due to not having data for catenary domes smaller than f/d = 0.3 and the similarity of the geometry at small f/d ratios, circular dome data was used to complete the graph for the different h/d ratios, see Figure 80 below. It should be noted that a circular and catenary dome are similar in shape for low h/d values.

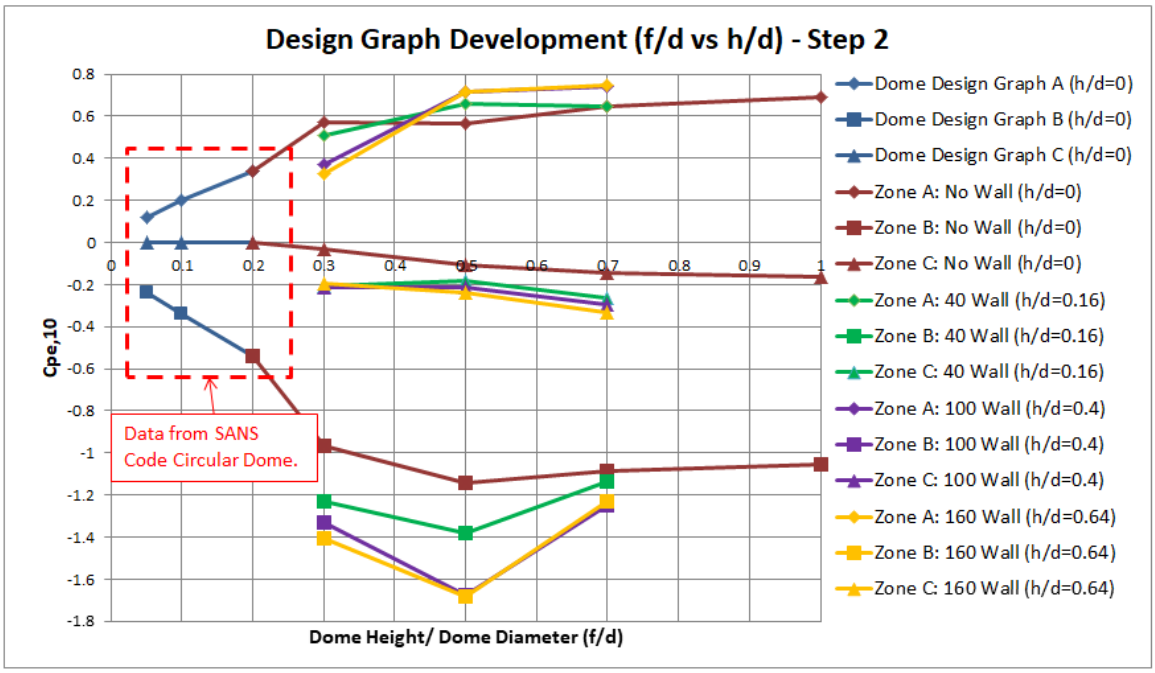


Figure 80: Design Graph Development (Step 2 of 4)

Step 3 shown in Figure 81, includes h/d ratios of 0.25 and 0.5. These were included for better comparison to the design lines used in the dome design graph in the SANS code. These new h/d ratios were obtained from linear interpolation between the measured experimental data. Therefore, h/d ratios of 0.16 and 0.4 were removed.

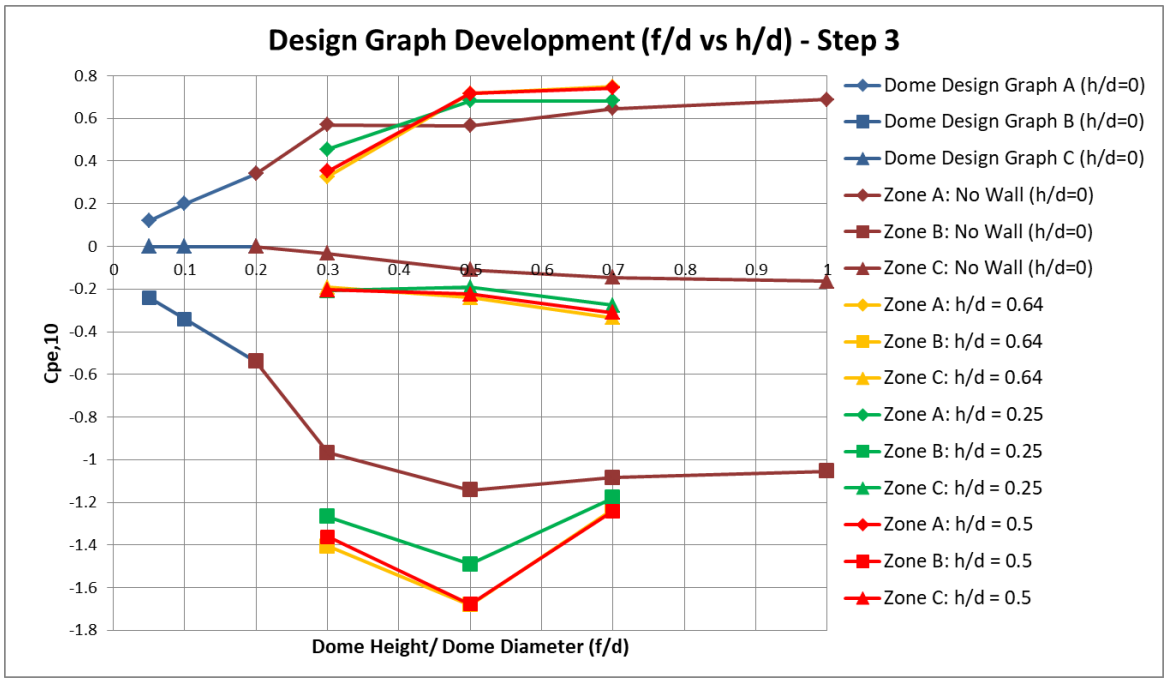


Figure 81: Design Graph Development (Step 3 of 4)

Step 4, now having included the data to build the catenary design graph, it was possible to start developing the final graph (see Figure 82). The 160mm wall data giving a h/d = 0.64 was kept for this final development of the design graph to show that the data converges at a h/d ratio ≥ 0.5. The light blue lines indicate the final catenary design graph.

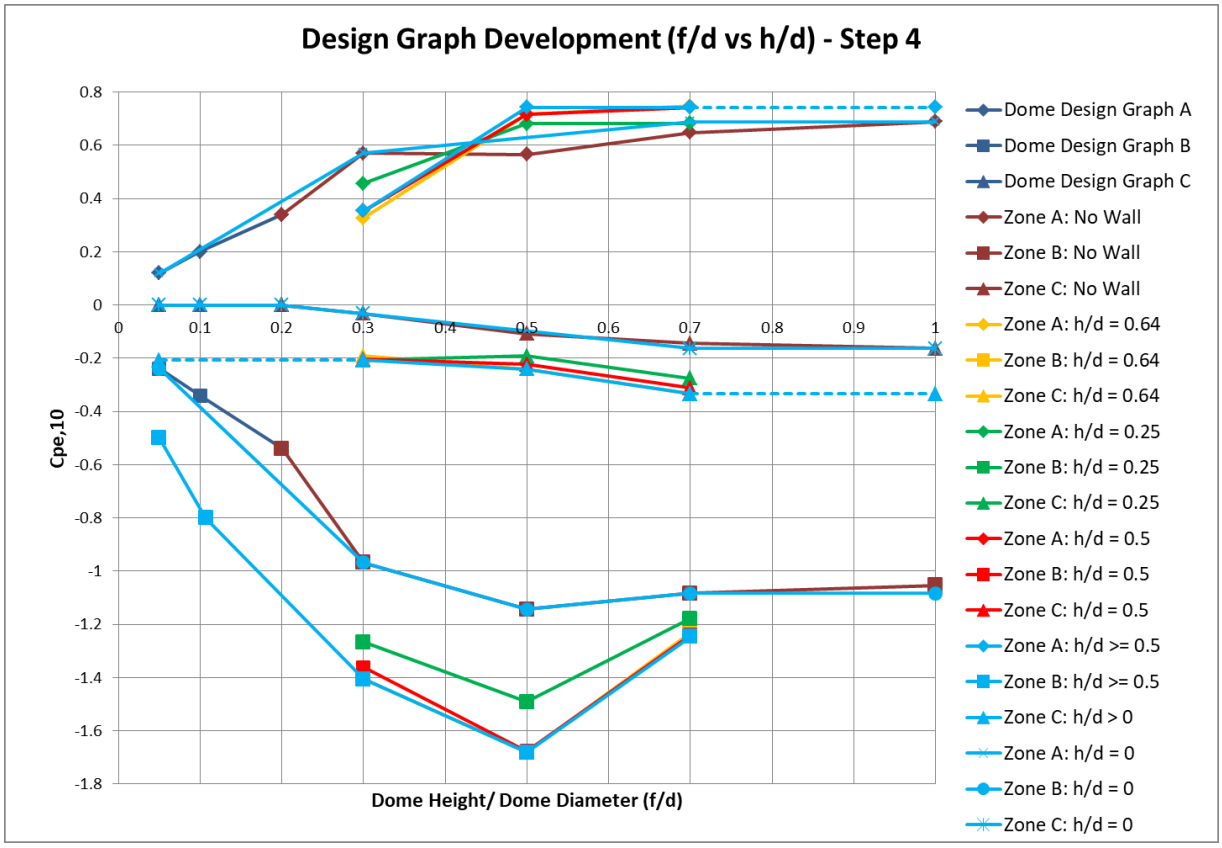


Figure 82: Design Graph Development (Step 4 of 4)

The zones as mentioned within the design development graphs are based on the same zones used for the circular dome design graph in SANS 10160-3-2010.

Description of each zone:

- Zone A – Where there was no wall (h/d = 0), the initial line from f/d = 0.05 to 0.3 is linear. From f/d = 0.3 to 0.7, a line which is higher than the test data was plotted. The reason for this was that at f/d = 0.5, if the point was lowered, then when linearly interpolating between different (h/d ratios or wall heights), the result would be unconservative. It can be seen at f/d = 0.5, that if linear interpolation is used, h/d = 0.25 would lie approximately between h/d = 0 and

0.5. This is also true for f/d = 0.3. At f/d = 0.7 to 1.0, data showed that when there was no wall, the pressure was uniform. This same straight line assumption was used for h/d ≥ 0.5, and it can be seen that the angle of the line between f/d = 0.5 and 0.7 was already very flat (i.e. approximately 0 degrees).

- Zone B - Where there was no wall (h/d = 0), the initial line from f/d = 0.05 to 0.3 is linear. This line does not conform to the initial h/d = 0 assumed line from the SANS10160-3:2010 dome design graph. It was decided to rather be conservative, and take a simplified straight line to data obtained from tests at f/d = 0.3. From f/d = 0.3 to 0.7, the design curve follows the test data curve. From f/d = 0.7 to 1.0, the pressure coefficients seem to drop slightly, but for design purposes this line was simplified as being straight (i.e. no gradient).

  Where there was a wall, the ratio of h/d ≥ 0.5 was chosen. The initial two data points of f/d = 0.05 and 0.1, was plotted directly from the SANS10160-3:2010 dome design graph. From f/d = 0.1 to 0.3, a linear line was plotted, ending on the test data from the h/d ratio = 0.64. The reason being that at this particular data point, it wasn't fully apparent that the data had converged at a h/d ratio of 0.5, as the negative pressure for h/d = 0.64 was seen to be higher (i.e -1.36 and -1.41 respectively). Convergence had occurred for f/d = 0.5 and 0.7, as the negative pressure for h/d = 0.5 and 0.64 was seen to be equivalent (i.e. -1.68 and -1.68 respectively). Therefore, the design graph followed these data points. No data was collected for a f/d ratio > 0.7, and for this particular case, a reasonable approximation for the design graph from f/d = 0.7 and 1.0 could not be extrapolated. A reasonable assumption would be that due to the catenary dome becoming so steep, the wall has less of an effect, and it is expected that the h/d = 0 and h/d ≥ 0.5 would start to converge at f/d = 1.0. Linear interpolation is assumed to simplify the Zone B graph between h/d = 0 and ≥ 0.5, but as seen in Figure 82, this may be slightly unconservative. The reason being that the h/d = 0.25 graph (green line) does not lie directly between the h/d ratios of 0 and 0.5.

- Zone C – Where there was no wall (h/d = 0), the initial line from f/d = 0.05 to 0.2 was linear, as per SANS10160-3:2010 dome design graph. From f/d = 0.2 to

0.7, there was a linear line which accurately approximates the test data. From f/d = 0.7 to 1.0, a straight line is assumed, which also best approximates the test data.

Where there was a wall, the ratio of h/d > 0 was chosen. From the graphs plotted for h/d = 0.16, 0.4, and 0.64, it can be seen that in Zone C, the data points are already convergent. To be conservative, a ratio of h/d > 0 was chosen, as it cannot be seen where the data started converging. Straight lines were seen as being acceptable for the graph from f/d = 0.05 to 0.3 and from f/d = 0.7 to 1.0, as both the graphs for h/d = 0 and > 0 seemed parallel between test data for f/d = 0.3 to 0.7. The straight line graph from f/d = 0.7 to 1.0 may be slightly unconservative based on the h/d = 0 graph between these points having a slight fall in angle.

6.2 COMPARISON OF DOME AND CATENARY DESIGN GRAPHS

To fully understand the difference between these two types of domes, a comparison can be made between the design graphs, as seen in Figure 84. Before this comparison can be made, it is important to understand the dome design graph in SANS10160-3:2010 code. The Dome 1.0 data from test results of this study was overlaid onto this graph, and is represented in Figure 83 below.

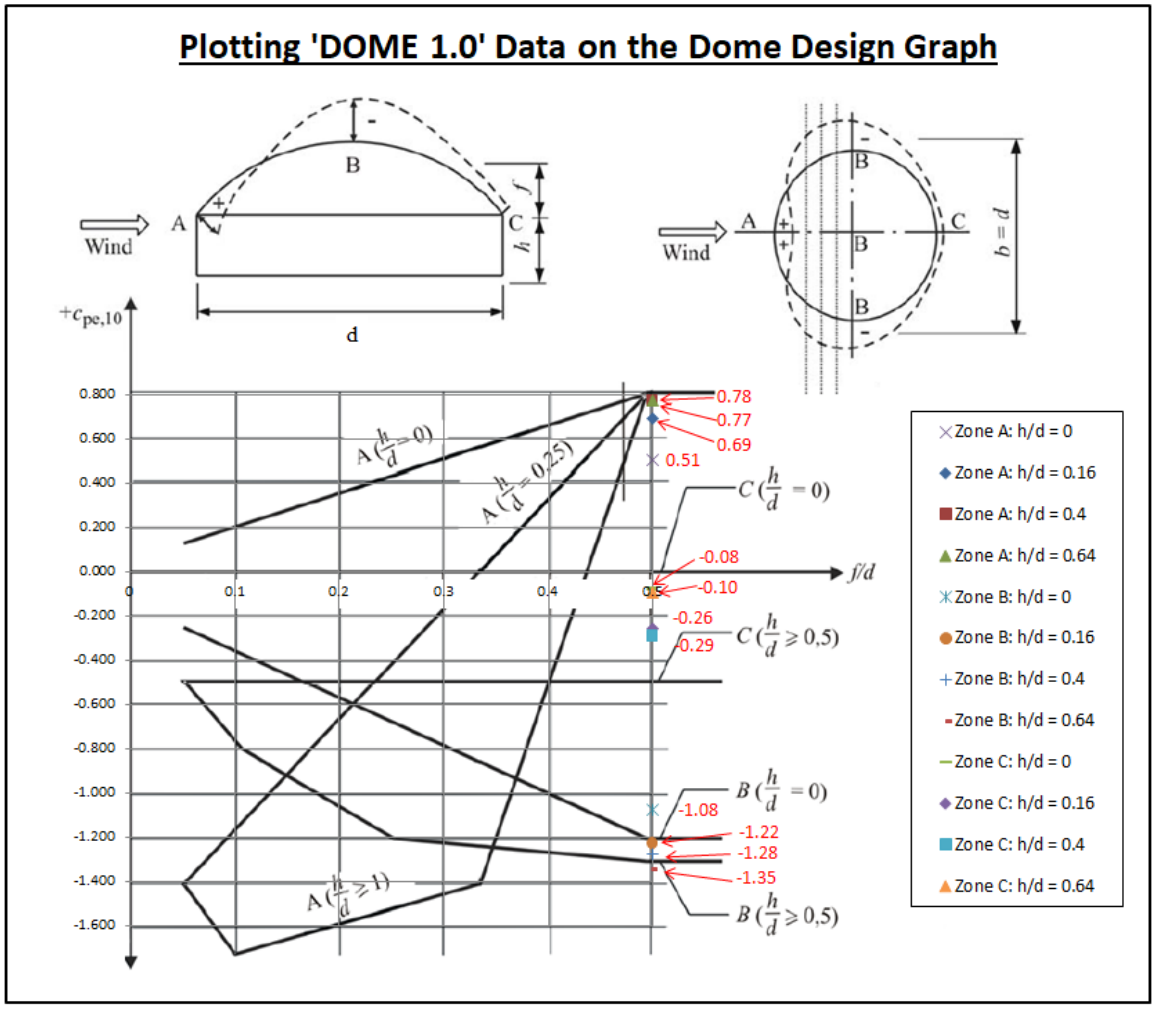


Figure 83: DOME 1.0 Test Data vs. Dome Design Graph

Comparison of different zones:

- Zone A: The peak external pressure coefficient was 0.78, and the design graph does approximate this. For lower h/d ratios, the values seem to be conservative.
- Zone B: The peak negative external pressure coefficient for h/d = 0.64 was -1.35, which closely represents the codes design graph. For h/d = 0, the design graph seems to be conservative.
- Zone C: It was immediately noticeable in this zone that the design graph is slightly conservative when it comes to h/d ratio ≥ 0.5 and unconservative when the h/d ratio is zero.

It must be noted, that the data is taken at 0, 90, and 180 degrees, for Zones A, B, and C respectively. This does not influence the Zone A readings, as the maximum positive pressure coefficient lies at zero degrees. However, this is not true for Zone C, as the maximum negative pressure increases the further from 180 degrees the readings are taken. See Figure 61 to Figure 72 pressure contours which make this clear to see.

The following was observed when considering data readings for 30 degrees on either side of 180 degrees (i.e. 150 to 210 degrees), see Table 10. If this approach is followed, the maximum negative pressure coefficient for Circular Domes in Zone C is -0.41, which is similar to Zone C h/d ≥ 0.5 from the SANS10160-3:2010 (Figure 83).

Table 10: Zone C - Maximum Pressure Coefficients for 150 to 210 Degrees

Zone C					
Model	**f/d**	**h/d = 0**	**h/d = 0.16**	**h/d = 0.4**	**h/d = 0.64**
CAT 0.6	0.3	-0.06	-0.41	-0.24	-0.28
CAT 1.0	0.5	-0.23	-0.23	-0.32	-0.35
CAT 1.4	0.7	-0.27	-0.29	-0.32	-0.40
CAT 2.0	1.0	-0.23			
DOME 1.0	0.5	-0.14	-0.41	-0.34	-0.32

From Table 10, CAT 0.6 and DOME 1.0 were similar in terms of having a peak negative pressure coefficient at h/d = 0.16, where CAT 1.0 and CAT 1.4 peak at h/d

ratio = 0.64. For this reason, it was best to provide a constant pressure coefficient to encapsulate all results. A pressure coefficient of -0.5 was chosen, based on the approximation that from linear extrapolation of the data to h/d = 1.0, no pressure coefficient exceeds this value of -0.5.

A new Catenary design graph taking the updated 'Zone C' into account, and comparing this graph to the dome design graph (SANS 10160-3:2010), can be seen in Figure 84 below.

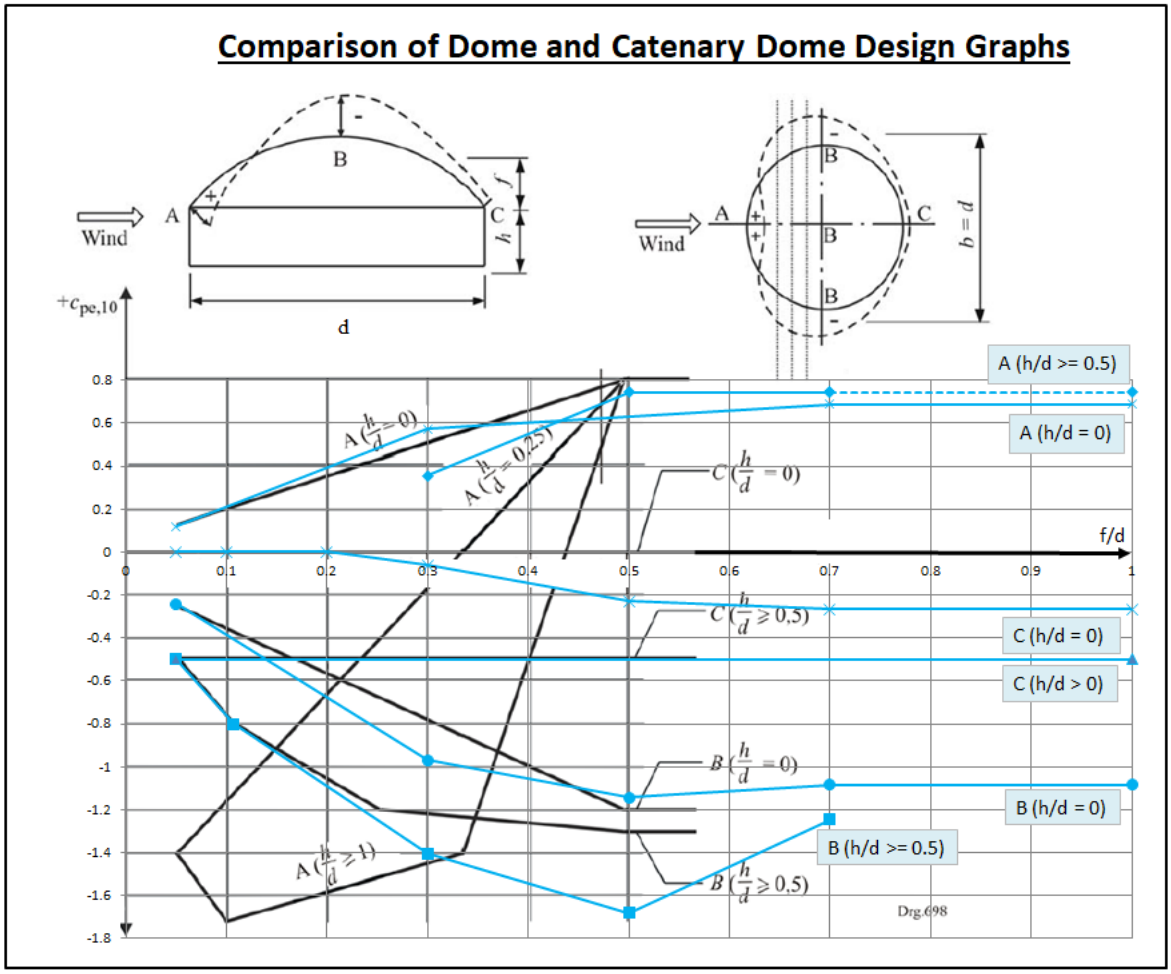


Figure 84: Dome and Catenary Dome Design Graph (Comparison)

Comparison of the catenary dome design graph to the circular dome design graph:

- Before comparing the three different zones, it is important to note that due to its nature, the circular dome cannot have a f/d ratio greater than 0.5. For Catenary domes, this f/d ratio can go to infinity. However, Figure 84 limits the design

graph to f/d = 1.0, which represents a very steep catenary dome (see illustration in Figure 85), and deemed to be extreme for practical purposes.

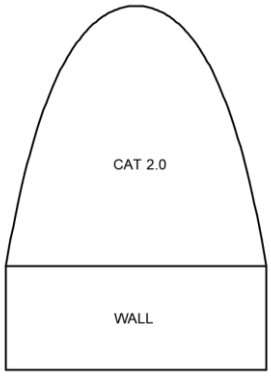


Figure 85: Illustration of CAT 2.0 Dome on a Wall (f/d = 1.0)

- Zone A – For h/d = 0, the catenary curve starts off slightly higher than the circular dome graph, which should almost match for these lower aspect ratio domes. This was due to the higher data point at f/d = 0.3. From f/d > 0.3, the peak positive pressure drops quite significantly and finally at f/d = 0.7 stabilises at a point slightly lower than that shown on the circular dome curve. The initial lower peak positive pressure coefficient is logical, as the dome is steepest at h/f = 0.5 and the catenary dome approaches a similar windward incident angle the greater the h/f ratio. A steeper face (greater f/d ratio) will produce a greater positive pressure coefficient.

  For h/d $\geq$ 0.5, the initial f/d = 0.3 reading was lower than the case were there was no wall. For the circular dome graph at this point, it shows that the pressure should be negative. The catenary dome and circular dome graphs do not agree here. During all tests, the windward pressure readings were always positive. This will be demonstrated further in Table 11 below.

Table 11: Pressure Coefficient Readings from 0 to 45 Degrees at Varying h/d Ratios

Model	h/d	Cpe @ Specific Degrees			
		0°	15°	30°	45°
CAT 0.6	0	0.57	0.52	0.32	0.05
	0.16	0.51	0.39	0.15	-0.17
	0.4	0.37	0.29	0.03	-0.33
	0.64	0.33	0.22	-0.05	-0.44
CAT 1.0	0	0.52	0.43	0.23	-0.07
	0.16	0.66	0.57	0.30	-0.07
	0.4	0.72	0.61	0.32	-0.10
	0.64	0.72	0.55	0.19	-0.34
CAT 1.4	0	0.49	0.42	0.22	-0.17
	0.16	0.65	0.57	0.28	-0.11
	0.4	0.74	0.62	0.25	-0.28
	0.64	0.75	0.67	0.31	-0.23
CAT 2.0	0	0.49	0.43	0.21	-0.13

From Table 11, it can be seen that between 30 at 45 degrees is the transition between positive and negative pressures. This is certainly helpful to the designer, to be able to apply the positive pressures to the correct zone. This approximation can only be made for Catenary domes with f/d ratio from 0.3 to 1.0. Additional research will be required to determine if this assumption is true for catenary domes with f/d ratios < 0.3.

As the f/d ratio passes 0.4, the maximum positive pressure exceeds the pressure for no wall. At f/d = 0.5, the peak positive pressure coefficient is reached (Cpe = 0.743), which is very similar to that of the circular dome tested (Cpe = 0.776).

- Zone B – For h/d = 0, the catenary curve is a straight line from f/d = 0.05 to f/d = 0.3. The coefficient at f/d = 0.3 is higher than the circular dome graph, which intern shifts the gradient of the straight line. These design lines where expected to be closer, and more data points between f/d = 0.05 and 0.3 are required. Currently this design line is seen as being slightly conservative, as the reading at f/d = 0.3 was taken as -0.97 from these tests and not -0.78 from the SANS10160-3:2010 circular dome graph. At f/d = 0.5, the negative pressure coefficient for the catenary dome is slightly lower than that of the circular dome

(i.e. -1.143 compared to -1.2). From f/d >0.7, the pressure coefficients stabilise at approximately -1.1.

For h/d ≥ 0.5, the catenary dome design curve approximately compares to the circular dome design curve up to f/d = 0.25. At f/d = 0.3, the catenary dome pressure coefficients were seen to be greater, and kept increasing until f/d = 0.5. At f/d = 0.5, the catenary dome and circular dome peak negative pressure coefficients are -1.7 and -1.3 respectively. After reaching the peak at f/d = 0.5, the curve reduces to approximately the same peak pressure coefficient as the circular dome design curve at f/d = 0.7. This shows that if designers used the circular dome graph from the SANS10160-3:2010 code for designing catenary domes, the peak negative pressure coefficient for catenary domes with walls would have been severely under-estimated between f/d ratios of 0.25 to 0.7, with a maximum error of 30%.

- Zone C – For h/d = 0, the catenary dome line matches the circular dome line from f/d = 0.05 to f/d = 0.2, as the data was a direct copy up to this point due to the dome shapes being very similar at low H/R ratios. At f/d = 0.3, the catenary dome was seen to have a small negative pressure coefficient, which increased until f/d = 0.7. After which the pressure became uniform. The SANS10160-3:2010 wind loading code circular dome graph assumes a constant zero pressure coefficient, at h/d = 0. From Figure 83, the negative pressure coefficient for a circular dome was -0.08, which is not zero, but not a significant negative pressure. However, for catenary domes, the “Zone C” pressure coefficient for h/d = 0 is of significance, and cannot be approximated to be zero (e.g. at f/d = 0.5, the pressure is -0.23).

  For h/d > 0, the catenary design curve approximately compares to the circular dome design curve for f/d ratios from 0.05 to 1.0. This was based on the previous discussion. The difference is that this catenary dome curve was based on a h/d > 0 and the circular dome curve was based on h/d ≥ 0.5. The reason for this was that at the lowest h/d ratio tested of 0.16, the pressure coefficient was -0.41 (see Table 10). Thus, interpolation of the graphs would not give the

correct pressure coefficients. Hence, the range of $h/d > 0$ was chosen, based on the current results obtained from testing.

It was noted that for all catenary dome graphs, pressure coefficients tended to become uniform at $f/d \geq 0.7$.

6.3 CATENARY DESIGN GRAPH

Based on the previous discussions and comparisons, the final Catenary Design Graph is shown in Figure 86.

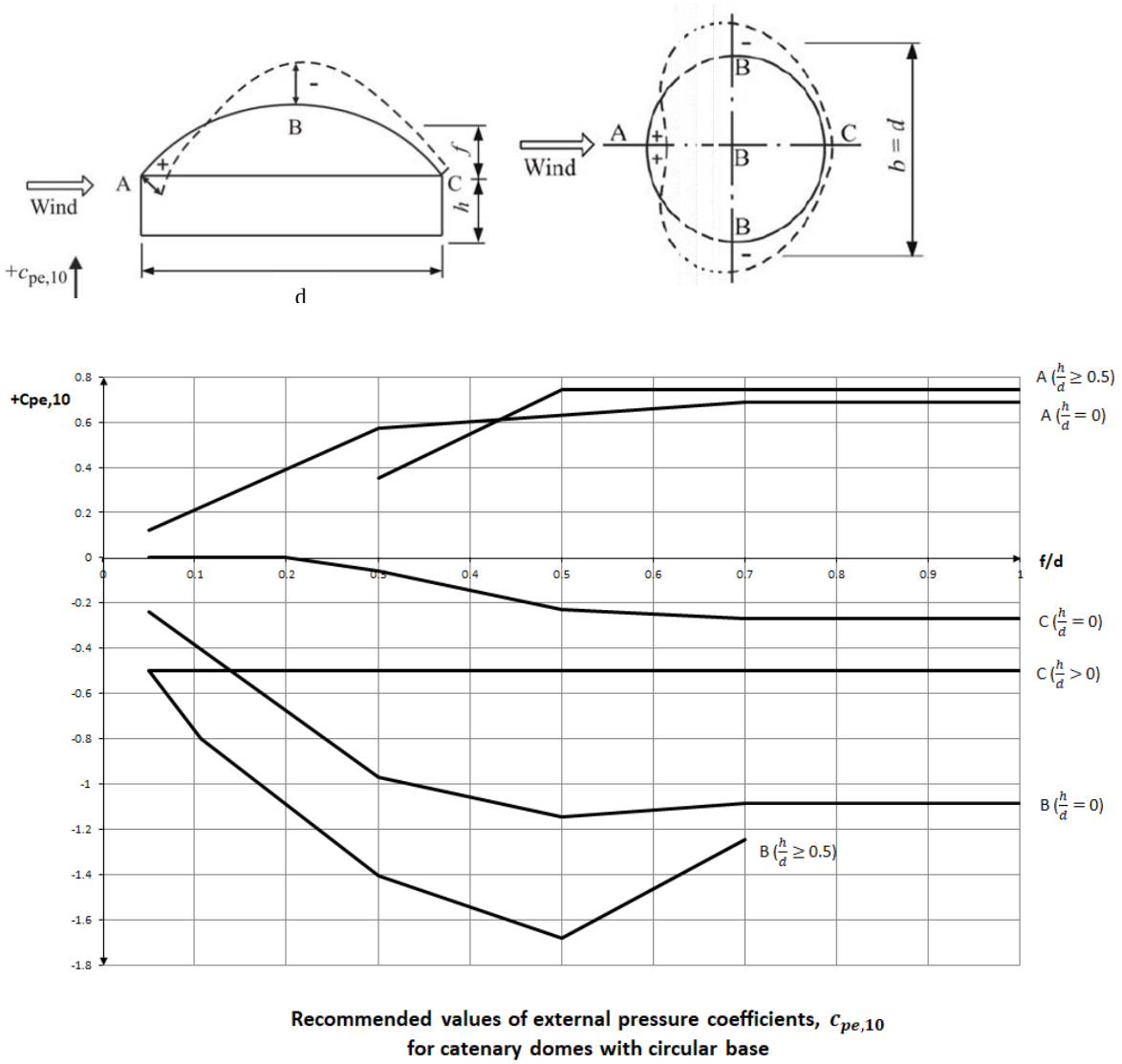


Figure 86: Catenary Dome Design Graph

Going further, one can estimate a figure to assist with the practical application of the design graph developed above (see Figure 87). This figure includes the previous discussion and, in short, the following is achieved:

- Zone A: Where the peak positive pressure coefficient is located. Linear interpolation between Zone A and Zone B is allowed.

- Zone B: The length of the peak negative pressure. Zone B extends to the edges, this was seen as the catenary dome H/R aspect ratio increased, the peak negative pressure zone moved away from the dome peak. The maximum negative peak pressure coefficients for the higher H/R ratio catenary domes are seen to be slightly forward of the dome centreline (towards the wind direction). Zone B was adjusted to reflect this.
- Zone C: Represents the negative pressures where readings were taken at a 30 degree angle. Linear interpolation between Zone B and Zone C is allowed.

This was an assumption based on f/d ratios of 0.3 to 1.0, and further research is required to prove/ disprove these assumptions especially for lower f/d ratios, and the division of the pressure Zones (i.e. A, B, and C).

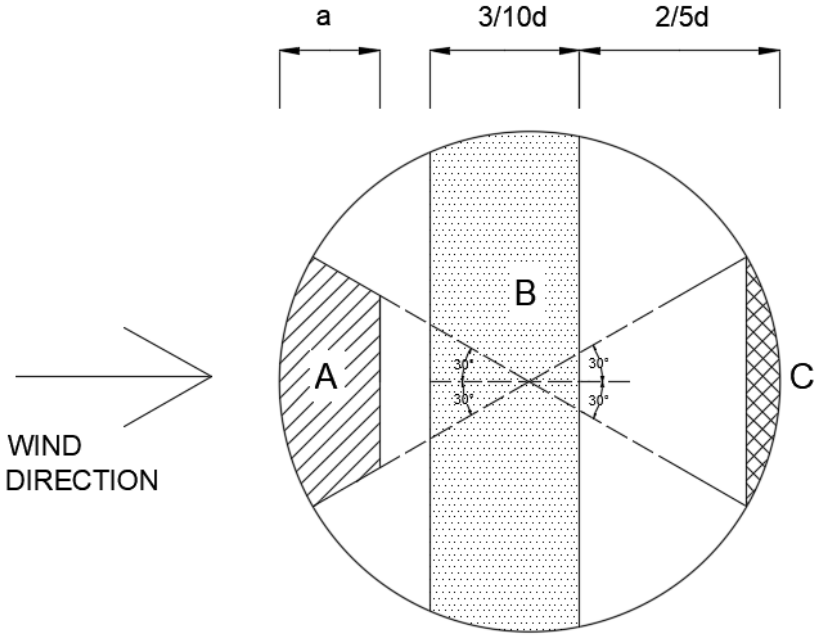


Figure 87: Illustration for Application of Wind Loads (f/d > 0.3)

Parameter “a” for use in Figure 87 is defined in Table 12. The determination of parameter “a” and development of Figure 87 was based on a few basic assumptions using the 0 to 180 degree pressure coefficient graphs as well as the 3D pressure contours.

Table 12: Defining dimension "a"

f/d Ratio	Dimension (a)
0.3	0.05d
0.5	0.20d
0.7	0.25d
1.0	0.30d

For design purposes, the code could also implement a further graph (see Figure 88) for member design (e.g. purlin design).

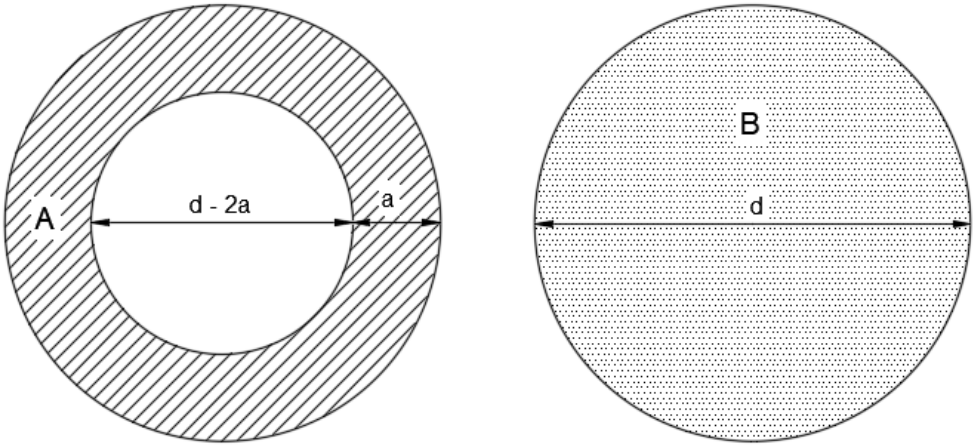


Figure 88: Positive and Negative Pressure Coefficients for Member Design (loading area >10m^2)

7 FUTURE WORK

The following areas are where future work is required to fully conclude this chapter for "Wind Loading on Catenary Domes":

1. Additional work should be done in a scaled boundary layer to confirm the graphs presented.
2. Confirm catenary design graph:
    a. Confirm the graphical inputs for f/d ratios of 0.3 to 1.0.
    b. Test catenary domes for f/d ratios of 0.05 to 0.2, or test domes with f/d ratios of 0.05 and 0.1 and a catenary dome where f/d = 0.2.
    c. Test CAT 2.0 dome model (f/d = 1.0) with walls.
    d. Test catenary domes on a higher wall, say h/d = 1.0, to determine if the data points did indeed converge as predicted with results from h/d of 0.4 and 0.64.
3. For the full data set, determine if the transition between positive and negative pressure zones is at 30 degrees, and if this continues to be true for catenary domes with f/d ratio less than 0.3.
4. Based on further analysis of the data, determine if the illustrations depicted in Figure 87 and Figure 88 can be used for a more practical understanding of applying the wind loads for design purposes, as well as parameter "a" defined in Table 12.

    Note: It is the Authors opinion that engineers need more experience with wind loading codes when it comes to selecting design pressure coefficients for complex shapes, including domed roofs. Selecting the worst combination positive and negative pressure coefficients as a shell load for domed roofs, will lead to uneconomical designs.

8 CONCLUSION

The wind tunnel data was analysed and a catenary dome design graph developed. The design graph showed that for Zone A, designing a catenary dome with no wall using the SANS10160-3:2010 circular dome design graph is seen as being conservative or close to correct. Where the catenary dome was raised off the floor, the positive pressures were greater than that predicted by the circular dome design graph (for f/d = 0.3 to approximately 0.475), and hence the catenary dome would have been under-designed. For Zone B, by using the SANS10160-3:2010 circular dome design graph, could have led to the catenary domes being under-designed. For Zone C, by using the SANS10160-3:2010 circular dome design graph, could likely have led to the catenary domes being under-designed. In general, catenary domes with $f/d \geq 0.3$ could have been under-designed based on the SANS10160-3:2010 external pressure coefficients for circular domes. For $f/d < 0.3$, further investigation is required. In conclusion, a catenary dome design graph is required to design for the appropriate wind loads and these wind loads should not be approximated off the current circular dome design graphs from SANS10160-3:2010, as this could lead to the roof structure being under-designed.

9 WORKS CITED

Auroville Earth Institute. (n.d.). *Stability Notions*. Retrieved August 13, 2018, from http://www.earth-auroville.com/stability_notions_en.php

Blackmore, P., & Tsokri, E. (2006). Wind loads on curved roofs. *Journal of Wind Engineering and Industrial Aerodynamics (94)*, 833-844.

Bradley, R. A. (n.d.). Chapter 7. Wind Loading on Catenary Earth Shells. *(PHD thesis in progress)*.

BS EN 1991-1-4:2005. (n.d.). Eurocode 1: Actions on structures Part 1-4. *General actions - Wind actions*, 50.

C.M. Cheng, C. F. (2009). Characteristics of wind loads on a hemispherical dome in smooth flow and turbulent boundary layer flow. *Journal of Wind Engineering and Industrial Aerodynamics*, 329-344.

Cheng C.M., F. C. (2008). Characteristics of wind loading on a hemispherical dome in smooth flow and turbulent boundary layer flow. *BBAA VI International Colloquium*.

Cook, N. J. (1990). The designer's guide to wind loading of building structures, Part 2: Static structures. Building Research Establishment (BRE).

Davenport A G, G. S. (2000). The revised Davenport roughness clasification for cities and sheltered country. *3rd Symposium on Urban Environment*, (pp. 7-8). CA, US.

Holmes, J. D. (2001). Wind Loading of Structures. London: Spon Press.

Liu, H. (1990). Wind Engineering, A Handbook for Structural Engineers. Prentice Hall.

Media Storehouse. (n.d.). *Framed Print of St Paul's Cathedral - Section thorugh Wren's Dome*. Retrieved Decemeber 20, 2018, from https://www.mediastorehouse.com/mary-evans-prints-online/st-pauls-cathedral-section-wrens-dome-4415642.html

Mistry, Y., & Bhayroo, T. (2014). *Pressure distribution on catenary vaults.* Johannesburg: Undergraduate Research (leading to MSc paper).

Quora. (2011, September 7). *What does the word "catenary" mean?* Retrieved April 11, 2015, from Quora: http://www.quora.com/What-does-the-word-catenary-mean

R A Bradley, M. G. (2016). Wind loading on catenary vault structures. *SAICE, Vol 58 No 4*, 29-47.

SANS 10160-3:2010. (n.d.). Basis of structural design and actions for buildings and industrial structures. *Part 3: Wind actions*.

Stathopoulos, &. B. (2007). Wind effects on buildings and design of wind-senstive structures. *CISM International Centre for Mechanical Sciences* (p. Vol 493). New York: Springer Science & Business Media.

Taylor, T. J. (1991). Wind pressures on a hemispherical dome. *Journal of Wind Engineering and Industrial Aerodynamics, 40*, 199-213.

Walks of Italy. (n.d.). *6 Surprising facts about the pantheon in Rome*. Retrieved August 13, 2018, from https://www.walksofitaly.com/blog/rome/pantheon-facts

Wikipedia. (2018, August 9). *Pantheon, Rome*. Retrieved April 11, 2015, from Wikipedia: en.m.wikipedia.org/wiki/Pantheon,_Rome

Wikipedia. (n.d.). *Dome*. Retrieved August 14, 2018, from https://en.wikipedia.org/wiki/Dome